GREEN SYNTHESIS: THE USE OF BROWN ALGAE IN THE SYNTHESIS OF PALLADIUM NANOPARTICLES AND APPLICATIONS IN CARBON – CARBON BOND FORMATION REACTIONS

UNIVERSITY *of the* WESTERN CAPE

BY

ELDON PIERRE DAMON
BSc. Chemical Science, BSc. Honours Chemical Science

A mini thesis submitted in partial fulfilment of the requirements for the
Degree of *Magister Scientiae* in Nanoscience in the
Department of Chemistry, University of the Western Cape, South Africa.

Supervisor
Prof Edith Antunes
Co-supervisor
Prof Denzil Beukes

January 2020

Declaration

I, Eldon Pierre Damon hereby declare that this dissertation *Green synthesis: The use of brown algae in the synthesis of palladium nanoparticles and applications in Carbon-Carbon bond formation reactions* is my own work and effort and that it has been not submitted for any degree or examination in any other university, and that all the sources I have used or quoted have been indicated and acknowledged as complete references.

Student_____ Date_____

Supervisor_____ Date_____

Co-supervisor_____ Date_____

Acknowledgements

Dedication

I would like to dedicate this work to my parents (Daniel and Shirley), my brother Daniello for they love, support, understanding, and sacrifices they have made.

Academic Output

The results that were obtained from this work were presented at an academic conference.

Conferences:

- Eldon P. Damon, Mokone Mmola, John J. Bolton, Denzil R. Beukes, and Edith M. Antunes. The use of a brown marine algae *Ecklonia radiata* aqueous extract, a supporting matrix for a palladium nanoparticle catalyst used in various organic reactions. Frank Warren Conference 2019, Alpine Heath Resort Drakensberg, 07 July 2019. Poster presentation.

Abstract

Due to the negative impact on the environment and the associated biological risks on human and animal life, the need for eco-friendly synthetic protocols is critical. With the rapid advancement in nanotechnology, this extends to the synthesis of nanomaterials. Eco-friendly nanoparticle synthesis protocols have led to the use of fungi, plants and other biological substances, due to their remarkable ability in reducing metal ions. This led to the formation of very efficient hybrid catalysts, which are partially organic/inorganic composites. Palladium nanoparticles have drawn much interest due to its potential in catalytic applications and in photovoltaic cell development.

In this study, the brown marine algae, *Ecklonia radiata*, was employed as a putative palladium nanoparticle bioreactor. Aqueous extracts of the algae were used as a supporting matrix for the synthesis of palladium nanoparticle (AE-PdNPs) catalysts according to the principles of green chemistry. The catalysts were then assessed for their capability in various carbon-carbon coupling reactions such as Suzuki-Miyaura, Sonogashira, and Heck coupling reactions. Selectivity studies were also performed. The PdNPs were compared to "model" polyvinylpyrrolidone palladium nanoparticles (PVP-PdNPs), synthesized according to literature methods. A variety of spectroscopic techniques were used to characterize the nanoparticles and the organic reaction products, including HRTEM, EDX, NMR, FTIR, DLS, TGA, UV-Vis, ICP-AES, GC-MS and XRD spectroscopy. qNMR was used to determine the product % yields. The aqueous extracts were characterised using NMR and a variety of assays, including total antioxidant potential, total reducing power and radical scavenging ability) to assess its ability to reduce the Pd metal salt. 2D NMR revealed polysaccharides and polyphenols to be the major and minor components, respectively, present in the extract. HRTEM images revealed the average size of the AE-PdNPs and PVP-PdNPs to be 12 nm and 8 nm, respectively. The images also showed the shapes of the NPs to be cubic for the AE-PdNPs and cubic or triangular for the PVP-PdNPs. SAED and XRD spectroscopy revealed the face-centred cubic phase and polycrystalline nature of the AE-PdNPs. No reliable data, other than the HRTEM images was obtained for the PVP-PdNPs. Zeta potential and DLS measurements confirmed the negative charge present on the surface of the nanoparticles, while the hydrodynamic radii were found to be 65 nm and 99 nm for the AE- and

PVP-PdNPs, respectively, substantiating the presence of the capping agents. ICP-AES analysis revealed the Pd content of the NPs to be 48.8 and 28.9 ppm for the AE- and PVP-PdNPs.

Following characterization, the PdNPs were assessed as potential catalysts in the Suzuki-Miyaura, Heck and Sonogashira carbon-carbon coupling reactions. Bromo and iodo substrates were employed, together with sterically hindered substrates, with a nitro moiety in the *ortho* or *para* positions. For the Suzuki-Miyaura reactions, both sets of PdNPs revealed slightly higher yields for the products synthesized using the bromo substrate (>90%), while low yields (40 – 55% yields) were obtained for the *ortho* substituted substrate in comparison to the *para* substrate (>90% yields). The Heck coupling reactions with butyl acrylate and 4-iodoacetphenone were successful (~70% yields), while reactions with 4-bromoacetophenone failed. However, the Sonogashira couplings did not proceed at all. With the series of reactions NPs showed some selectivity, with the AE-PdNPs consistently producing higher yields for the products obtained. This may be due to overall nature of the NPs, or due to the higher platinum loading content for the AE-PdNPs.

Table of Contents

List of Figures

List of Tables

List of Schemes

List of Abbreviations and Symbols

AA	Ascorbic Acid
AAE	Ascorbic Acid Equivalent
AE	Aqueous Extract
AE-PdNPs	Aqueous Extract – Palladium Nanoparticles
AgNPs	Silver Nanoparticles
ATR	Attenuated Total Reflection
AuNPs	Gold Nanoparticles
CCD	Charge-coupled device
COSY	Correlated Spectroscopy
DLS	Dynamic Light Scattering
DPPH	2,2-diphenyl-1-picrylhydrazyl
EDX	Energy Dispersive X-Ray Spectroscopy
E. radiata	*Ecklonia radiata*
F-C reagent	Folin-Ciocalteu reagent
fcc	Face centered cubic
FEG	Field-emission Gun
FTIR	Fourier Transform Infrared Spectroscopy
GA	Gallic Acid
GAE	Gallic Acid Equivalents
GC-MS	Gas Chromatography- Mass Spectroscopy
^{1}H	Proton
H_2O	Water
hrs	Hours
HMBC	Heteronuclear Multiple Bond Correlation
HRTEM	High Resolution Transmission Electron Microscopy
HSQC	Heteronuclear Single Quantum Coherence
ICP-AES	Inductively Coupled Plasma-Atomic Emission Spectroscopy
IR	Infrared
J	Coupling Constant
JCPDS	Joint Committee on Powder Diffraction Standards
KCl	Potassium Chloride
K_2PdCl_4	Potassium Tetrachloropalladate
$K_3Fe(CN)_6$	Potassium Ferricyanide
mA	milliamperes
MeOH	Methanol
Min	Minutes
MNPs	Metallic Nanoparticles

multi.	Multiplicity
NMs	Nanomaterials
NMR	Nuclear Magnetic Resonance
NPs	Nanoparticles
OAE	Organic Aqueous extract
OAE-PdNPs	Organic Aqueous Extract-Palladium Nanoparticles
PDI	Polydispersity Index
PdNPs	Palladium nanoparticles
PEG	Polyethylene Glycol
PVP	Polyvinylpyrrolidone
PVP-PdNPs	Polyvinylpyrrolidone capped-Palladium Nanoparticles
SAED	Selected Area Electron Diffraction
SEM	Scanning Electron Microscope
SPR	Surface Plasmon Resonance
TCA	Trichloroacetic Acid
TEM	Transmission Electron Microscopy
TGA	Thermal Gravimetric Analysis
TLC	Thin Layer Chromatography
UV-Vis	Ultraviolet - Visible Spectrophotometry
XRD	X-ray Powder Diffraction Spectroscopy
ZnO	Zinc Oxide
Θ	Bragg Diffraction Angle (Theta)
λ_{max}	Maximum wavelength
ζ	Zeta potential

Chapter 1: Introduction

1.1. Nanoscience and Nanotechnology

The last few years have drawn significant scientific interest in the field of nanoscience and nanotechnology, especially in the development of metallic nanomaterials due to their unique properties and the numerous applications discovered for these nanoparticles. Nanomaterials include all materials which are at the nanoscale level, where one dimension at less than 100 nm. These include nanoparticles, nanorods, nanotubes, nanofibers, quantum dots, etc. (Huo and Worden, 2007). These nanomaterials are primarily synthesized by using two methods, namely, chemical or physical methods (Huo and Worden, 2007). The synthesis of metallic nanoparticles (MNPs) is capturing the interest of the scientific community, due to the unique properties they possess compared to the bulk material properties of the same element (Parker *et al.*, 2014). To produce these nanomaterials, there are various synthetic routes that could be followed, however, most of these synthetic methods make use of toxic reagents, which may have a negative impact on the environment, and also on human and animal life (Kuppusamy *et al.*, 2015).

1.2. Green Chemistry

The field of Green Chemistry is a fairly recent field emerging in chemistry, which focuses mainly on the sustainability of the environment and the economy (Anastas and Eghbali, 2010). In 1998 Anastas and Warner (1998) introduced twelve principles that they believed Green Chemistry should cover. The principles include various topics such as making use of renewable natural materials, introducing catalysts into reaction systems, and the use of solvents that are more environmentally friendly. Green Chemistry can also be applied in the field of synthetic chemistry, whereby it maximizes the desired product yield and minimizes the yield of by-products. The use of water as a solvent is not only environmentally friendly, but it is also inexpensive, readily available and non-toxic (Li and Trost, 2008). Unterlass (2016), in a review article, mentioned the various Green synthetic routes which could be followed to produce materials from renewable resources by making use of hybrid materials (inorganic-organic) that can be employed in various applications. In another review article, Sheldon (2016) mentioned that catalysis has a pivotal role to play in the developing of sustainable technologies. The article also makes mention of how the catalytic technologies

could be used to improve the economy, as it allows for the conversion of waste biomass to valuable products (Sheldon, 2016). It is out of concern for the environment that various research groups started to make use of waste biomass in the synthesis of hybrid materials. Gholinejad *et al.*, (2017) synthesized carbon quantum dots from vanillin in order to modify their magnetic nanoparticles. In the article, the author and co-workers mentioned that vanillin is eco-friendly and a naturally abundant compound, found in plants and in wood (Gholinejad *et al.*, 2017). The success obtained from the use of waste biomass is the reason why researchers started to look for various alternative materials. For example, Bankar *et al.,* (2010) made use of banana peel extracts to synthesize their palladium nanoparticles. Plants and seaweeds have been recognized as a critical tool to clean-up the environment; due to its ability to take up metals from contaminated areas such as sewage run-off (Parker *et al.*, 2014). The new trend in the use of biobased materials to synthesize nanomaterials has therefore led researchers to make use of plants, teas, marine algae, and proteins to make new nanomaterials and also use these biobased materials as a support for the nanomaterials (Chen *et al.*, 2014; Kora and Rastogi, 2015; Arsiya, Sayadi and Sobhani, 2017; Mallikarjuna *et al.*, 2017). Making use of green synthetic routes allows for the easy up-scale of reactions, where chemical and physical synthetic methods are abandoned where possible in favour of energy-saving, non-toxic reagents, protecting the environment (Ajdari *et al.*, 2016). Besides the use of biomass, researchers have also been using proteins, viruses, and bacteria as a reducing agent to synthesize metallic nanoparticles (Parker *et al.*, 2014). It is especially the marine algae which show the most promising results for the synthesis of nanoparticles in particular, as extracts obtained from the marine algae contains compounds which not only reduce the metal salt, but they also cap the surface of the nanoparticle in order to maintain its size in the nanometer range (Azizi *et al.*, 2013). Yu *et al.,* (1999) showed that marine algae can be used to recover and remove heavy metal ions from the environment, as these algae act as a biosorbent materials.

1.3. Marine Algae

There are a variety of marine macroalgae and they are classified according to the pigmentation of their main body (Azizi *et al.*, 2013). The classes are *chlorophytes* (Green algae), *phaeophytes* (Brown algae) and *rhodophytes* (Red algae) (Azizi *et al.*, 2013). Marine algae have been very useful as a food source and as medicine (Nakai *et al.*, 2006). It has been reported that marine algae consist of polysaccharides, polyphenols, fatty acids, amino acids, sterols, etc.; however, it is the polysaccharides and polyphenols which researchers deem the most important in nanoparticle synthesis (Nakai *et al.*, 2006). It has been reported that aqueous

extracts of brown marine algae, in particular are rich in polyphenols and polysaccharides (Ananthi *et al.*, 2010). Marine algae contain various functional groups and bioactive molecules within its structure which serves the dual purpose of being a capping agent (for the surface of the metal nanoparticle), as well as being a reducing agent (to reduce the metal ion salt) (Azizi *et al.*, 2013). Polysaccharides are reported to be water-soluble and are also non-toxic, which allows for aqueous extracts of brown marine algae to be used in various biological applications (Ajdari *et al.*, 2016). In an article published by Daun *et al.,* (2015), the authors reported that polysaccharides are able to behave as both a capping and a reducing agent. The process of capping and reducing to form nanoparticles is done simultaneously (since the algae contain the requisite organic compounds) therefore decreasing the number of synthetic steps and also the overall costs involved with the typical synthesis of nano particles. In an article on seaweeds, Parker *et al.*, (2015) made use of a brown seaweed *Laminaria digitata* (brown algae) to form palladium nanoparticles, by the direct impregnation of the marine algae with a palladium metal salt. The metal salt is toxic, and the plant will reduce the salt to the zero valent metal state. This therefore remove the use of toxic chemicals in the synthesis of metallic nanoparticles, barring the use of the metal salt.

1.4. Carbon-Carbon Coupling Reactions (Suzuki, Heck, Sonogashira)

Some of the most relevant carbon-carbon coupling reactions in organic synthetic reactions include the Suzuki, Heck and Sonogashira reactions. The Suzuki-Miyaura carbon-carbon coupling reaction is reported to be mostly used in the synthesis of biaryl compounds and has been extensively used in natural product synthesis (Callam, C. S.; Loward, 2001) to form carbon-carbon bonds between two sp^2-sp^2 hybridized compounds (Zim, Monteiro and Dupont, 2000). What makes the Suzuki-Miyaura reactions so important, is that it's used by pharmaceutical companies to form various high-value compounds. One of these compounds is Losartan (Figure 1.1), which is a hypertension drug (Martin *et al.*, 2015, Larsen *et al.*, 1994). Besides the pharmaceutical industry, the Suzuki-Miyaura coupling reaction is also important in the synthetic chemical industry, where it is used to produce the fungicide, Boscalid for the agricultural industry (Glasnov and Kappe, 2010).
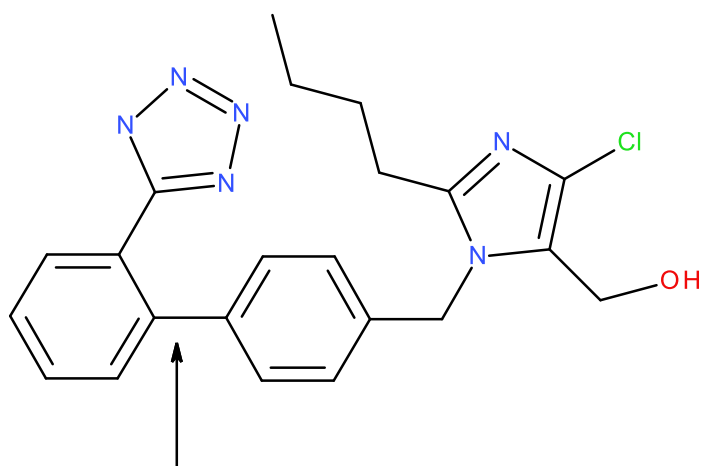
Suzuki-Miyaura Coupling Reaction

Figure 1.1: The structure of Losartan (Larsen et al., 1994).

Another important carbon-carbon coupling reaction is the Sonogashira reaction. These reactions allow for the coupling of aryl halides and terminal alkynes (Chinchilla and Nájera, 2007). This coupling reaction is used in the synthesis of some natural products, whereby it is used as a skeleton framework for the formation of other compounds (Thorand and Krause, 1998). In an article which was published by Wagner and Comins (2006), the Sonogashira coupling reaction was used to synthesize Altinicline (SIB-1508Y, Figure 1.2), which is an anti-Parkinson's agent.
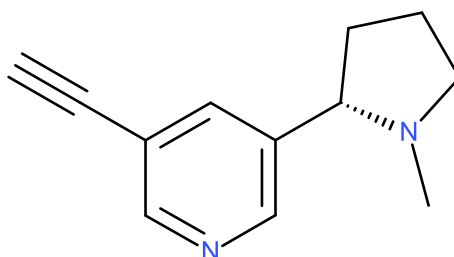
Figure 1.2:The structure of altinicline (Wagner and Comins, 2006).

The Heck carbon-carbon coupling reaction is a reaction which is mostly used in industry, where olefins are used to make high-value products (Reetz and de Vries, 2004). The Heck reaction is not only limited to the industry, but it is also important from an academic point of view, due to the ease with which the Heck reaction can be applied (Beletskaya and Cheprakov, 2000; Reetz and de Vries, 2004). Ding *et al.*, (2013) made use of the Heck reaction in synthesising sesquiterpene

compounds with lactone derivatives as part of their investigation in testing these compounds against various leukaemia cell lines.

These three carbon-carbon coupling reactions are thus very important in the synthesis of various coupling products and intermediates, varying from natural products to polymer formation (Gonzµlez-arellano *et al.*, 2007). Chemical industries make use of these coupling reactions to form pharmaceutical compounds as well as agrochemical compounds such as fungicides (Balsane, Shendage and Nagarkar, 2015). These three coupling reactions are catalytic reactions and according to literature, palladium complexes are mostly used. However, palladium nanoparticles have recently received favourable attention in catalysis, due to their ease of preparation (Balsane, Shendage and Nagarkar, 2015).

1.5. Aims, Objectives, and Hypothesis of the Study

The aim of this study is to synthesize palladium nanoparticle catalysts from an extract of the brown marine algae *Ecklonia radiata.* The secondary aim of this study is to test the palladium nanoparticle's catalytic activity in various carbon-carbon coupling reactions and compare it against a model palladium nanoparticle.

The objectives of this study are as follows:

1. To prepare both aqueous- and organic extracts from the brown seaweed *Ecklonia radiata.*
2. To make use of various characterization techniques on both extracts from the seaweed.
3. The use of the aqueous and organic extracts to synthesize the palladium nanoparticle catalysts.
4. Perform characterization on both these palladium nanoparticle catalysts.
5. To use the palladium nanoparticle catalysts prepared using the organic and aqueous extracts in a "screening" carbon-carbon Suzuki coupling reaction.
6. Choose the most appropriate palladium nanoparticle catalyst which complies with the "Green Chemistry Principles" and compare it against a palladium nanoparticle catalyst from literature.
7. Characterize the palladium nanoparticle catalyst as prepared according to the literature as a model Palladium nanoparticle.

8. And finally, to use these palladium nanoparticles catalysts in various carbon-carbon coupling reactions, and to determine their catalytic efficiency and selectivity in coupling reactions.

1.6. Hypothesis

The palladium nanoparticle catalyst produced from the extracts of the brown seaweed *Ecklonia radiata* can efficiently catalyse the various carbon-carbon coupling reactions. The palladium nanoparticles are also likely to out-perform the palladium nanoparticle catalyst synthesized according to the literature.

1.7. Research Questions

1) Do the extracts from the brown seaweed allow for the formation of palladium nanoparticles?
2) Which of the extracts produces the best palladium nanoparticles for the purpose of the study?
3) What are the characteristics of the palladium nanoparticles?
4) Are the palladium nanoparticles synthesised, an effective catalyst?
5) Are the palladium nanoparticles a better catalyst compared to the model palladium nanoparticles synthesized according to the literature?

1.8. Thesis Outline

The thesis is divided into 5 chapters and is briefly described.

Chapter 1 provides a general introduction of the project including the aims, objectives, hypothesis and research questions.

Chapter 2 gives an overview of the literature review with respect to the biosynthesis of metallic nanoparticles from marine algae, characterization of metallic nanoparticles and the carbon-carbon coupling reactions.

Chapter 3 includes the preparation of the extracts, characterization of the extracts, synthesis of the palladium nanoparticles as well as the results obtained

from the characterization of the nanoparticles. This chapter also contains the methods and materials used, as well as the discussion on the results obtained.

Chapter 4 presents information with regards to the various carbon-carbon coupling reactions as well as the results obtained. The chapter ends with a discussion of the results obtained.

Chapter 5 presents the conclusions and future perspectives of this study.

1.9.   Bibliography

Ajdari, Z., Rahman, H., Shameli, K., Abdullah, R., Ghani, M., Yeap, S., Abbasiliasi, S., Ajdari, D. and Ariff, A. (2016) 'Novel gold nanoparticles reduced by *Sargassum glaucescens*: Preparation, characterization and anticancer activity', *Molecules*, 21(3), pp. 1-17.

Ananthi, S., Raghavendran, H.R., Sunil, A.G., Gayathri, V., Ramakrishnan, G. and Vasanthi H.R. (2010) 'In vitro antioxidant and in vivo anti-inflammatory potential of crude polysaccharide from *Turbinaria ornata* (Marine Brown Alga)', *Food and Chemical Toxicology*, 48(1), pp. 187–192.

Anastas, P. and Eghbali, N. (2010) 'Green Chemistry : Principles and Practice', *Chem. Soc. Rev.*, 39(1), pp. 301–312.

Arsiya, F., Sayadi, M.H. and Sobhani, S. (2017) 'Green synthesis of palladium nanoparticles using *Chlorella vulgaris*', *Materials Letters*, 186, pp. 113–115.

Azizi, S., Namvar, F., Mahdavi, M., Ahmad, M.B. and Mohamad, R. (2013) 'Biosynthesis of silver nanoparticles using brown marine macroalga, *Sargassum muticum* aqueous extract', *Materials*, 6(12), pp. 5942–5950.

Azizi, S., Ahmad, M.B., Namvar, F. and Mohamad, R. (2014) 'Green biosynthesis and characterization of zinc oxide nanoparticles using brown marine macroalga *Sargassum muticum* aqueous extract', *Materials Letters*, 116, pp. 275–277.

Balsane, K. E., Shendage, S. S. and Nagarkar, J. M. (2015) 'Efficient Sonogashira and Suzuki-Miyaura coupling reaction catalyzed by Pd-Nanoparticles', *J. Chem. Sci.*, 127(3), pp. 425–431.

Bankar, A., Joshi, B., Kumar, A.R. and Zinjarde, S. (2010) 'Banana peel extract mediated novel route for the synthesis of palladium nanoparticles', *Materials Letters*, 64(18), pp. 1951–1953.

Beletskaya, I. P. and Cheprakov, A. V. (2000) 'Heck reaction as a sharpening stone of palladium catalysis', *Chemical Reviews*, 100(8), pp. 3009–3066.

Bindhani, B. K. and Panigrahi, A. K. (2014) 'Green synthesis of chitosan based gold nanoparticles using leaf extracts of *Terminalia catappa L*. and study of their effects on cancerous cells', *World. Appl. Sci. J.*, 32(6), pp. 1153–1158.

Bonet, F., Delmas, V., Grugeon, S., Urbina, R.H., Silvert, P-Y. and Tekaia-Elhsissen, K. (1999) 'Synthesis of monodisperse Au, Pt, Pd, Ru and Ir nanoparticles in ethylene glycol', *NanoStructured Materials*, 11(8), pp. 1277–1284.

Callam, C. S.; Loward, T. L. (2001) 'Suzuki Cross-Coupling Reaction: Synthesis of Unsymmetrical Biaryls in Organic Laboratory', *J. Chem. Edu.,* 78(7), pp. 947–8.

Chen, Q., Wang, C., Cheng, L., He, W., Cheng, Z. and Liu, Z. (2014) 'Biomaterials Protein modified upconversion nanoparticles for imaging-guided combined photothermal and photodynamic therapy', *Biomaterials*, 35(9), pp. 2915–2923.

Chinchilla, R. and Nájera, C. (2007) 'The Sonogashira Reaction:ʼ A Booming Methodology in Synthetic Organic Chemistry', *Chemical Reviews*, 107(3), pp. 874–922.

Daun H, W. D. and L. Y. (2015) 'Green Chemistry for Nanoparticle Synthesis', *Chem.Soc.Rev.*, 44, pp. 5778–5792.

Ding, Y. H., Fan, H., Long, J., Zhang, Q. and Chen, Y. (2013) 'The application of Heck reaction in the synthesis of guaianolide sesquiterpene lactones derivatives selectively inhibiting resistant acute leukemic cells', *Bioorg. Med. Chem. Lett.*, 23(22), pp. 6087–6092.

Gholinejad, M., Najera, C., Hamed, F., Seyedhamzeh, M., Bahrami, M. and Kompany-Zareh, M. (2017) 'Green synthesis of carbon quantum dots from vanillin for modification of magnetite nanoparticles and formation of palladium nanoparticles : Efficient catalyst for Suzuki reaction', *Tetrahedron*, 73(38), pp. 5585–5592.

Glasnov, T. N. and Kappe, C. O. (2010) 'Toward a Continuous-Flow Synthesis of Boscalid', *Adv. Synth. Catal*., 352, pp. 3089–3097.

Gonzμlez-arellano, C., Abad, A., Corma, A., Garcia, H., Iglesias, M. and Sanchez, F. (2007) 'Catalysis by Gold (I) and Gold (III): A Parallelism between Homo- and Heterogeneous Catalysts for Copper-Free Sonogashira Cross-Coupling Reactions '. *Angew. Chem. Int. Ed,* 46, pp. 1536–1538.

Huo, Q. and Worden, J. G. (2007) 'Monofunctional gold nanoparticles : synthesis and applications', *J. Nanopart. Res.*, 9, pp. 1013–1025.

Joshi, M., Bhattacharyya, A. and Ali, S. W. (2008) 'Characterization techniques for nanotechnology applications in textiles', *Indian. J. Fibre. Text. Res.*, 33(3), pp. 304–317.

Kora, A. J. and Rastogi, L. (2015) 'Green synthesis of palladium nanoparticles using gum ghatti (*Anogeissus latifolia*) and its application as an antioxidant and catalyst', *Arabian Journal of Chemistry*, 11, pp. 1–9.

Kuppusamy, P., Ichwan, S. J. A., Parine, N. R., Yusoff, M. M.*,* Maniam, G. P. and Govindan, N. (2015) 'Intracellular biosynthesis of Au and Ag nanoparticles using ethanolic extract of *Brassica oleracea L* . and studies on their physicochemical and biological properties', *JES*, 29, pp. 151–157.

Kyriakou, G., Beaumont, S. K., Humphrey, S. M., Antonetti, C. and Lambert, R. M. (2010) 'Sonogashira coupling catalyzed by gold nanoparticles: Does homogeneous or heterogeneous catalysis dominate?', *ChemCatChem*, 2(11), pp. 1444–1449.

Larsen, R. D., King, A. O., Chen, C. Y., Corley, E. G., Foster, B. S., Roberts, F. E., Yang, C.,

Lieberman, D. R., Reamer, R. A., Tschaen, D. M., Verhoeven, T. R. and Reider, P. J. (1994) 'ChemInform Abstract: Efficient Synthesis of Losartan, a Nonpeptide Angiotensin II Receptor Antagonist.', *J. Org. Chem*, 59, pp. 6391-6394.

Li, C. and Trost, B. M. (2008) 'Green chemistry for chemical synthesis', *PNAS,* 105(36), pp. 13197–13202.

Mallikarjuna, K., Bathula, C., Buruga, K., Shrestha, N. K., Noh, Y. Y. and Kim, H. (2017) 'Green synthesis of palladium nanoparticles using fenugreek tea and their catalytic applications in organic reactions', *Materials Letters*, 205, pp. 138–141.

Mandali, P. K. and Chand, D. K. (2013) 'Palladium nanoparticles catalyzed Suzuki cross-coupling reactions in ambient conditions', *CATCOM*, 31, pp. 16–20.

Martin, A. D., Siamaki, A. R., Belecki, K. and Gupton, B. F. (2015) 'A convergent approach to the total synthesis of telmisartan via a Suzuki cross-coupling reaction between two functionalized benzimidazoles', *J. Org. Chem.*, 80(3), pp. 1915–1919.

Mmola, M., Le Roes-Hill, M., Durrell, K., Bolton, J. J., Sibuyi, N., Meyer, M. E., Beukes, D. R. and Antunes, E. (2016) 'Enhanced antimicrobial and anticancer activity of silver and gold nanoparticles synthesised using Sargassum incisifolium aqueous extracts', *Molecules*, 21(1633), pp. 1-22.

Momeni, S. and Nabipour, I. (2015) 'A Simple Green Synthesis of Palladium Nanoparticles with Sargassum Alga and Their Electrocatalytic Activities Towards Hydrogen Peroxide', *Appl. Biochem. Biotechnol.*, 176(7), pp. 1937–1949.

Moreno-Mañas, M., Pleixats, R. and Villarroya, S. (2001) 'Fluorous phase soluble palladium nanoparticles as recoverable catalysts for Suzuki cross-coupling and heck reactions', *Organometallics*, 20(22), pp. 4524–4528.

Nakai, M., Kageyama, N., Nakahara, K. and Miki, W. (2006) 'Phlorotannins as radical scavengers from the extract of Sargassum ringgoldianum', *Marine Biotechnology*, 8(4), pp. 409–414.

Parker, H. L., Rylott, E. L., Hunt, A. J., Dodson, J. R., Taylor, A. F., Bruce, N. C. and Clark, J. H. (2014) 'Supported palladium nanoparticles synthesized by living plants as a catalyst for Suzuki-Miyaura reactions', *PLoS ONE*, 9(1), pp. 1–6.

Parker, H. L., Dodson, J. R., Budarin, V. L., Clark, J. and Hunt, A. J. (2015) 'Direct synthesis of Pd nanoparticles on alginic acid and seaweed supports', *Green Chem.*, 17(4), pp. 2200–2207.

Reetz, M. T. and de Vries, J. G. (2004) 'Ligand-free Heck reactions using low Pd-loading.', *Chem. Commun.*, 1, pp. 1559–1563.

Sawoo, S., Srimani, D., Dutta, P., Lahiri, R. and Sarkar, A. (2009) 'Size controlled synthesis of Pd nanoparticles in water and their catalytic application in C-C coupling reactions', *Tetrahedron*, 65(22), pp. 4367–4374.

Sheldon, R. A. (2016) 'Green chemistry, catalysis and valorization of waste biomass', *J. Mol. Catal. A: Chem.*, 422, pp. 3–12.

Stalin Dhas, T., Kumar, V. G., Abraham, L. S., Karthick, V. and Govindaraju, K. (2012) '*Sargassum myriocystum* mediated biosynthesis of gold nanoparticles', *Spectrochim.*

Acta-Part A: Mol. Biomol. Spec., 99, pp. 97–101.

Thareja, R. K. and Shukla, S. (2007) 'Synthesis and characterization of zinc oxide nanoparticles by laser ablation of zinc in liquid', *Applied Surface Science,* 253, pp. 8889–8895.

Thiruvengadathan, R., Korampally, V., Ghosh, A., Chanda, N., Gangopadhyay, K. and Gangopadhyay, S. (2013) 'Nanomaterial processing using self-assembly- bottom-up chemical and biological approaches', *Rep. Prog. Phys.,* 76(6), pp. 1-90.

Thorand, S. and Krause, N. (1998) 'Improved procedures for the palladium-catalyzed coupling of terminal alkynes with aryl bromides (Sonogashira coupling)', *J. Org. Chem.*, 63(23), pp. 8551–8553.

Turunc, E., Binzet, R., Gumus, I., Binzet, G. and Arslan, H. (2017) 'Green synthesis of silver and palladium nanoparticles using *Lithodora hispidula* (Sm.) Griseb. (*Boraginaceae*) and application to the electrocatalytic reduction of hydrogen peroxide', *Materials Chemistry and Physics*, 202, pp. 310–319.

Unterlass, M. M. (2016) 'Green Synthesis of Inorganic-Organic Hybrid Materials: State of the Art and Future Perspectives', *Eur. J. Inorg. Chem.*, 2016(8), pp. 1135–1156.

Wagner, F. F. and Comins, D. L. (2006) 'Expedient five-step synthesis of SIB-1508Y from natural nicotine', *J. Org. Chem.*, 71(22), pp. 8673–8675.

Yadav, T. P., Yadav, R. M. and Singh, D. P. (2012) 'Mechanical Milling : a Top Down Approach for the Synthesis of Nanomaterials and Nanocomposites', *Nanoscience and Nanotechnology,* 2(3), pp. 22–48.

Yu, Q., Matheickal, J. T., Yin, P. and Kaewsarn, P. (1999) 'Heavy metal uptake capacities of common marine macro algal biomass', *Water Research*, 33(6), pp. 1534–1537.

Zhang, B., Misak, H., Dhanasekaran, P. S., Kalla, D. and Asmatulu, R. (2011) 'Environmental Impacts of Nanotechnology and Its Products', *Proceedings of the 2011 Midwest Section Conference of the American Society for Engineering Education*, pp. 1–9.

Zim, D., Monteiro, A. L. and Dupont, J. (2000) 'PdCl2(SEt2)2 and Pd(OAc)2: simple and efficient catalyst precursors for the Suzuki cross-coupling reaction', *Tetrahedron Letters*, 41(43), pp. 8199–8202.

Chapter 2: Literature Review

2.1. Nanoscience and Nanotechnology

Nanoscience and nanotechnology is a relatively new field of science, where the properties of nanoscale materials are studied and observed to be very different from their bulk counterpart (Huo and Worden, 2007). At the Nanoscale (1 – 100 nm), the physical and chemical properties and characteristics of materials change, due to the quantum confinement effect (Zhang *et al.*, 2011; Mmola *et al.*, 2016). The quantum confinement effect is the phenomenon that results from the fact that as nanomaterials get smaller in size, there is an increase in the size of the electron bandgap (Manzoor, et al., 2009). Manzoor, *et al.,* (2009) stated that semiconductors such as ZnO on the nanoscale contain a wide bandgap, which therefore makes it available for various applications such as solar cells. A wide bandgap also causes the materials' optical properties to change. ZnOs' wide bandgap causes it to be transparent in the visible region, with absorption in the UV (Ultra Violet) range (Kripal, et al., 2011).

Nanomaterials have at least one of its dimensions confined to the nanometer region (Zhang *et al.*, 2011). These materials are small in size, allowing for a large surface to volume ratio, making them ideal for various applications such as electronics, optics, medicine, as sensors, and especially catalysts (Bonet *et al.*, 1999; Momeni and Nabipour, 2015). As the size of the material is getting smaller, the more the ratio between the surface area to volume increases, therefore making more of the nanomaterial surface available for sensing and catalytic activity (Figure 2.1).

sides = 3
surface = 3^2 x 6 = 54
volume = 3^3 = 27

surface/volume = 2

sides = 2
surface = 2^2 x 6 = 24
volume = 2^3 = 3

surface/volume = 3

sides = 1
surface = 1^2 x 6 = 6
volume = 1^3 = 1
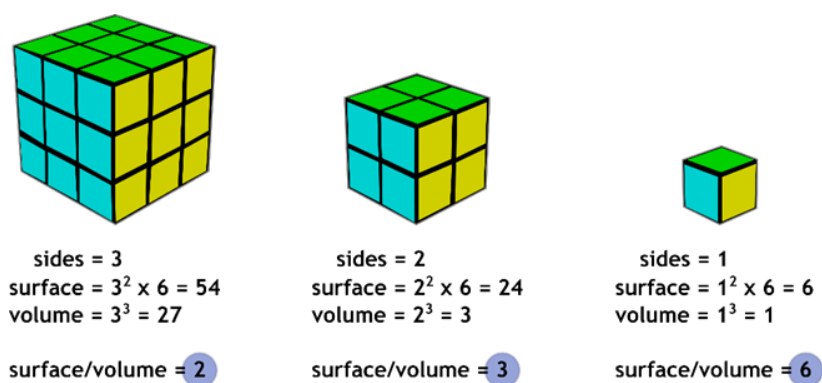
surface/volume = 6

Figure 2.1: The surface area to volume ratio explanation (Hamers, 2014).

The synthesis or the development of these nanomaterials can be accomplished using one of two approaches, namely, a top-down or bottom-up approach. The top-down approach is mainly used to produce nanocomposites, where metals are

mechanically milled down to form small metallic particles in powder form (Yadav, Yadav and Singh, 2012). On the other hand, the bottom-up approach, also known as atom-atom self-assembly, is widely regarded to be the most cost-effective method (Thiruvengadathan *et al.*, 2013). Figure 2.2 illustrates the Top-down and Bottom-up approaches graphically, which presents an understanding of how nanomaterials could be produced (Rajan, et al., 2016).
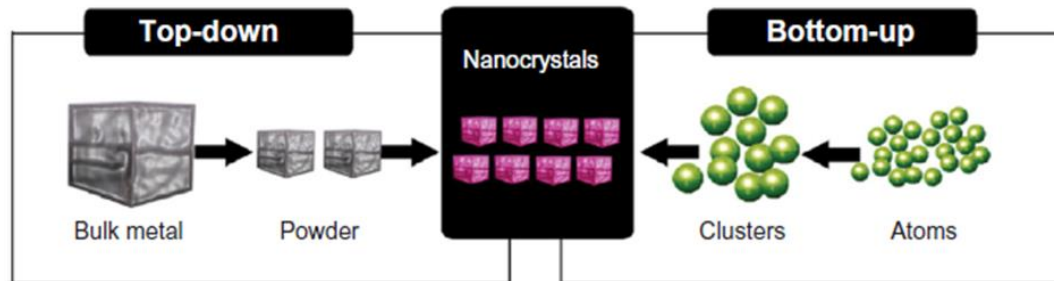
Figure 2.2: The differences between the Top-down and Bottom-up approaches that are followed for the development of nanomaterials (Rajan, et al., 2016).

Of all the nanomaterials produced, metallic nanoparticles are generally regarded to be the most promising nanomaterial, since it has a broader variety of applications it can be used, due to its shape and size. Because metallic nanoparticles can be easily synthesised from biological materials, it can be applied in biomedical fields and also have environmental friendly benefits (Azizi *et al.*, 2014). The nanomaterials produced must undergo vigorous characterisation, so that their size, morphology, dimensions, and optical properties and therefore their application can be better understood (Joshi, Bhattacharyya and Ali, 2008).

2.2. Characterization Techniques

2.2.1. High-Resolution Transmission Electron Microscopy (HR-TEM)
HR-TEM is an electron microscope that is used to image a sample at an atomic scale (Joshi, *et al*., 2008). The working principle behind HR-TEM is that an electron gun is used to generate a beam of electrons which interacts with the sample as it passes through it (Joshi, *et al*., 2008). Figure 2.3 is a graphical description of the component setup of an HR-TEM system. An image of the sample is formed when the electrons that are transmitted through the sample are detected by a sensor, allowing the user to examine the sample in detail (Joshi, *et al*., 2008). The images obtained from the HR-TEM allows for the determination of morphology, crystallography, size of the nanomaterials, and also the particle size distribution (Azizi *et al.*, 2013).
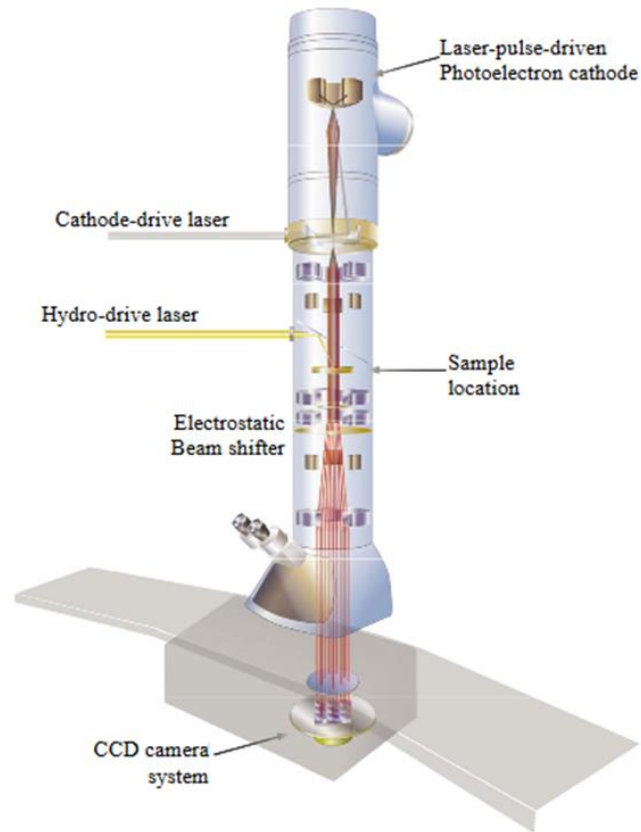
Figure 2.3: The HR-TEM component setup as illustrated by (Aseyev, et al., 2013).

Figure 2.4 presents a TEM image of silver nanoparticles as synthesised by Azizi *et al.,* (2013), while Bonet *et al.,* (1999) showed monodisperse gold nanoparticles as seen in Figure 2.5. The gold nanoparticles in Figure 2.5, are shown to be monodisperse, with the same size and shape, appearing to be decahedral in shape whereby ethylene glycol was used as a reducing agent and polyvinylpyrrolidone (PVP) capping agent.
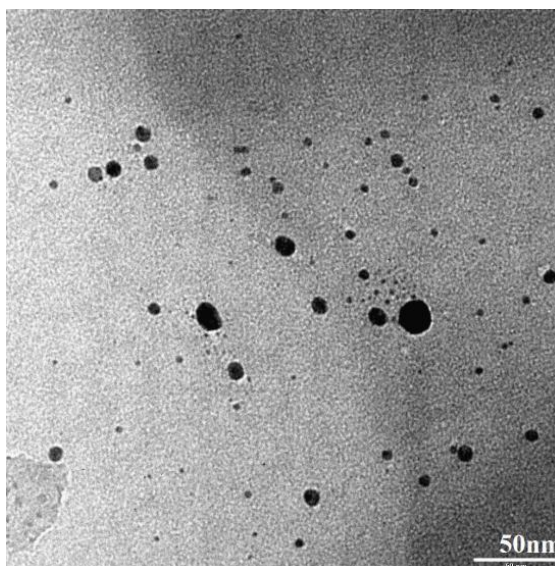
Figure 2.4: TEM image of silver nanoparticles synthesized from marine algae (Azizi et al., 2013).
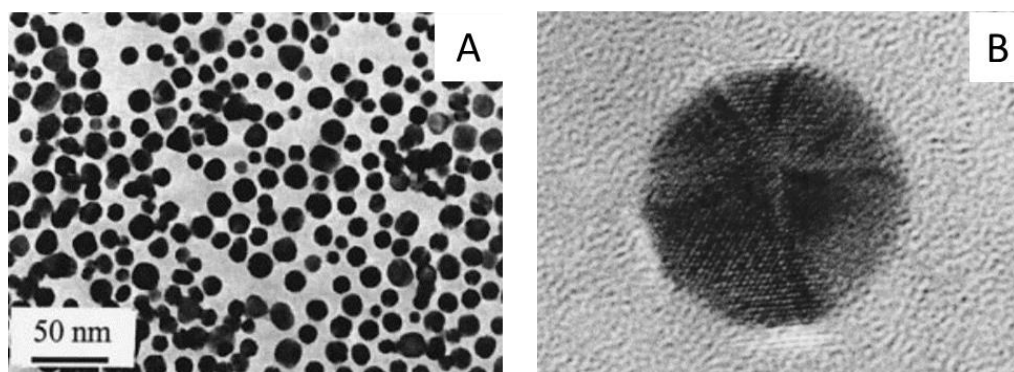
Figure 2.5: TEM image of gold nanoparticles and the HR-TEM image of a single decahedral gold nanoparticle which is 116 Å in size (Bonet et al., 1999).

2.2.2. Energy Dispersive X-ray (EDX) Analysis

Energy dispersive X-ray analysis is an analytical technique that is used to determine the elements that are present within the sample *(Joshi, et al.*, 2008). This technique is used together with HR-TEM, but can also be coupled with a Scanning Electron Microscope (SEM). The working principle of this characterization technique is, as the electrons pass through the sample from the electron beam, X-rays are being emitted from the surface of the sample which is related to the specific energies of the various elements (Joshi, *et al.*, 2008). Figure 2.6 shows data obtained from EDX, revealing the presence of palladium for palladium nanoparticles, however, the authors do not explain the presence of platinum (Pt) and sodium (Na) in the EDX data obtained (Turunc *et al.*, 2017).
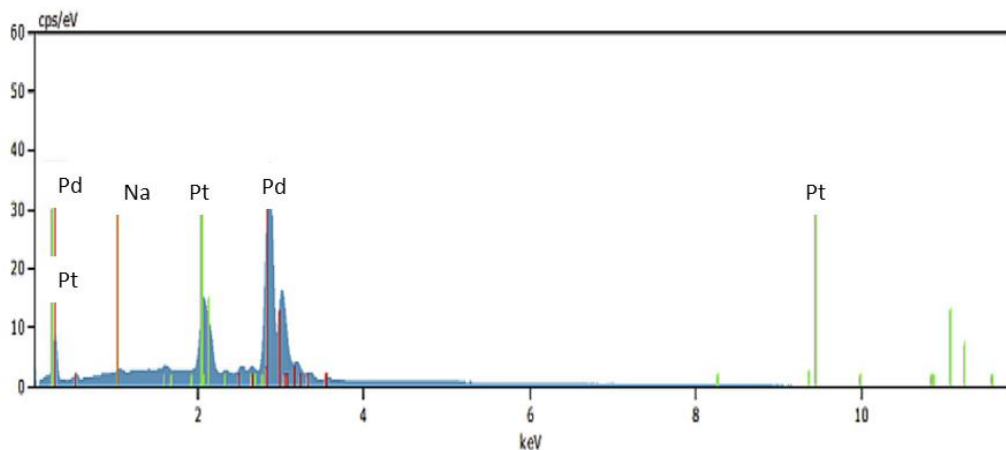
Figure 2.6: EDX data obtained for palladium nanoparticles, illustrating the elemental composition of the palladium nanoparticles (Turunc et al., 2017).

2.2.3. Ultraviolet-Visible (UV-Vis) Spectroscopy

UV-Visible spectroscopy is an absorbance characterisation technique that can be used to quickly determine the concentration, bioconjugation, shape, and size of the nanoparticles, particularly for gold and silver nanoparticles (Joshi,*et al.*, 2008). The basic principle behind the technique involves ultraviolet/visible light passing through the sample at various wavelengths in a step-wise manner, with the detector recording the absorbance (Joshi, *et al.*, 2008). Figure 2.7 shows a typical UV-Visible spectrum obtained for silver nanoparticles (Turunc *et al.*, 2017).
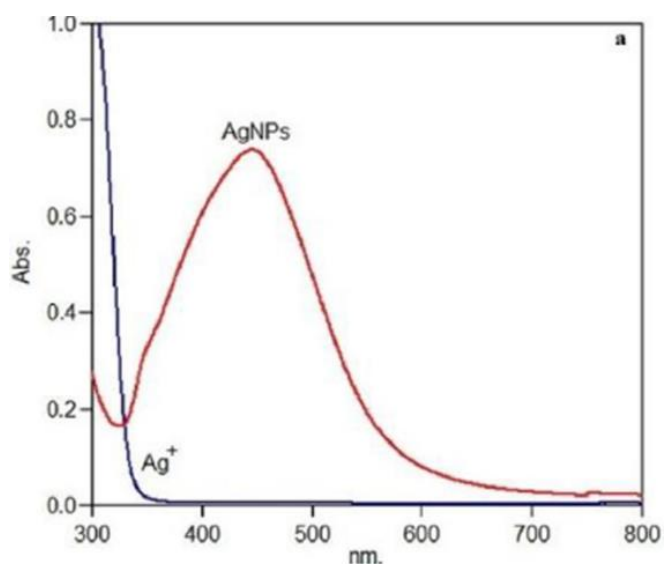
Figure 2.7: An UV-Visible spectrum of silver nanoparticles (AgNPs) as reported by Turunc, et al., (2017).

It is clear in Figure 2.7 that the surface plasmon resonance (SPR) peak for silver nanoparticles falls within the range 420-500 nm (Joshi, *et al.*, 2008) as expected. When light passes through a sample, the free electrons present on the surface of the sample start to oscillate at the same frequency as the light wave (Eustis & El-

Sayed, 2006). This is known as SPR absorption. Eustis & El-Sayed, (2006) also state that the SPR value is dependent on the shape and sizes of the sample. Gold nanoparticles, on the other hand, have a typical SPR value between 500-550 nm, while a gold nanorod typically reveals an SPR band at 650-1100 nm depending on the diameter of the nanorods (Eustis & El-Sayed, 2006).
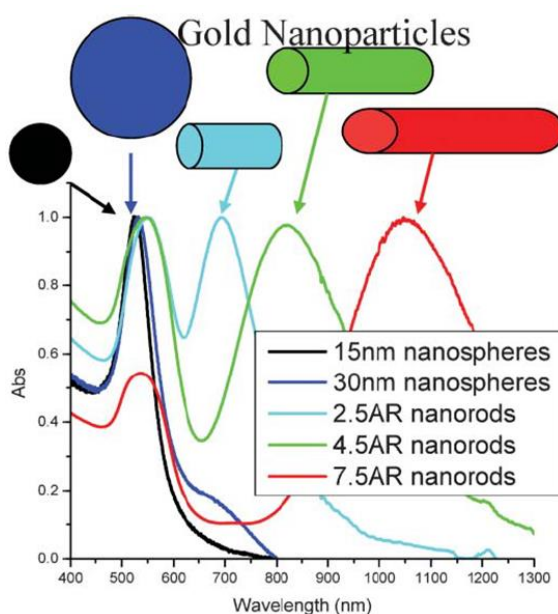
Figure 2.8: The UV-Visible spectrum of various gold nanomaterials (Eustis & El-Sayed, 2006).

2.2.4. Fourier Transform Infra-Red (FTIR) Spectroscopy

FTIR spectroscopy is an important characterisation technique as it allows the identification of any possible organic molecules and that may be present as a reducing agent and also in the capping of the surface of the nanoparticles, once the NPs have formed (Azizi *et al.*, 2014). Figure 2.9 shows the surface of the AgNPs which were capped with biomolecules from an extract (Azizi *et al.*, 2013). Azizi *et al.*, (2014) mentioned the sulphate and hydroxyl functional groups that are present in the aqueous extract causes the reduction of the silver metal salt to form AgNPs. Azizi *et al.*, (2014) states that the hydroxyl peak found in Figure 2.9 (a) at 3217 cm^{-1} is part of the compound that is responsible for the reduction to form AgNPs, this peak is absent (Figure 2.9 (b)) after the AgNPs were formed. Azizi *et al.*, (2014) further mentioned that sulphated polysaccharides are responsible for the reduction and capping of the AgNPs.
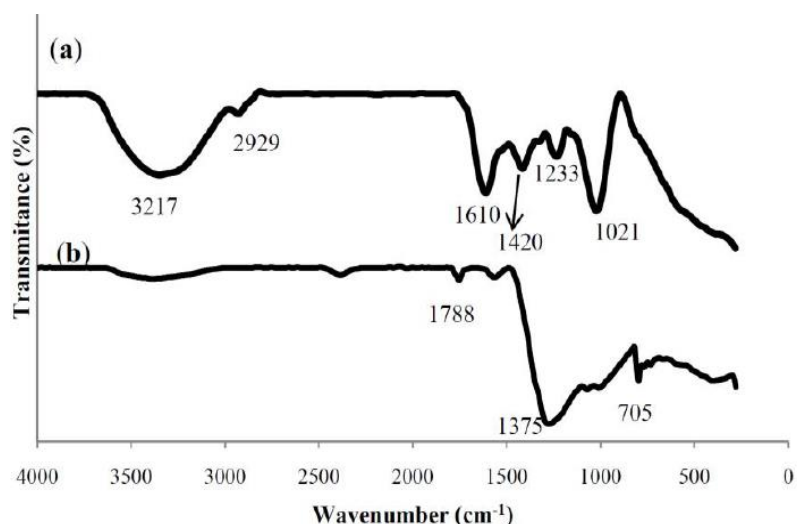
Figure 2.9: FTIR spectra of (a) aqueous extract of S. muticum, (b) AgNPs formed from S. muticum as reported by Azizi et al.(2013). The disappearance of the peaks 1233 cm⁻¹ and 1021 cm⁻¹in Figure 2.9 (a) after the synthesis of the AgNPs Figure 2.9 (b) is the sulphated groups that are responsible for the reduction of AgNPs.

2.2.5. X-Ray Diffraction (XRD)

X-ray powder diffraction is one of the most useful techniques used to determine the crystal structure of nanomaterials, crystalline size and shape, as well as lattice planes. It also enables a comparison of the diffraction peaks to those of standards according to the Joint Committee on Powder Diffraction Standards (JCPDS) data (Kora and Rastogi, 2015). The angle (θ) at which the sample diffracts the X-rays produces reflections and these provide important information about the crystal structure of the sample. In an article on nanomaterials, Giannini *et al.*, (2016) mentioned that the broader reflections are, the smaller the crystal lattice of the nanomaterial. Giannini *et al.*, (2016) further mentioned that the reflections represent the Miller indices (*h,k,l*) for each plane of the crystal lattice and can be used to calculate the size of the nanomaterials. Kora and Rastogi (2015) made use of the Debye-Scherrer equation (equation 2.1) in order to calculate the particle sizes, by using the Miller indices such as (111) which represents the main reflections for the crystal unit cell for the plane (Giannini, *et al.*, 2016). Figure 2.10 shows an XRD powder diffraction pattern which was obtained for PdNPs as reported by Turunc *et al.* (2017).

$$d = \frac{k\lambda}{\beta cos\theta} \qquad (2.1)$$

Is the Debye – Scherrer equation where:

d is the size of the crystal (nm)

k is the Scherrer constant (0.9)

λ is the wavelength of the X-ray source (nm)

β is the half-height width of the XRD peak from the diffractogram

θ is the Braggs diffraction angle of the XRD peak from the diffractogram
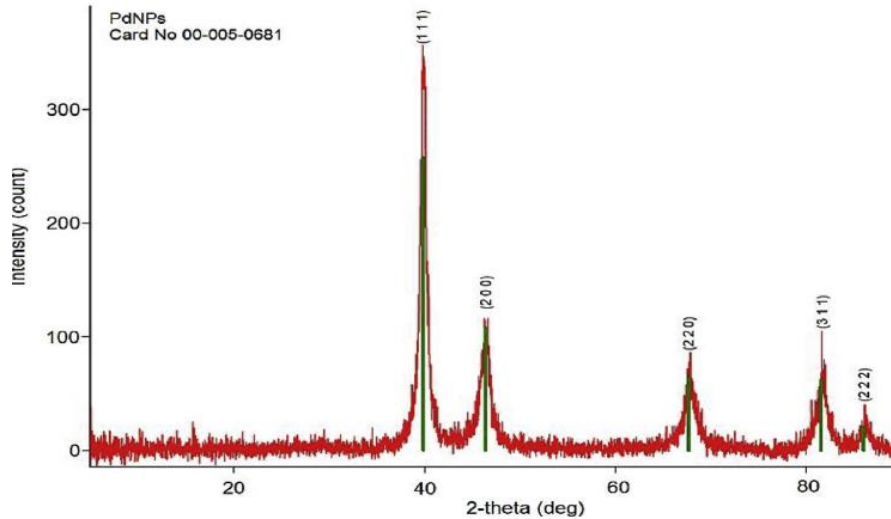
Figure 2.10: XRD pattern obtained for PdNPs as reported by (Turunc et al., 2017).

2.2.6. Thermogravimetric analysis (TGA)

Thermogravimetric analysis (TGA) is an analytical technique that is used to characterise any changes to the thermal behaviour and gather information about the purity of the sample (Mansfield, *et al.*, 2014). Mansfield *et al.*, (2014) mentioned that TGA can be used to determine the coating of the nanoparticles, however, samples need to be dry. The samples are heated at a constant rate to high temperatures such as 800 °C, under a nitrogen atmosphere, while the decomposition of the sample is monitored (Shekhar, *et al.*, 2012). Figure 2.11 shows a TGA thermogram for the PdNPs hybrid composites synthesised by Jiang & Gao, (2006) to test the different generations of dendrimers that capped the surface of the hybrid composites.
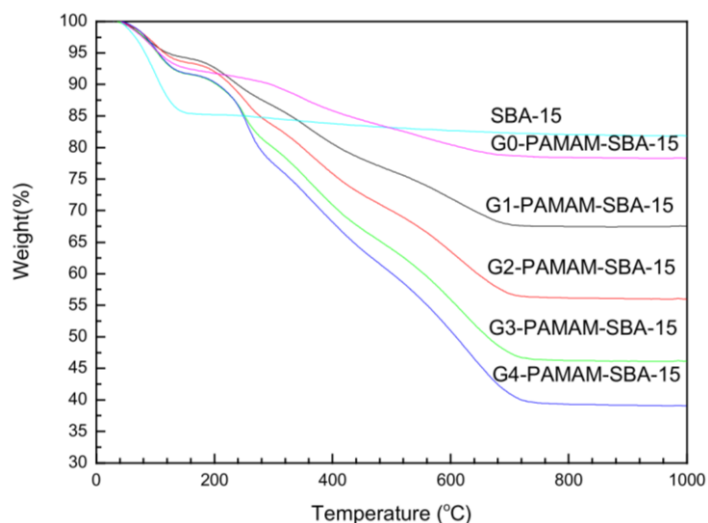
Figure 2.11:TGA profile for the various dendrimer generations that are linked with SBA-15, which also indicates the stability of the different dendrimers (Jiang & Gao, 2006).

2.2.7. Nuclear magnetic resonance (NMR)

Nuclear magnetic resonance is a quantitative analytical technique that is used to analyse various known and unknown compounds. Briefly, the sample is placed in a strong external magnetic field, where the nuclei present in the sample will react at a frequency that is characteristic to the nuclei present in the sample. In this way it can be used to determine the structure of molecules (Hatzakis, 2019). With a variety of 1D and 2D experiments available information can be obtained about the compounds. It is these experiments that assists researchers to try and get structural information on compounds such as polysaccharides (Ye, *et al.*, 2010).

2.2.8. Gas chromatography–mass spectrometry (GC-MS)

Gas chromatography-mass spectrometry is an analytical technique that is used to analyse various compounds. Hussain & Maqbool (2014) reported that GC-MS can separate volatile and semi-volatile compounds from each other according to retention time, however, it needs to be coupled with an MS system in order to identify the compounds that have been separated. In an article on the biosynthesis of gold nanoparticles, Dhas *et al.*, (2012), made use of GC-MS to determine the capping agent present on the surface of the gold nanoparticles. GC-MS was also used for the identification of pharmaceutical compounds that were synthesised using the Suzuki-Miyaura carbon-carbon coupling reaction (Bright, *et al.*, 2013). Besides GC-MS being used as a tool to identify compounds, it was also used in a study to show how 1-nitro-4-phenyl benzene causes cancer in rats (Ning & Xiaobai, 1997).

2.2.9. Inductively coupled plasma atomic emission spectroscopy (ICP-AES)

ICP-AES in an analytical technique which can measure most of the elements on the periodic table, with the exception being C, H, O, N, the halides and inert gasses. The instrument can detect concentrations of analytes within the hundreds of mg/L to ng/L range and it is a technique that was used by Fan *et al.*, (2017) to determine the loading of Pd in their PdNPs. Fan *et al.*, (2017) also made use of ICP-AES to determine whether the PdNPs underwent leaching after being used in the Suzuki-Miyaura reactions. Schimpf *et al.*, (2002) employed ICP-AES analysis to identify the amount of gold that was present on their catalyst.

2.2.10. Dynamic Light Scattering (DLS) and Zeta Potential

Pecora, R (2000) has reported that dynamic light scattering (DLS) is an experimental technique that is used to characterise the nanoparticles in solution. The DLS technique measures the size of the NPs, the size distribution and the polydispersity of the NPs. Pecora, R (2000) reported that the drying of a sample, may causes changes to the nature of the NPs, when it gets measured. Jans *et al.*, (2009) reported that DLS is a technique which can be used to study the bioconjugation of NPs. Jans *et al.*, (2009) also reported that DLS are very sensitive, as it can be used to monitor agglomeration of MNPs, and furthermore, DLS can also be used for protein-protein interactions. Gnanasekar *et al.,* (2017) reported in their article that zeta potential could be used to study the stability of the MNPs. The authors further mentioned in their report that zeta potential is used as a measuring tool for the electrostatic potential on the MNPs surface.

2.3. Synthesis of metallic nanoparticles

There are many synthetic methods documented for the synthesis of metallic nanoparticles (MNPs), with both bottom-up and top-down approaches available. In the article published by Thareja and Shukla (2007), the authors utilized the top-down synthetic approach by employing a pulsing laser where the ablation of solid zinc metal in a liquid solution formed zinc oxide nanoparticles. The authors further state that making use of the laser ablation method for a metallic sample in liquid media, allows media such as deionized water, to behave as a capping agent for the zinc oxide nanoparticles. Thareja and Shukla, (2007) reported that a reasonably good particle size distribution could be obtained this way. Bonet *et al.*, (1999), on the other hand, made use of a bottom-up approach, in the synthesis of various MNPs, using polyvinylpyrrolidone (PVP) and ethylene glycol as capping and reducing agents, respectively. The addition of PVP not only capped the surface of the MNPs, but also assisted the ethylene glycol in reducing the metal ions to form

MNPs. This method used by Bonet *et al.*, (1999) to synthesize the MNPs allowed for narrow size distribution. Bindhani and Panigrahi (2014), made use of an ethanolic leaf extract of the plant *Terminalia catappa* to synthesize gold nanoparticles (AuNPs) and by making use of Chitosan. These AuNPs were not only synthesized in an environmentally friendly manner, they were also used in biological studies since the bioavailability of the NPs was enhanced. Kora and Rastogi (2015), made use of a similar approach, however, unlike Bindhani and Panigrahi (2014), gum ghatti from the tree *Anogeissus latifolia* was used as a reducing and capping agent for the synthesis of palladium nanoparticles (PdNPs). Kora and Rastogi (2015), reported on the synthesis of polydisperse, spherically shaped PdNPs which showed excellent catalytic activities in the reduction and degradation of various dyes and nitro compounds. Parker *et al.*, (2014) on the other hand, employed a living plant, *Arabidopsis thaliana*, to synthesize PdNPs. As mentioned previously, Azizi *et al.* (2014, 2013) used an aqueous extract from the brown marine algae, *Sargassum muticum,* to synthesize zinc oxide nanoparticles (ZnO NPs) and AgNPs (Azizi *et al.*, 2013). Azizi *et al.*, (2013, 2014) reported, in both cases, that the aqueous extract, were successful in reducing the metal ions to form nanoparticles, where the secondary metabolites present in the extract were also effective in capping the surface of the nanoparticles.

Parker *et al.* (2015) made use of the brown marine algae *Laminaria digitata* and alginic acid, which is also found in brown marine algae, to successfully synthesize palladium nanoparticles, following which the catalytic activity of the PdNPs was tested. By making use of a biosynthesis protocol, raw materials such as marine algae, Parker *et al.,* (2015) demonstrated that algae can be used to capture toxic heavy metals from wastewater sources and that these metals could also be recovered. Dhas *et al.*, (2012) reported on the use of an aqueous extract of *Sargassum myriocystum* to reduce and cap the surface of gold nanoparticles, with the authors identifying that 1-cyclopentyl-4-(3-cyclopentylpropyl) dodecane to be responsible for capping and stabilising the AuNPs upon analysing the GC-MS data. Similarly, Ajdari *et al.* (2016) fabricated AuNPs by making use of the brown marine algae *Sargassum glaucescens* aqueous extracts. These AuNPs were then tested for anticancer activity against various cancer cell lines, where the AuNPs showed no activity against normal human cells (MCF-10A) and did show anticancer activity against cervical cancer (HeLa) cell line.

2.4. Capping- and Reducing agents

Capping agents are reported to be stabilisers as they are used in the synthesis of metallic nanoparticles to protect the metallic nanoparticles from agglomeration (Cookson, 2012). There are many types of capping agents available, however

organic ligands are the most commonly used, especially if these organic ligands have a heteroatom present too (Cookson, 2012). Cookson, (2012) further reported that capping agents that are extracted from natural materials such as plants, have huge potential as they have low toxicity and are highly soluble in water. Kripal, *et al.*, (2011) made use of the sulphur-based ligand thioglycerol as a capping agent for their ZnO NPs. In another article, PdNPs were capped by an aqueous extract from *Chlorella vulgaris* (Arsiya, et al., 2017).

It is stated in the article that was published by Rajan, *et al.*, (2016), that the reducing agents are responsible for reducing the metal ions to their zerovalent state, as metallic nanomaterials only form at the zerovalent state. Rajan, *et al.*, (2016) explained how silver at its oxidation state (Ag^+) gets reduced to Ag^0 and form nanocrystals. Arsiya, *et al.*, (2017) did also use the aqueous extract from *Chlorella vulgaris* to reduce palladium metal ions from its oxidation state (Pd^{2+}) to its zerovalent state (Pd^0) to form PdNPs. In the case of Arsiya, *et al.*, (2017), the aqueous extract behaves as both the reducing and capping agent, and that is due to the compounds that are present in the aqueous extract. Kanchana, *et al.*, (2010) made use of aqueous extracts from leaves of *Solanum trilobatum* to form their PdNPs. Therefore, promising results were obtained when extracts of renewable biomaterials such as plants, fruits, marine algae were used in the synthesis of metallic nanoparticles, and that is due as seen from Arsiya, *et al.*, (2017) and Kanchana, *et al.*, (2010) that these aqueous extracts behave as both reducing- and capping agent, which means that toxic reducing- and capping agents are no longer needed.

2.5. Applications for metallic nanoparticles (MNPs)

Metallic nanoparticles have such a large and diverse field of applications that it can be used for, that they cannot be restricted to a specific field. Fan, *et al.*, (2017) used palladium nanoparticles (PdNPs) as a catalyst in Suzuki-Miyaura reactions, reporting a five time recyclability, before it starts to lose its activity. Kripal, *et al.*, (2011) studied ZnO NPs' photoconductivity and photoluminescence, making the ZnO NPs a candidate for electronics. In an article published by Li, *et al.*, (2002) on PVP-PdNPs, the authors were able to synthesise nanoparticles with narrow size distribution and use it as a catalyst in the Suzuki-Miyuara reaction as well. It has been reported that a low ratio of metal to capping (Thiebaut, 2004) results in a narrow size distribution of nanoparticles which in turn exhibits better catalytic activity over broad size distributed nanoparticles. This is due to the high surface area to volume ratio that are obtained. Renero-Lecuna *et al.*, (2019) performed a study in how various nanomaterials interact with human cells (HeLa cells) reporting that the morphology of the carbon nanotubes, is the reason why they

are toxic to human cells. However, the authors also stated that these carbon nanotubes and graphene oxide are ideal for adsorption of molecules due to their high surface to volume ratio and they may be employed in other applications such as catalysis, electronics, etc. Khan *et al.*, (2019) states that nanoparticles should be small and have a narrow size distribution for it to be used in biomedical applications.

2.6. Catalysis: carbon-carbon coupling reactions

Parker *et al.* (2014) reported on the excellent catalytic activity of the PdNPs in Suzuki-Miyaura carbon-carbon coupling reactions. The recyclability of the PdNP catalyst was also evaluated. Moreno-Mañas *et al.,* (2001) also made use of PdNPs as catalysts for both the Suzuki and Heck coupling reactions, reporting that it was possible to do five successful catalytic runs under fluorous conditions before needing to replace the catalyst. Mandali and Chand (2013) reported on Suzuki coupling reactions carried out at room temperature and normal atmospheric conditions. Interestingly, Kyriakou *et al.* (2010) demonstrated that AuNPs could also be used as a catalyst in the Sonogashira coupling reactions with the authors comparing the differences between using homogeneous and heterogeneous AuNPs catalytic systems. Kyriakou *et al.,* (2010) found that the Sonogashira coupling reaction favoured heterogeneous AuNPs catalyst, implying that nanoparticles will behave more selectively in coupling reactions as heterogeneous catalysts. Sawoo *et al.* (2009) reported using water as a solvent for the Suzuki, Heck, and Sonogashira coupling reactions together with water-soluble PdNP catalysts. The water solubility was imparted by the polyethyleneglycol (PEG) used as a capping reagent for the PdNPs. Thus, with the use of these PdNPs, the reactants in the coupling reactions are easily able to come into contact with the surface of the PdNPs, which allows for improved catalytic activity.

2.7. What makes a good catalyst?

According to Hemalatha *et al.* (2013), a good catalyst is one which has a large surface area available for catalytic activity and also being selective when forming the product. Hemalatha *et al.* (2013) further reported that nanoparticles have a high potential to be used as a catalyst (nanocatalyst) due to its high surface to volume ratio which allows for more active sites for the catalyst. The authors concluded that the selectivity shown by metallic nanoparticles depends on the

crystallography of the nanoparticles and also the crystal plane that the active sites are present on. Li *et al.* (2002) mentioned that a good catalyst should have a high catalytic activity and that it should also have a high turnover frequency (TOF) and that the catalytic activity depends on the size and shape of the catalyst, where NPs have the highest number of active sites for catalytic reactions.

2.8. Discussion

The literature provides clear evidence that various biomaterials such as plants and marine algae could be used in the synthesis of nanomaterials. Biosynthesis of nanomaterials allows for nanomaterials such as metallic nanoparticles to be used in biological applications, since, according to the literature, metallic nanoparticles have the potential for drug delivery. Biosynthesized nanoparticles result in nanoparticles that are water-soluble, allowing for certain chemical reactions to be carried out in water as a solvent. This, therefore, allows for chemical reactions to be carried out under more environmentally friendly reaction conditions as researchers are slowly moving away from the use of toxic chemicals and harsh reaction conditions. The use of metallic nanoparticles as a catalyst in various reactions has shown promising results that can be ascribed to the unique properties it possesses over the bulky, traditional metallic catalysts. The use of palladium nanoparticles as a catalyst also appears to have superior catalytic activity compared to the more traditional Pd/C catalysts Scheuermann *et al.,* (2009). The main reason why the metallic nanoparticles is superior in catalytic activity over the traditional Pd/C catalysts, is due to their shape, size and also because they have more active sites available (due to their high surface to volume ratios), to catalyse the reaction.

The use of brown marine algae appears to be more efficient in forming metallic nanoparticles compared to other types of marine algae, and this can be ascribed to the fact that brown marine algae contain the highest amount of polysaccharides and polyphenols, which are believed to act as both the capping and reducing agent for nanoparticles being synthesized.

Therefore, by using the easily available brown marine algae *Ecklonia radiata* (kelp) to synthesize water-soluble palladium nanoparticles, a green chemistry approach will be followed, and water can also be used in the synthetic organic reactions. Studying these palladium nanoparticles is important in order to understand whether they are able to effectively allow carbon-carbon coupling reactions, how selective they are in catalysing the various coupling reactions and whether it may be reused.

2.9. Bibliography

Ajdari, Z., Rahman, H., Shameli, K., Abdullah, R., Ghani, M.A., Yeap, S., Abbasiliasi, S., Ajdari, D and Ariff, A. (2016) 'Novel gold nanoparticles reduced by Sargassum glaucescens: Preparation, characterization and anticancer activity', *Molecules*, 21(123), pp. 1-17.

Anderson, R., Stegenga, H. & Bolton, J. (2016) *Seaweeds of the South African South Coast.* [Online]
Available at: https://southafrseaweeds.uct.ac.za
[Accessed 17 October 2019].

Arsiya, F., Sayadi, M. H. & Sobhani, S. (2017) 'Green synthesis of palladium nanoparticles using *Chlorella vulgaris*'. *Materials Letters,* 186, pp. 113-115.

Aseyev, S. A., Weber, P. M. & Ischenko, A. A. (2013) 'Ultrafast Electron Microscopy for Chemistry, Biology and Material Science', *Journal of Analytical Sciences, Methods and Instrumentation,* 3, pp. 30-53.

Azizi, S., Namvar, F., Mahdavi, M., Ahmad, M. B. and Mohamad, R. (2013) 'Biosynthesis of silver nanoparticles using brown marine macroalga, *Sargassum muticum* aqueous extract', *Materials*, 6(12), pp. 5942–5950.

Azizi, Ahmad, M. B*.,* Namvar, F. and Mohamad, R*.* (2014) 'Green biosynthesis and characterization of zinc oxide nanoparticles using brown marine macroalga Sargassum muticum aqueous extract', *Materials Letters*, 116, pp. 275–277.

Bindhani, B. K. and Panigrahi, A. K. (2014) 'Green synthesis of chitosan-based gold nanoparticles using leaf extracts of *Terminalia catappa L*. and study of their effects on cancerous cells', *World Applied Sciences Journal*, 32(6), pp. 1153–1158.

Bonet, F., Delmas, V., Grugeon, S., Urbina, R. H., Silvert, P. Y. and Tekaia-Elhsissen, K. (1999) 'Synthesis of monodisperse Au, Pt, Pd, Ru and Ir nanoparticles in ethylene glycol', *Nanostructured Materials*, 11(8), pp. 1277–1284.

Bright, T. V., Dalton, F., Elder, V. L., Murphy, C.D., O'Connor, N.K. and Sandford, G., (2013). 'A convenient chemical-microbial method for developing fluorinated pharmaceuticals', *Org. Biomol. Chem.,* 11, pp. 1135-1142.

Dhas, T., Kumar, G., Abraham, L.S., Karthick, V. and Govindaraju, K. (2012) '*Sargassum myriocystum* mediated biosynthesis of gold nanoparticles', *Spectrochim. Acta-Part A: Mol. Biomol. Spec.,* 99, pp. 97-101.

Eustis, S. & El-Sayed, M. A. (2006) 'Why gold nanoparticles are more precious than pretty gold: Noble metal surface plasmon resonance and its enhancement of the radiative and nonradiative properties of nanocrystals of different shapes', *Chem.Soc.Rev.*, 35, pp. 209-217.

Fan, H., Qi, Z., Sui, D., Mao, F., Chen, R. and Huang, J. (2017) 'Palladium nanoparticles in cross-linked polyaniline as highly efficient catalysts for Suzuki - Miyaura reactions', *Chinese Journal of Catalysis,* 38(3), pp. 589-596.

Hatzakis, E. (2019) 'Nuclear Magnetic Resonance (NMR) Spectroscopy in Food Science: A Comprehensive Review', *Comprehensive Reviews in Food Science and Food Safety,* 18(1), pp. 189-220.

Huo, Q. and Worden, J. G. (2007) 'Monofunctional gold nanoparticles : synthesis and applications', *J. Nanoparticle. Res.*, 9, pp. 1013–1025.

Giannini, C., Ladisa, M., Altamura, D., Siliqi, D., Sibillano, T. and De Caro, L. (2016) 'X-ray Diffraction: A Powerful Technique for the Multiple-Length-Scale Structural Analysis of Nanomaterials'. *Crystals,* 6(8), pp. 1-22.

Gnanasekar, S., Murugaraj, J., Dhivyabharathi, B., Krishnamoorthy, V., Jha, P. K., Seetharaman, P., Vilwanathan, R. and Sivaperumal, S. (2017) 'Antibacterial and cytotoxicity effects of biogenic palladium nanoparticles synthesized using fruit extract of *Couroupita guianensis Aubl', J. Appl. Biomed.,* 16, pp. 59-65.

Jans, H., Liu, X., Austin, L., Maes, G. and Huo, Q. (2009) 'Dynamic light scattering as a powerful tool for gold nanoparticles bioconjugation and biomolecular binding studies', *Anal. Chem.,* 81, pp. 9425-9432.

Jiang, Y. & Gao, Q. (2006) 'Heterogeneous Hydrogenation Catalyses over Recyclable Pd(0) Nanoparticle Catalysts Stabilized by PAMAM-SBA-15 Organic-Inorganic Hybrid Composites', *J. Am. Chem. Soc.,* 128(3), pp. 716-717.

Joshi, M., Bhattacharyya, A. and Ali, S. W. (2008) 'Characterization techniques for nanotechnology applications in textiles', *Indian. J. Fibre. Text. Res.*, 33(3), pp. 304–317.

Kanchana, A., Devarajan, S. & Ayyappan, S. R. (2010) 'Green synthesis and characterization of palladium nanoparticles and its conjugates from *Solanum trilobatum* leaf extract', *Nano-Micro Letters,* 2(3), pp. 169-176.

Kora, A. J. and Rastogi, L. (2015) 'Green synthesis of palladium nanoparticles using gum ghatti (*Anogeissus latifolia*) and its application as an antioxidant and catalyst', *Arabian Journal of Chemistry*, 11(7), pp. 1–9.

Kyriakou, G., Beaumont, S. K., Humphrey, S. M., Antonetti, C. and Lambert, R.M. (2010) 'Sonogashira coupling catalyzed by gold nanoparticles: Does homogeneous or heterogeneous catalysis dominate?', *ChemCatChem*, 2(11), pp. 1444–1449.

Li , Y., Boone , E. & El-Sayed, M. A. (2002) 'Size Effects of PVP-Pd Nanoparticles on the Catalytic Suzuki Reactions in Aqueous Solution', *Langmuir,* 18, pp. 4921-4925.

Mandali, P. K. and Chand, D. K. (2013) 'Palladium nanoparticles catalyzed Suzuki cross-coupling reactions in ambient conditions', *CATCOM*, 31, pp. 16–20.

Mansfield, E., Tyner, K. M., Poling, C. M. & Blacklock, J. L. (2014) 'Determination of Nanoparticle Surface Coatings and Nanoparticle Purity Using Microscale Thermogravimetric Analysis', *Anal. Chem.,* 86(3), pp. 1478-1484.

Mmola, M., Le Roes-Hill, M., Durrell, K., Bolton, J. J., Sibuyi, N., Meyer, M. E., Beukes, D.R. and Antunes, E. (2016) 'Enhanced antimicrobial and anticancer activity of silver and gold nanoparticles synthesised using *Sargassum incisifolium* aqueous extracts', *Molecules*, 21(1633), pp. 1-22.

Momeni, S. and Nabipour, I. (2015) 'A Simple Green Synthesis of Palladium Nanoparticles with *Sargassum Alga* and Their Electrocatalytic Activities Towards Hydrogen Peroxide', *Appl. Biochem. Biotech.*, 176(7), pp. 1937–1949.

Moreno-Mañas, M., Pleixats, R. and Villarroya, S. (2001) 'Fluorous phase soluble palladium nanoparticles as recoverable catalysts for Suzuki cross-coupling and heck reactions', *Organometallics*, 20(22), pp. 4524–4528.

Ning, S. & Xiaobai, X., (1997) 'Reductive metabolism of 4-nitrobiphenyl by rat liver fraction', *Carcinogenesis,* 18(6), pp. 1233-1240.

Parker, H. L., Rylott, E.L., Hunt, A.J., Dodson, J.R., Taylor, A. E., Bruce, N. C. and Clark, J. H. (2014) 'Supported palladium nanoparticles synthesized by living plants as a catalyst for Suzuki-Miyaura reactions', *PLoS ONE*, 9(1), pp. 1–6.

Parker, H. L., Dodson, J.R., Budarin, V.L., Clark, J. and Hunt, A. J. (2015) 'Direct synthesis of Pd nanoparticles on alginic acid and seaweed supports', *Green Chem.*, 17(4), pp. 2200–2207.

Pecora, R. (2000). 'Dynamic light scattering measurement of nanometer particles in liquids', *Journal of Nanoparticle Research,* 2, pp. 123-131.

Sawoo, S., Srimani, D., Dutta, P., Lahiri, R. and Sarkar, A. (2009) 'Size controlled synthesis of Pd nanoparticles in water and their catalytic application in C-C coupling reactions', *Tetrahedron*, 65(22), pp. 4367–4374.

Scheuermann, G. M., Rumi, L., Steurer, P., Bannwarth, W. and Mulhaupt, R. (2009) 'Palladium nanoparticles on graphite oxide and its functionalized graphene derivatives as highly active catalysts for the Suzuki-Miyaura coupling reaction', *J. Am. Chem. Soc.,* 131, pp. 8262-8270.

Schimpf, S., Lucas, M., Mohr, C., Rodemerck, U., Bruckner, A., Radnik, J., Hofmeister, H. and Claus, P. (2002) 'Supported gold nanoparticles: In-depth catalyst characterization and application in hydrogenation and oxidation reactions', *Catalysis Today,* 72(1), pp. 63-78.

Shekhar, S. H., Lyons, G., McRoberts, C., McCall, D., Carmichael, E., Andrews, F. and McCormack, R. (2012) 'Brown seaweed species from Strangford Lough: compositional analyses of seaweed species and biostimulant formulations by rapid instrumental methods', *J. Appl. Phycol.,* 24(5), pp. 1141-1157.

Thareja, R. K. and Shukla, S. (2007) 'Synthesis and characterization of zinc oxide nanoparticles by laser ablation of zinc in liquid', *Applied Surface Science*, 253, pp. 8889–8895.

Thiruvengadathan, R., Korampally, V., Ghosh, A., Chanda, N., Gangopadhyay, K. and Gangopadhyay, S. (2013) 'Nanomaterial processing using self-assembly- bottom-up chemical and biological approaches', *Reports on Progress in Physics,* 76(6), pp. 1-90.

Turunc, E., Binzet, R., Gumus, I., Binzet, G. and Arslan, H. (2017) 'Green synthesis of silver and palladium nanoparticles using *Lithodora hispidula* (Sm.) Griseb. (*Boraginaceae*) and application to the electrocatalytic reduction of hydrogen peroxide', *Materials Chemistry and Physics*, 202, pp. 310–319.

Yadav, T. P., Yadav, R. M. and Singh, D. P. (2012) 'Mechanical Milling : a Top Down Approach for the Synthesis of Nanomaterials and Nanocomposites', *Nanoscience and Nanotechnology,* 2(3), pp. 22–48.

Ye, L., Li, J., Zhang , J. & Pan, Y. (2010) 'NMR characterization for polysaccharide moiety of a glycopeptide', *Fitoterapia,* 81(2), pp. 93-96.

Zhang, B., Misak, H., Dhanasekaran, P. S., Kalla, D. and Asmatulu, R. (2011) 'Environmental Impacts of Nanotechnology and Its Products', *Proceedings of the 2011 Midwest Section Conference of the American Society for Engineering Education*, pp. 1–9

Chapter 3: Synthesis and characterization of palladium nanoparticles

3.1. Introduction

This chapter deals with the preparation of the seaweed extracts, and the synthesis and characterization of variously prepared palladium nanoparticles (PdNPs). The chapter also covers the preliminary investigations carried out with respect to the catalytic ability of the prepared PdNPs. This provided guidance to the most feasible synthetic routes to take for the NPs. The topics covered in this chapter are:

1. Preparation of a variety of aqueous extracts (AE) for the *Ecklonia radiata* seaweed.
2. Characterization of these variously prepared aqueous extracts.
3. Synthesis of the PdNPs using the aqueous extracts to produce the AE capped PdNPs (AE-PdNPs).
4. Synthesis of polyvinylpyrrolidone capped PdNPs (PVP-PdNPs) according to literature methods, which would be employed as a model PdNP.
5. Characterization of the variously prepared PdNPs.
6. Test of the catalytic ability of the AE-PdNPs in a model Suzuki carbon-carbon coupling reaction.

3.2. Materials and methods

3.2.1. Chemicals and reagents

The materials used for this section of the study, which included potassium tetrachloropalladate (K_2PdCl_4), sodium carbonate (Na_2CO_3), Folin-Ciocaleu's reagent (F-C reagent), Gallic acid (GA), phosphate buffer (pH 6.6), potassium ferricyanide [$K_3Fe(CN)_6$], trichloroacetic acid (TCA), ferric chloride ($FeCl_3.6H_2O$), Ascorbic acid (AA), 2,2-diphenyl-1-Picrylhydrazyl (DPPH), palladium chloride ($PdCl_2$) and polyvinylpyrrolidone (PVP), were all purchased from Sigma Aldrich and used without further purification. Distilled methanol, ethanol, concentrated

hydrochloric acid (10.44 M) and deionized water (15.0 MΩ.cm^{-1}) were used to synthesize the PdNPs. Deionized water was also used to wash glassware. For the Suzuki coupling reactions, phenylboronic acid, 4-iodoanisole, potassium carbonate (K_2CO_3), dimethylformamide (DMF), diethyl ether, ethyl acetate (EtOAc), sodium hydroxide and anhydrous magnesium sulphate ($MgSO_4$) were all purchased from Sigma Aldrich and used without further purification.

3.2.2. Equipment

3.2.2.1. UV-Visible Spectroscopy
The UV-Visible spectra of the various samples were collected using an Agilent Technologies Varian Cary 60 UV-Vis spectrometer in the range from 190 nm to 800 nm. 3 mL aliquots of the samples were placed in a 1 cm pathlength quartz cuvette. Agilent Cary WinUV (Agilent Technologies) software (version 5.0.0.1004) was used to collect the data, while the data was analysed and plotted with Origin (OriginLab) software (version 8.5.1).

3.2.2.2. Fourier Transform Infra-Red (FTIR) spectroscopy
Aqueous extracts and other samples were analysed in its powder form, using a Perkin Elmer Spectrum 400 FT-IR spectrometer equipped with an ATR accessory. The data was collected using Perkin Elmer Spectrum software, (version 10.5.4).

3.2.2.3. Thermogravimetric Analysis (TGA)
TGA data, using a Perkin-Elmer TGA 4000 instrument, was collected for the sample powders under inert, nitrogen gas, conditions. The gas flow rate was set at 20 mL/minute, while the heating rate was set at 10°C/minute from 30°C to 850°C. The data were collected and analysed using the Pyris software (version 11.0.3) installed on the TGA workstation.

3.2.2.4. NMR spectroscopy
A Bruker 400 MHz Avance IIIHD Nanobay spectrometer equipped with a 5 mm BBO probe at 298 K was used to obtain 1D and 2D NMR spectra, with the exception of the aqueous extracts which were recorded at 333 K in D_2O. Standard 1D and 2D NMR pulse sequences were employed, with D_2O (δ_H 4.70), DMSO-d_6 (δ_H 2.50) or CDCl$_3$ (δ_H 7.25) as the deuterated solvent. Quantitative NMR was performed using the Bruker Topspin 3.6.2. qNMR analysis software where DCM (2.66 mg of 99.5% purity) was used as the internal standard. The Topspin 3.6.2. Eretic 2 NMR quantification analysis tool was also employed for comparison.

3.2.2.5. X-Ray Diffraction (XRD)

A Bruker AXS D8 Advance powder diffractometer (voltage 40 kv, current 40 mA) was used to collect the XRD patterns. A CuK_α (λ=0.154 nm) monochromatic radiation source was used to produce the X-ray powder pattern and the reflections were recorded in the 2-theta (2Θ) range of 15-85°.

3.2.2.6. High-Resolution Transmission Electron Microscopy (HRTEM)

The PdNP samples were submitted as a colloidal solution (labelled OAE-PdNPs, AE-PdNPs in water and PVP-PdNPs in ethanol) for HRTEM analyses. A Tecnai F20 HRTEM instrument equipped with a field-emission gun (FEG) operating in a bright field mode and a 200 kV accelerating voltage to generate an electron beam produced the images obtained. One drop of the solution was placed on a holey carbon-coated copper/nickel grid and the specimen dried under a Xenon lamp. The electron micrographs/images produced were analysed using ImageJ software (version 2) and the size and morphology of the NPs subsequently recorded.

3.2.2.7. Energy Dispersive X-ray (EDX) analysis

Liquid nitrogen was used to cool the lithium doped silicon EDX detector which was coupled to the HRTEM instrument, and used to collect data.

3.2.2.8. Dynamic Light Scattering (DLS) spectroscopy and Zeta Potential measurements

DLS and zeta potential measurements were carried out using a Malvern Zetasizer Nanoseries instrument with the Zetasizer software (version 7.11). After the synthesis of the PdNPs, briefly, 3 mL of the solution was used for the DLS determinations, where measurements were taken in triplicate to give the mean hydrodynamic size of the PdNPs. Similarly, the zeta potential of the PdNPs was determined using 1 mL of the PdNP solutions and the mean potential was recorded in triplicate.

3.2.2.9. Inductively Coupled Plasma—Atomic Emission Spectroscopy (ICP-AES)

A Thermo ICAP 6200 ICP-AES instrument was used to determine the concentration of palladium in the NP samples using the ITEVA software. To quantify the Pd in the solutions, a primary wavelength for Pd at 340.458 nm was used. Briefly, 50 mL of the AE-PdNPs sample solution was first passed through a 0.45 μm microfilter to remove any large particles and to protect the instrument. The sample was

transferred into a 50 mL centrifuge tube and sent for ICP-AES analysis. 50 mL of the PVP-PdNPs solution was transferred into a 100 mL round bottom flask. The solvent (ethanol) was removed under reduced pressure using a rotavap and 50 mL of H_2O added and the sample stirred. The PVP-PdNPs sample solution was passed through a 0.45 µm microfilter into a 50 mL centrifuge tube and sent for analysis. The results obtained are reported as mg/L or parts per million (ppm).

3.2.2.10. Gas Chromatography-Mass Spectrometry (GC-MS)

GC-MS analysis was performed on an Agilent 7820A GC with 5977E msd. The software that was used to retrieve data was the Masshunter B07.02.1938. Briefly, the samples for GC-MS was prepared by diluting 1 mg of sample in 2 mL DCM analysis.

3.2.3. Methods

3.2.3.1 Seaweed extraction

The *E. radiata* seaweed was collected in Port Alfred, along the coast of the Eastern Cape, South Africa, and stored at -20°C until further use.

From the collected *E. radiata*, two aqueous extracts were prepared. The first aqueous extract was generated by an organic extraction process. Firstly, about 15 g of the kelp was extracted with methanol followed by extraction with dichloromethane-methanol (1:2). This kelp sample was allowed to dry and then extracted with boiling water for 60 minutes. This extract was called ED18-OAE. Secondly, another 15 g of *E. radiata* underwent a direct extraction method where it was boiled in water for 60 minutes. This extract was called ED18-AE. The two aqueous extracts were placed on a freeze-drier and the samples stored in 50 mL centrifuge tubes in a cool, dry and dark cupboard until further use.

3.2.3.2. Total polyphenolic content

The total polyphenolic content of both the aqueous extracts (ED18-AE and ED18-OAE) was determined using a modified method of Tobwala, *et al*. (2014). Briefly, 1 mg/mL, 5 mg/mL and 10 mg/mL samples of each of the aqueous extracts were prepared, where 125 µL of each of the sample extracts was mixed with 625 µL of the F-C reagent that was diluted 10-fold (1.00 mL F-C reagent and 9.00 mL H_2O) in clean, dry vials. The newly formed mixture was incubated at room temperature (RT) for 5 min, after which 500 µL of a 75 mg/mL Na_2CO_3 solution was added to each vial. After the addition of the Na_2CO_3 solution, the vials containing the mixtures underwent vortex mixing and was once again incubated at RT for 90 min

in a dark cupboard. Standards using gallic acid (GA) were also prepared in the same way, however, the concentrations of the GA standards were 50 µg/mL, 75 µg/mL, 100 µg/mL, 150 µg/mL, 250 µg/mL, 500 µg/mL and 750 µg/mL. The mixtures were pipetted (100 µL) into the 96 well microplates in triplicates, and the absorbance measured at 760 nm. The results were expressed as GAE/mg (gallic acid equivalents) of dried kelp.

3.2.3.3. Total reducing power

The total reducing power of both aqueous extracts (ED18-AE and ED18-OAE) was determined using a modified method of Tobwala, *et al*. (2014). Firstly, standards of ascorbic acid (AA) were prepared for use as the standard curve. The concentrations of the AA standards were as follows: 50 µg/mL, 75 µg/mL, 100 µg/mL, 150 µg/mL, 250 µg/mL, 500 µg/mL and 750 µg/mL. The assay was carried out on the aqueous extracts in glass vials. Homogeneous mixtures were prepared which consisted of 2.5 mL (0.2 M) phosphate buffer (pH 6.6), 2.5 mL of 1% potassium ferricyanide and 1.0 mL of the extracts. The aqueous extracts were also prepared in different concentrations at 1 mg/mL, 5 mg/mL and 10 mg/mL. The prepared solutions were placed in a warm water (50°C) bath for 20 min. These samples were added to a 15 mL centrifuge tubes containing 2.5 ml of 10% TCA solution. The mixtures were subsequently centrifuged at 6000 rpm for 10 min, before 2.5 mL of the top layer was transferred into clean glass vials. To the mixture in the glass vials, 2.5 mL of water and 0.5 mL of 0.1% ferric chloride were added, and the mixture mixed well. The mixtures were allowed to settle for 5 min before 100 µL of the mixtures were pipetted into 96 well microplates in triplicates, and the absorbance measured at 700 nm. The results obtained were expressed as AAE/mg (ascorbic acid equivalents) of dried kelp.

3.2.3.4. Radical scavenging power assay

The radical scavenging power of both aqueous extracts (ED18-AE and ED18-OAE) was determined using a modified method of Tobwala, *et al*. (2014). Firstly, a DPPH solution was prepared using MeOH as a solvent. Secondly, concentrations of 1 mg/mL, 5 mg/mL and 10 mg/mL samples of each of the aqueous extracts were prepared. In clean glass vials, 2.9 mL DPPH ($1x10^{-4}$ M) was mixed with 0.1 mL of the extracts that were prepared. The mixtures were placed in a dark cupboard at RT for 30 min before it was used. Briefly, 100 µL of the mixtures were pipetted into 96 well microplates, as triplicates and the absorbance measured at 520 nm against the blank samples (triplicates) of DPPH. The radical scavenging power of the extracts was calculated using the equation $\left[1 - \frac{A1}{A2}\right] x 100\%$, where A1 is the absorbance of the mixture and A2 is the absorbance of the DPPH blank samples.

3.2.3.5. Synthesis of palladium nanoparticles (PdNPs)

Briefly, 25 mg of each of the freeze-dried aqueous extracts (OAE and AE) was dissolved in 25 mL of deionized water to prepare a solution of 1 mg/mL. 14.25 mL of this solution was mixed with 750 µL of a K_2PdCl_4 (0.1M) solution containing 135 mL of deionized water. The synthesis was carried out for 24 hours at 80°C under reflux. The palladium nanoparticles are reported as OAE-PdNPs and AE-PdNPs for the OAE and AE samples, respectively. The PdNPs were freeze-dried, however, they also appeared to be a highly hygroscopic, needle-like, light powder. As a result, the PdNPs were kept and used as a solution, as the light, hygroscopic powder presented a health and safety risk, and difficulties in working with the sample. The amount of Pd in the NP solution was determined using ICP-AES.

A modified method was used in the synthesis of the polyvinylpyrrolidone capped PdNPs (PVP-PdNPs) (Narayanan & El-Sayed, 2003). Briefly, a precursor was prepared where 89 mg of the $PdCl_2$ metal salt was weighed out and mixed with 6 mL of HCl (0.2M) and 244 mL of deionized water, to form the precursor H_2PdCl_4 (2 mM) solution. 15 mL of this H_2PdCl_4 (2 mM) solution, 21 mL of deionized water and 67 mg PVP were placed in a 100 mL round bottom flask (RBF), and an additional 4 drops of HCl (1 M) added. The reaction mixture was heated for 3 hours under reflux at 80 °C. As soon as the refluxing started, 14 mL of ethanol was added. After 3 hours, a dark brown solution formed, and the solution was lyophilized. A sticky, gummy paste resulted which could be due to the PVP polymer, and therefore the decision was made to also keep the PVP-PdNPs in solution and use it as it is. The amount of Pd in the NP solution was also determined using ICP-AES.

3.2.3.6. Synthesis of 1-methoxy-4-phenyl benzene (3.3)

The method used was modified and adapted based on literature (Oliveira, et al., 2015) (Figure 3.1).
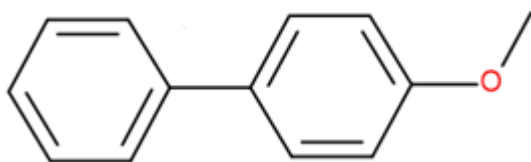
Figure 3.1: The structure of 1-methoxy-4-phenyl benzene (Structure 3.3).

Briefly, 18.4 mg of phenylboronic acid (**3.1**, 0.15 mmol eq.), 23.6 mg of 4-iodoanisole (**3.2**, 0.10 mmol eq.), 27.5 mg of potassium carbonate (0.20 mmol eq.), 1.8 mg of the AE-PdNPs catalyst (40.18 mL) and 400 µL of dimethylformamide were all added in sequence to a round bottom flask and heated for 24 h at 130 °C under inert conditions. The product formed was first extracted with diethyl ether

and then with ethyl acetate. The organic layer was then dried under reduced pressure. The crude product was used as is.

3.3. Results and Discussion

3.3.1. Seaweed description and extraction

The brown marine algae, *Ecklonia radiata (E. radiata)*, is a kelp species which is classified under the order of *Laminariales* (Guiry & Guiry, 2019). Figure 3.2 and 3.3 shows photographs of a blade and the kelp in its natural environment (Anderson, et al., 2016).

Firstly, 30 g of the frozen brown seaweed was left in a beaker to defrost overnight. The seaweed was washed with deionized water to remove any sand particles or other materials and placed in a mortar. Liquid nitrogen was added and the seaweed crushed to obtain a fine powder (Figure 3.4). The powder was divided into two (15 g) portions and stored at -20°C until further use.

Figure 3.2: Photograph of a single E. radiata blade.

Figure 3.3: E.radiata in its natural habitat (Anderson, et al., 2016).

Figure 3.4: The crushed seaweed in powdered form.

The first portion (15 g) was extracted with 500 mL of distilled methanol for 60 min at RT. The mixture was allowed to stand, resulting in a lime-green crude extract as shown in Figure 3.4 to give 430 mg of extract (labelled ED18-OE1).
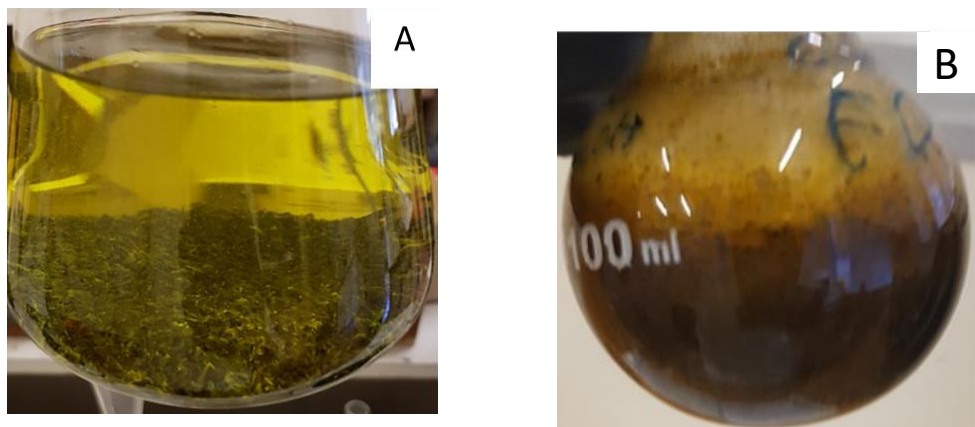
Figure 3.5: MeOH extract (ED18-OE1) of E. radiata: A) solution and B) after solvent removal.

The kelp powdered grains were then dried and then extracted with 500 mL of a DCM: MeOH (2:1) mix for 60 min at RT and the dark green extract solution decanted. The kelp powder was subsequently subjected to a second extraction using 500 mL of DCM: MeOH (2:1) mix where the solution changed to a light brown colour. The two DCM: MeOH extracts were combined and dried to give 70 mg of extract (labelled ED18-OE2). The kelp powder was then dried in a fume hood for 7 days.
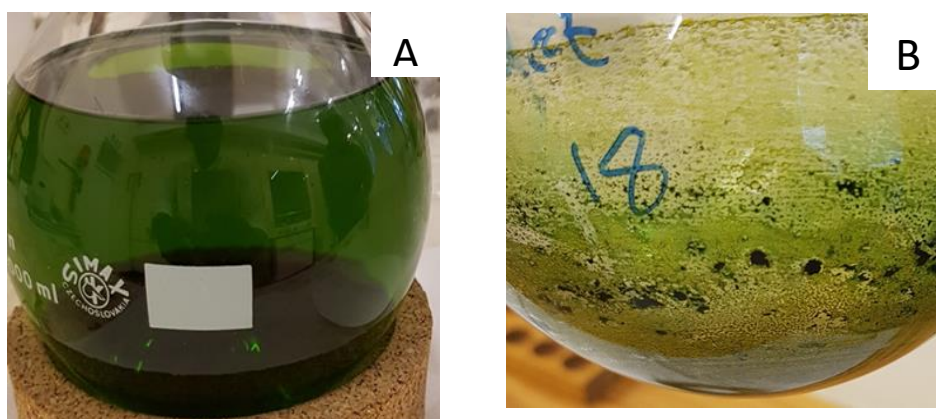
Figure 3.6: DCM: MeOH extract (ED18-OE2) of E. radiata: A) solution and B) after solvent removal.

The remaining, dried kelp powder (4.50 g), following the MeOH and DCM extractions, was subsequently subjected to an aqueous extraction using 100 mL of deionized water and heated at 120 °C under reflux for 140 min when the solution started to change from a transparent colour to a dark-brown. The mixture was vacuum filtered, the solution stored in a fridge (4 °C) overnight and the solution freeze-dried. The lyophilized material (656 mg), labelled ED18-OAE appeared as a soft needle-like, porous material, light brown in colour (Figure 3.7).

Figure 3.7: The sample ED18-OAE obtained after freeze-drying.

A second, untreated powdered, portion (4.50 g) of kelp was directly extracted by adding 100 mL of deionized water (Figure 3.8(A)). The mixture was heated at 120 °C for 140 min under reflux resulting in a dark brown solution as illustrated in (Figure 3.8(B)). The solution was filtered and freeze-dried to give the dark brown, highly hygroscopic, aqueous extract, ED18-AE (Figure 3.8(C).
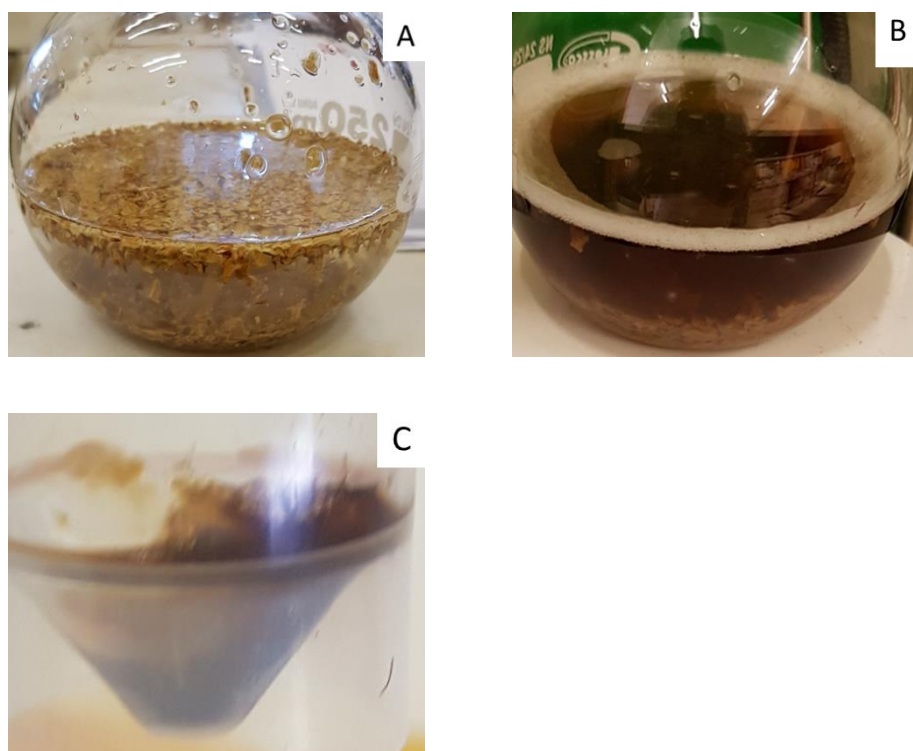
Figure 3.8: Aqueous extraction of E. radiata (ED18-AE): A) at the start of the extraction, B) at the end of the aqueous extraction and C) after lyophilization.

Two kelp aqueous extracts (ED18-AE and ED18-OAE) were therefore prepared, where one aqueous extract sample (ED18-OAE) was subjected to organic extraction prior to the aqueous extraction step. Both extract samples were placed in a dark cupboard and stored at room temperature in air-tight containers.

3.3.2. Characterization of the aqueous extracts obtained from *Ecklonia radiata*

3.3.2.1. UV-Visible Spectroscopy

UV-visible absorption spectroscopy was used to characterize and identify any differences between the two aqueous extracts, i.e. the aqueous extract (AE) and the organic aqueous extract (OAE). Briefly, a stock solution was prepared and diluted to obtain a final concentration of 0.22 mg/mL which was used to measure the UV-Visible spectra.

Figure 3.9 shows the UV-Visible spectra of both the AE and OAE samples in deionized water. An absorbance band is observed at approximately 273 nm, which could be due to polyphenols which are present in brown marine algae, as it is these polyphenols which give the characteristic dark brown colour to the marine algae and the aqueous extracts (Gomez-Guzman, et al., 2018). The AE spectrum appears

to have a higher absorbance intensity than the OAE spectrum, which possibly indicates that there is a greater quantity of polyphenols present in the AE than the OAE extract. This prediction was later confirmed by the results obtained in the total polyphenolic content assay (section 3.3.1.5).
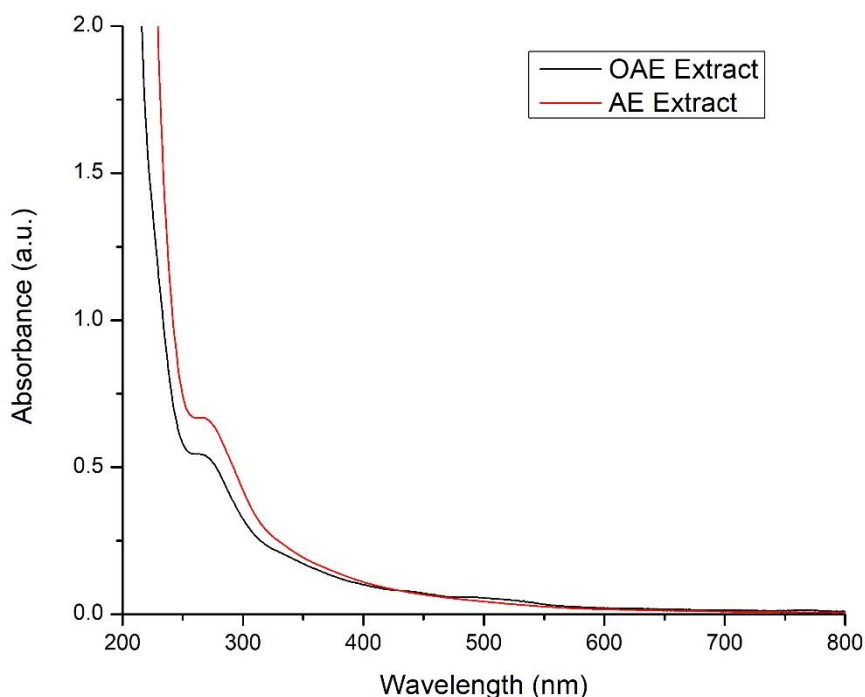
Figure 3.9: The UV-Visible spectra of the different aqueous extracts of E. radiata (using deionized water as a solvent).

3.3.1.2. FTIR spectroscopy

FTIR spectra provide a fingerprint for a compound, as it gives an indication of the various functional groups present in a material. The stretches and bands observed are unique to each functional group at a specific wavenumber (cm^{-1}). Figure 3.10 shows the various functional groups present in the IR spectra of AE extract (top) and the OAE (bottom). Both spectra appear to be identical, with peak position and intensities the same. A broad peak appears at approximately 3300 cm^{-1}, which is attributed to the OH functional moieties present in the sample, which supports the presence of polyphenols (Gomez-Guzman, et al., 2018). Other peaks which appear at approximately 1620 cm^{-1} can be assigned to the aromatic ring whereby the C=C bonds undergo bending, while the peak at approximately 1390 cm^{-1} may be described as the OH bending of phenols. Another important peak is found at approximately 1040 cm^{-1} which is reported to be an indication that there are polysaccharides present in the aqueous extracts (Gomez-Ordonez & Ruperez, 2011). The latter was confirmed using NMR spectroscopy.
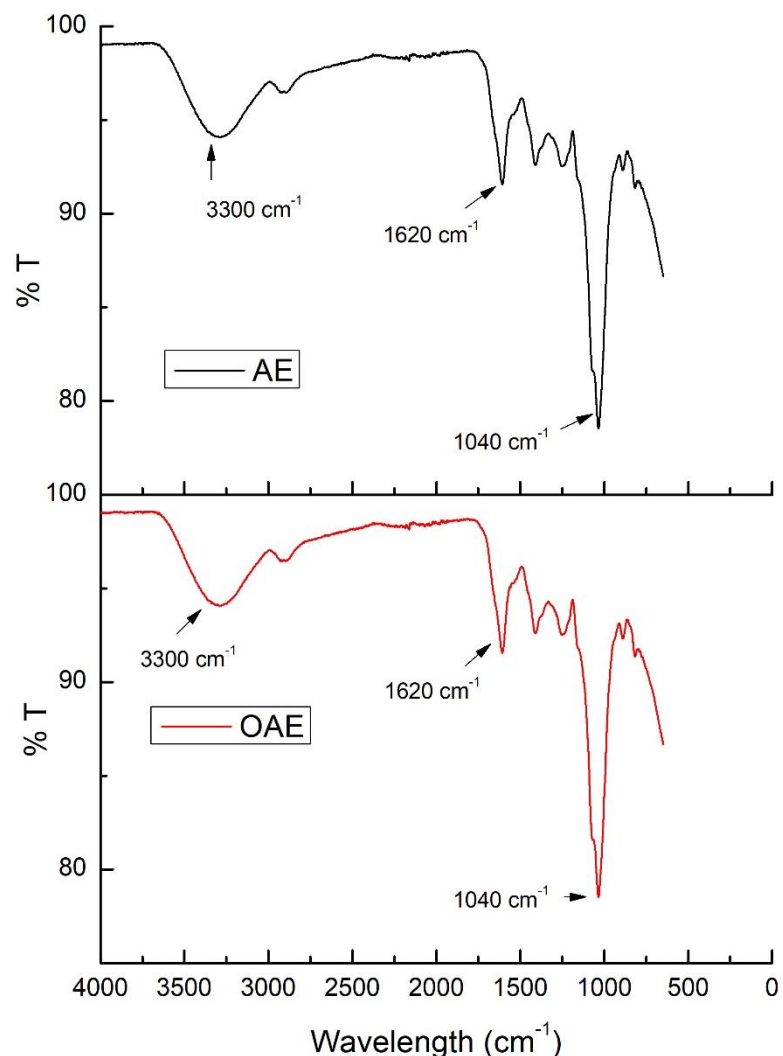
Figure 3.10: The FTIR spectra of the aqueous extracts AE (top) and OAE (bottom) from E. radiata.

3.3.1.3. TGA (Thermal Gravimetric Analysis)

Figure 3.11 shows the TGA profile obtained for the various aqueous extracts from *E. radiata.* Since both samples are highly hygroscopic, a slight loss in mass may be observed in the initial heating step. From 50 °C to 100 °C, a mass loss is indeed observed for AE (0.47 %) which may be assigned to loss of water from the sample, but it may also be due to a loss of OH moieties on the polyphenols. The latter could be confirmed by TGA coupled to a mass spectrometer, however this equipment was not available. A mass loss (5.13 %) was then observed between 200 °C and 300 °C, while a significant mass loss (20.40 %) between 200 °C and 300 °C was observed. This may be attributed to the combustion of organic materials. After 300 °C, a gradual mass loss (53.87 %) is observed and can be assigned to the complete decomposition of organic material, leaving only ashes, NaCl and KCl (which is likely to be present in seaweeds) remaining. The salts have very high melting points (> 1400 °C) and the remaining 20.13 % is likely due to NaCl and KCl.

This was later confirmed using EDX analyses (section 3.3.2.4). Similar results were obtained for the OAE sample, with a small, initial mass loss in water (3.03 %). However, the sample did not undergo any mass loss between 100 °C and 200 °C, which could be since the small, volatile organic molecules were removed during the organic extraction process which the AE sample did not undergo. The OAE sample shows a steeper, more pronounced mass loss from 200 °C to 300 °C, which could be due to organic material that was not removed during the initial extraction steps with the organic solvents. In this region, the AE sample shows the presence of more organic material than the OAE extract, which was expected.
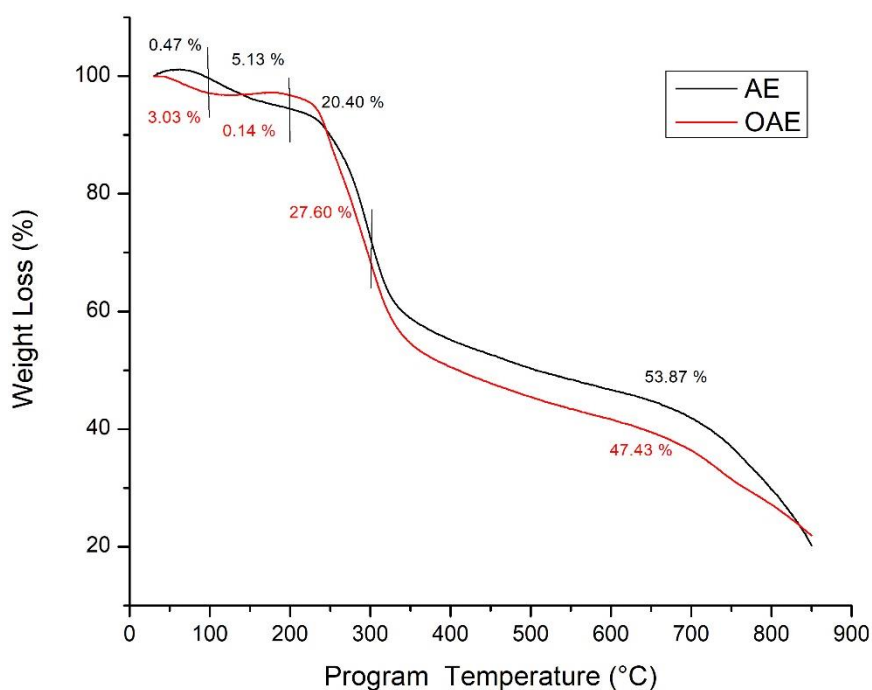
Figure 3.11: TGA profiles obtained for the aqueous extracts, AE and OAE of E. radiata.

3.3.1.4. NMR spectroscopy

Figure 3.12 shows the ^{1}H NMR spectra for the various aqueous extracts. These spectra were obtained with water suppression (o1 set to 4.70 ppm) at 333 K on a 400 MHz instrument. The proton spectra reveal the possible presence of polysaccharides (~δ_H 3-4) as the major constituent of the extract, and some aromatic compounds (~δ_H 6-8) present in a much smaller quantity, especially for the OAE sample. The latter chemical shifts may be due to the presence of polyphenols.
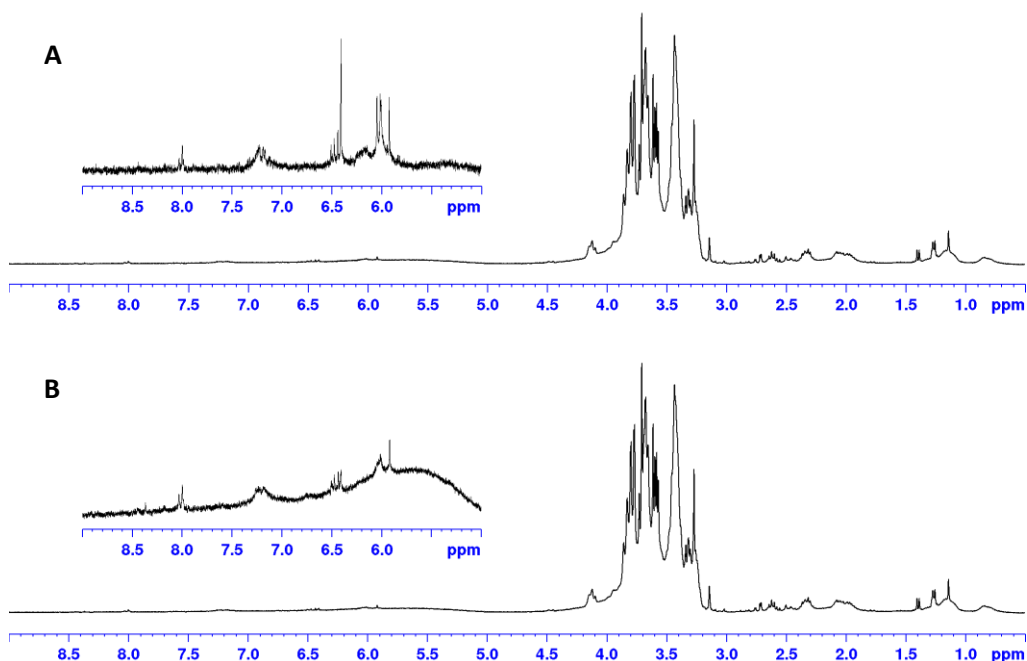
Figure 3.12: ^{1}H NMR spectra for the A) aqueous (AE) and B) organic aqueous (OAE) extracts obtained for E. radiata acquired in D_2O at 333K (400 MHz). The spectra were obtained with water suppression using the standard pulse program zgesgp. Insets show the regions from δ_H 5 − 9 for each spectrum.

Figures 3.13 and 3.14 show the multiplicity edited HSQC (Heteronuclear Single Quantum Coherence) spectra obtained for the extracts (also at 333K). HSQC is an important 2D experiment, as it gives information about one bond (^1J) proton-carbon bond correlation. In this way, the experiment is able to give an indication of the major components that are present in a specific sample, since both the ^{1}H and associated ^{13}C chemical shifts are obtained. HSQC spectra also allow for the spreading out of overlapping signals, allowing for a more detailed view of signal peaks. The data shown in Figures 3.13 and 3.14 shows characteristic signals for polysaccharides at δ_C 60-80 and δ_H 3-4 (Monsur, et al., 2017), confirming our initial suspicion. The NMR spectra also show that the aqueous extracts contain polysaccharides as a major component, while a second aromatic, possibly polyphenolic, component is present as a minor constituent due to the signals present in the range of ~δ_H 6-8. The HSQC spectra reveal that the latter aromatic protons are attached to carbon signals at ~δ_C 100-120 ppm. However, with the intensity being so weak, we could only unequivocally confirm the presence of polyphenols using a variety of assays.
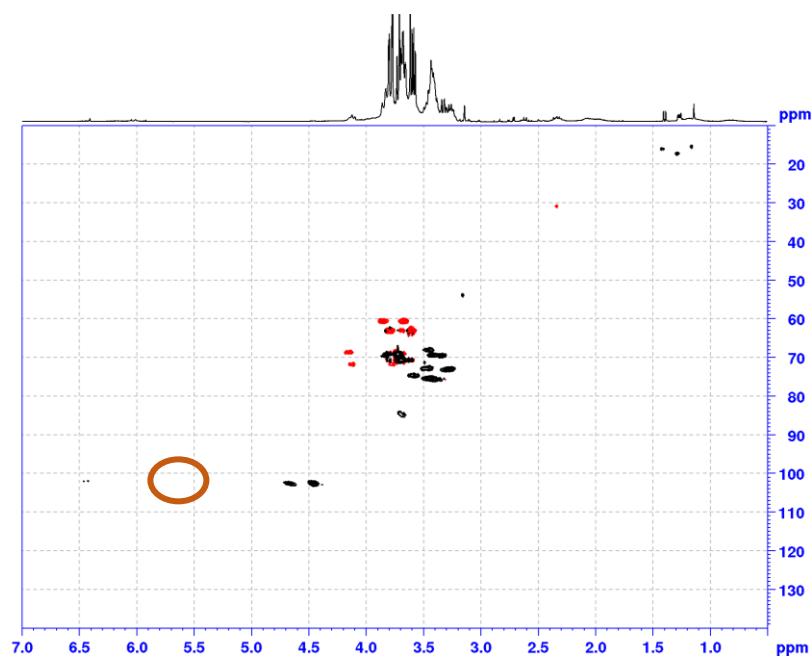
Figure 3.13: Multiplicity-edited HSQC spectrum obtained for the aqueous extract of E. radiata (333K, D_2O; 400 MHz). The 1D projection showed along the F2 dimension in the ^1H spectrum obtained with water suppression. Methylene signals are shown in red, while methyl and methine signals are shown in black.
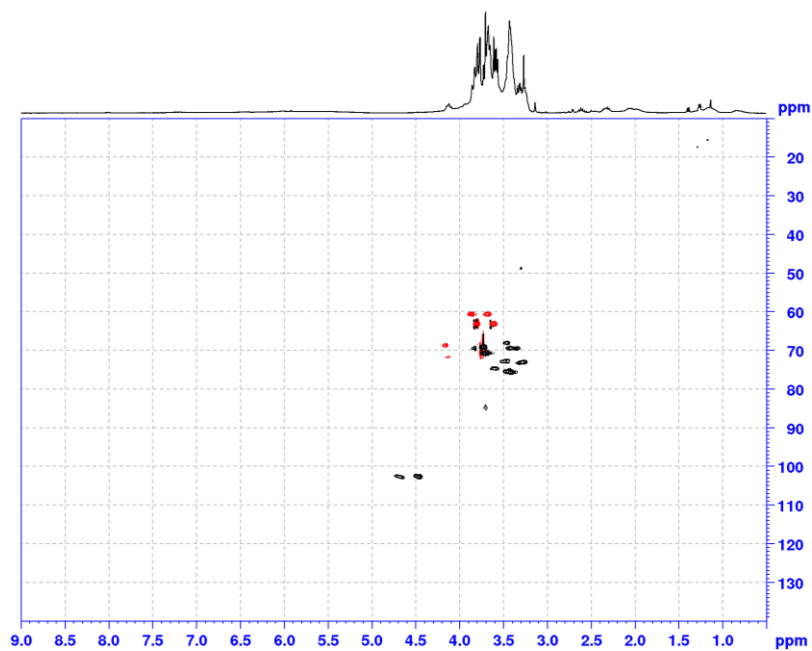
Figure 3.14: Multiplicity-edited HSQC spectrum obtained for the organic aqueous extract of E. radiata (333K, D_2O; 400 MHz). The 1D projection showed along the F2 dimension in the ^1H spectrum obtained with water suppression. Methylene signals are shown in red, while methyl and methine signals are shown in black.

These two components are vital to the biosynthesis, or green synthesis, of NPs, as the polysaccharides are expected to act as a capping agent for the NP surface, while the polyphenols are expected to act as a reducing agent for the metal salt to produce PdNPs.

3.3.1.5. Total polyphenolic content, total reducing power, and radical scavenging power assays

The total polyphenolic content assay indicates the amount of polyphenols which is present in the aqueous extracts of *E. radiata.* The purpose of the polyphenol component is to reduce the metal ion to form the metal NPs. Therefore, the greater the amount of polyphenols present in the aqueous extracts, the more efficient the metal NP formation. The method used to evaluate the polyphenolic content was carried out according to a method described by Tobwala *et al.* (2014). The authors reported that the total polyphenolic content can be measured in terms of gallic acid (in μg) equivalence (GAE) per mg of dried material (Tobwala, et al., 2014). The results obtained for the total polyphenolic content of the extracts is shown in Table 3.1. The two extracts were prepared at three concentrations each (1, 5, 10 mg/ml) and the absorbance measured in triplicate at 760 nm. It is clear that for each concentration, the polyphenolic content in relation to GAE equivalents was twice as high for the AE sample (216 μg GAE/ mg) compared to the same concentration of the OAE sample (99 μg GAE/ mg) at 5mg/mL for example.

Table 3.1: Results obtained for total polyphenolic content (760 nm) and total reducing power (700 nm) assays was carried out for each of the aqueous extracts of E. radiata using UV-Visible spectroscopy.

Sample	Total Polyphenolic Content	Total Reducing Power
	Concentration (μg GAE/mg)	Concentration (μg AAE/mg)
OAE (1mg/ml)	0.00	241.83
OAE (5mg/ml)	99.44	46.83
OAE (10mg/ml)	252.62	201.83
AE (1mg/ml)	7.47	321.83
AE (5mg/ml)	216.41	561.83
AE (10mg/ml)	408.53	926.83

The total reducing power of the constituents present in the *E. radiata* aqueous extracts was also analysed according to Tobwala *et al*. (2014). The total reducing power assay presents information about the reducing ability of the polyphenols in the reduction of Fe^{3+} ion to Fe^{2+} ion (Tobwala, et al., 2014), giving an indication of the ability of the aqueous extracts to reduce the metal salt and form metal NPs. In this study, it will provide information on the ability of the polyphenols to reduce the palladium metal ion solution from Pd^{2+} to Pd^0, as the oxidation state of Pd in PdNPs is the zero valency (Pd^0) state. Tobwala, *et al*., (2014) determined the total reducing power of polyphenols in terms of µg ascorbic acid equivalence (AAE) per mg of dried material. The results reported in Table 3.1 indicates that once again the aqueous extract has the highest reducing (927 µg AAE/ mg at 10 mg/ mL) ability as it contains at least triple the amount of ascorbic acid equivalents at the various concentrations, compared to the organic aqueous extract (OAE)(202 µg AAE/ mg) at the same concentration.

A total radical scavenging power assay was also carried out on the aqueous extracts of *E. radiata.* As before, the assay was carried out according to Tobwala *et al*. (2014). The assay assesses the ability of the extracts to find a radical and use this radical to reduce DPPH to its stable form of DPPH-H (Tobwala, et al., 2014), as seen in Figure 3.15.
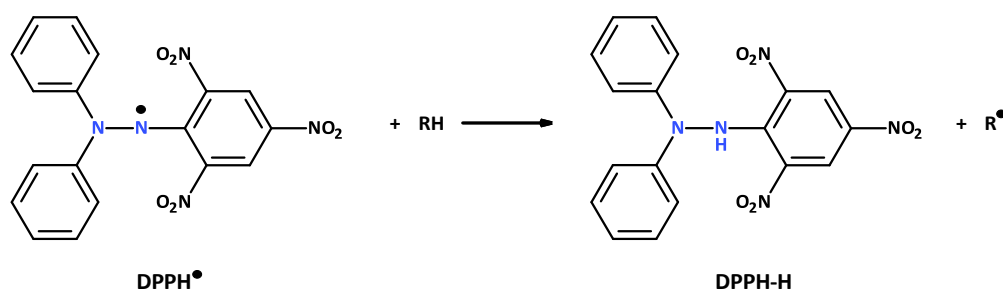
Figure 3.15: An illustration of how DPPH is reduced to its stable form of DPPH-H.

Figure 3.16. shows the radical scavenging power of the extracts at various concentrations (1, 5, 10 mg/mL), for each of the extracts. Once again the aqueous extract (AE) consistently appears to have the highest radical scavenging power (60% at 10 mg/mL) compared to the OAE sample (45% at 10 mg/mL).
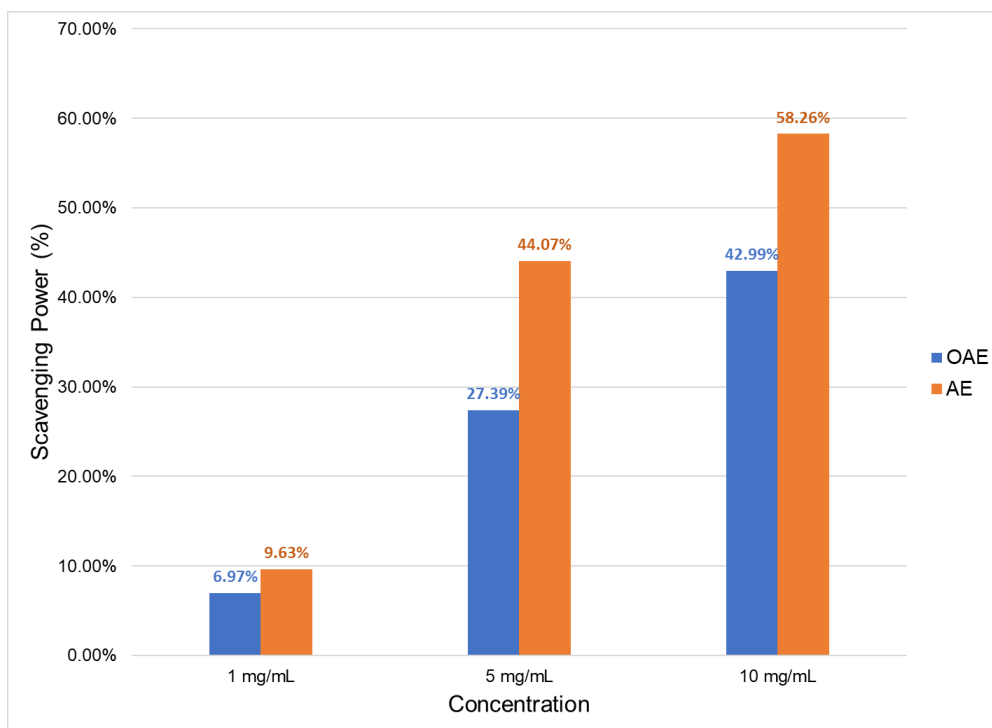
Figure 3.16: The results obtained in triplicate from the radical scavenging power assay for the aqueous extracts of E. radiata at 520 nm.

Overall, it appears that the AE sample is far superior in terms of the total phenolic content, total reducing power and radical scavenging power compared to the OAE sample. We, therefore, expected that the AE extract would produce PdNPs with greater ease and, hopefully, superior quality.

The results obtained clearly show that the aqueous extracts of the kelp *E. radiata* have the ability and potential to form metallic nanoparticles. The results obtained from the assays states that the aqueous extract AE has a much higher polyphenolic content and a better reducing ability than the organic aqueous extract OAE. AE also has a better radical scavenging ability, which makes it the best suited to produce metallic nanoparticles. The possible reason why AE is performing better than OAE could be that OAE had all the smaller sized polyphenolic molecules removed during the organic extraction process. This could be the main reason why AE outperformed OAE, however Mmola *et al*. (2016) reported the opposite. Mmola *et al*. (2016) carried out these assays on the seaweed *Sargassum incisifolium,* therefore the results could be due to type of brown algae that are used and also the species, as the physical properties of the extracts that were obtained from *E. radiata* are also different to that which Mmola *et al*. (2016) reported. It is therefore possible that these factors all play a role in the performance of the extracts, however, other *Ecklonia* species need to undergo the

same extraction methods and assays in order to prove if this phenomenon is only occurring in *E.radiata* species or if this is also found in other species.

3.3.2. Synthesis and characterization of the AE- and PVP- PdNPs

PdNPs were prepared as outlined in the Methods section (section 3.2.3.5) using the aqueous extracts (AE and OAE) and polyvinylpyrrolidone. The latter was prepared in an attempt to provide a model catalyst since PVP capped PdNPs have been reported in the literature to be efficient catalysts for organic coupling reactions (Narayanan & El-Sayed, 2003). Once the NPs were formed, they were subjected to a variety of characterization techniques to interrogate their properties.

3.3.2.1. UV-Visible spectroscopy

UV-Visible spectra were obtained for the PdNPs prepared with the aqueous extracts (OAE-PdNPs and AE-PdNPs) and PVP (PVP-PdNPs) and these are shown in Figures 3.17 and 3.18 in deionized water.
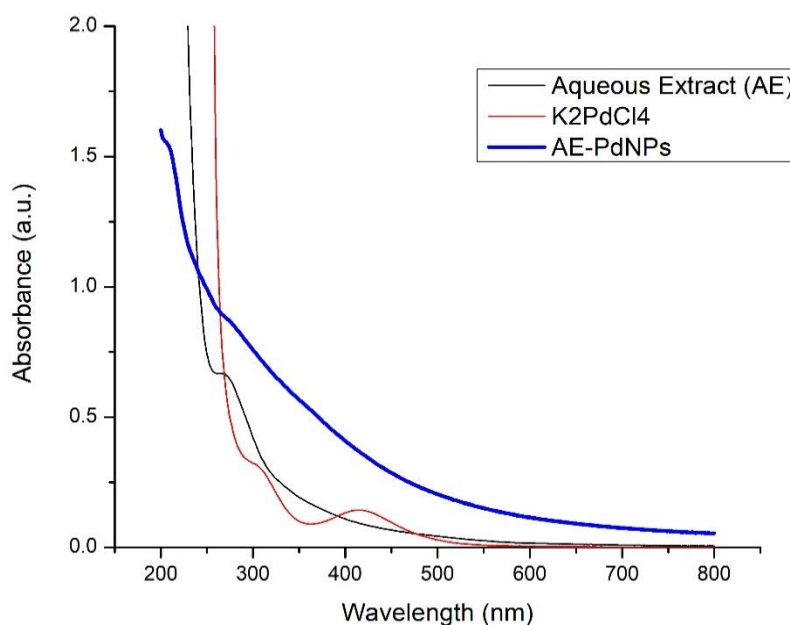
Figure 3.17: The UV-Visible spectra for the starting materials i.e. the metal salt (K_2PdCl_4), aqueous extract (AE), and the AE-PdNPs (in water).

Figures 3.17 and 3.18 show the UV-visible spectra of the palladium metal salt solution (in water) with two weak bands found at approximately 300 nm and 430 nm. These absorption bands are due to the charge transfer between the ligands to the metal when water is used as a solvent (Kettemann, et al., 2015). During the

reaction, when the Pd salt solution was added to each of the aqueous extracts, the colour of the solution changes from yellow to dark brown, which is an indication of PdNP formation (Viswadevarayalu, *et al.*, 2016). Additionally, the disappearance of the band at 430 nm during the syntheses of both sets of PdNPs, is due to the reduction of Pd^{2+} to Pd^0, which could indicate the successful formation of the PdNPs (Viswadevarayalu, et al., 2016) The UV-Vis spectra do comply with the spectra that are found in the literature (Turunc, et al., 2017), however, OAE-PdNPs have a small bump which indicates that not all the polyphenols were used in the synthesis of the PdNPs. Turunc, et al., (2017) did report that the disappearance of λ_{max} is a sign that Pd^{2+} was converted to Pd^0 and that PdNPs did form, therefore, this suggests that both the extracts did form PdNPs. However, since the aqueous extract solutions are already brownish in colour (thus masking the absorbance band at 430 nm), this could only be unequivocally confirmed with images obtained from HR-TEM.
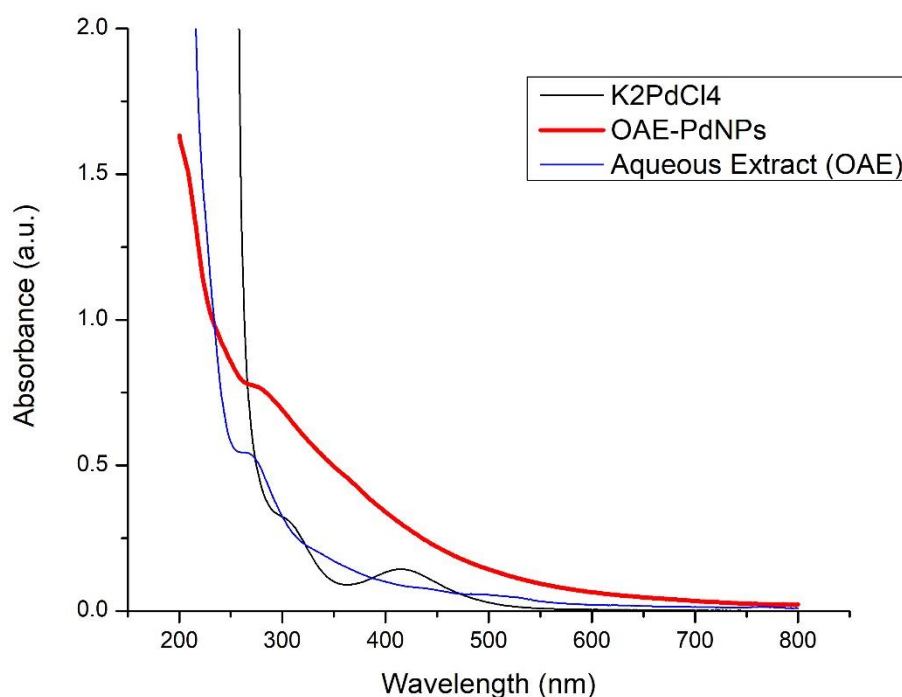
Figure 3.18: UV-Visible spectra for starting materials i.e. the metal salt (K₂PdCl₄), organic aqueous extract (OAE), and the OAE-PdNPs (in water).

The UV-Visible spectra relevant to the PVP-PdNPs is shown in Figure 3.19 together with the spectrum for the metal salt precursor (H_2PdCl_4) in water. The UV-visible spectra, in this case, clearly show the successful formation of PVP-PdNPs, since PVP itself is UV transparent and the UV-visible spectra of the PdNP is not ambiguous. As seen in Figure 3.19, the spectra reveal absorption peaks at around 325 nm and 420 nm, with the latter absorption band being due to the Pd^{2+} ion (Viswadevarayalu, et al., 2016). The disappearance of the peak at 420 nm,

48

together with lack of absorption peaks for the NPs, indicates the successful formation of the PVP-PdNPs since the NPs are dark brown to black in colour and a colloidal solution is obtained. Figure 3.20 shows the UV-Visible spectra of both the PVP- and AE-PdNPs to enable comparison. As is immediately apparent in Figure 3.20, the aqueous extract does contribute to the increase in absorbance intensity between 700 and 250 nm, of the AE-PdNPs, since the extract itself is brown in colour. This makes comparison of the two sets of NPs by UV/Visible spectroscopy difficult.
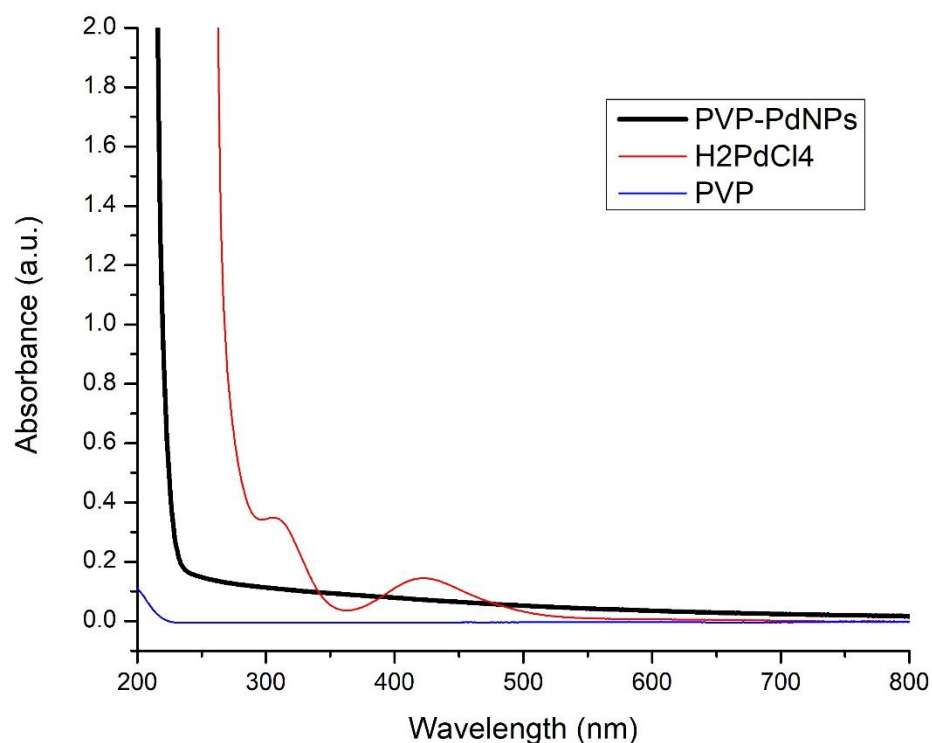
Figure 3.19: UV-Visible spectra for the metal salt precursor (H_2PdCl_4), PVP and PVP-PdNPs (in water).
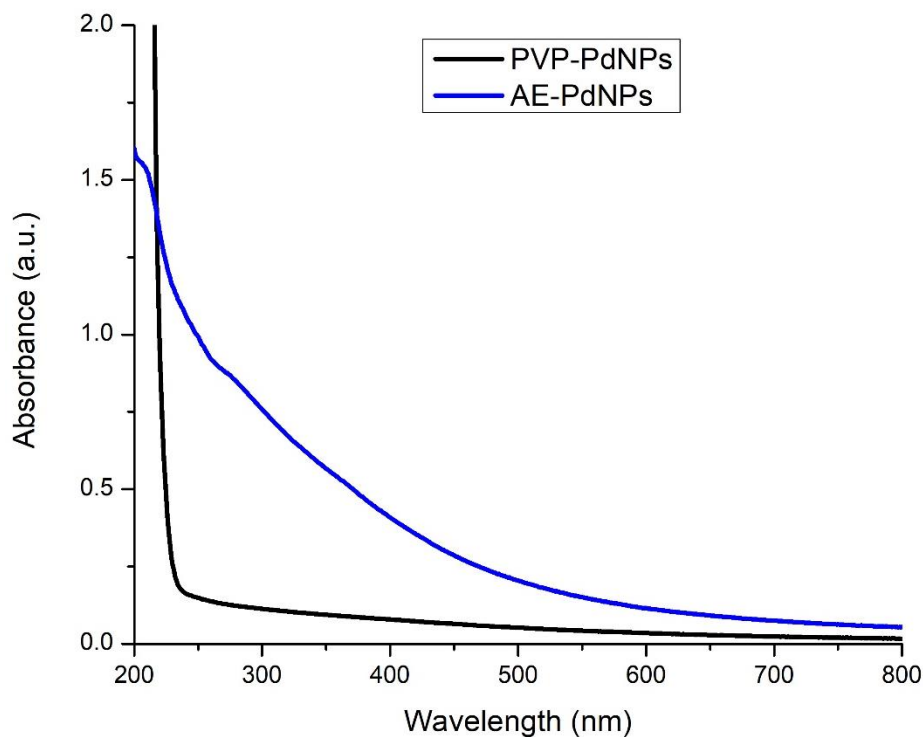
Figure 3.20: Comparison of the absorption spectra for the AE- and PVP- capped PdNPs (in water).

3.3.2.2. High-Resolution Transmission Electron Microscopy (HRTEM)

The respective HRTEM images obtained for the PdNPs prepared with the aqueous extracts is shown in Figure 3.21 (A and B). The images show that the PdNPs are roughly cubically shaped, with some evidence of twinning. Twinning is reported to be a defect in the NPs structure which is the result of the NPs being polycrystalline (Quintanilla, et al., 2010). Polycrystallinity is also reported to improve the catalytical activity of NPs (Quintanilla, et al., 2010). A variety of sizes were obtained, as revealed in the images, with the average particle size for the PdNPs found to be approximately 12 nm and 7 nm for the AE-PdNPs and OAE-PdNPs, respectively. The sizes were determined by measuring the size of 10 NPs in the images obtained for the AE-PdNPs and 7 NPs for OAE-PdNPs by using the software program ImageJ.
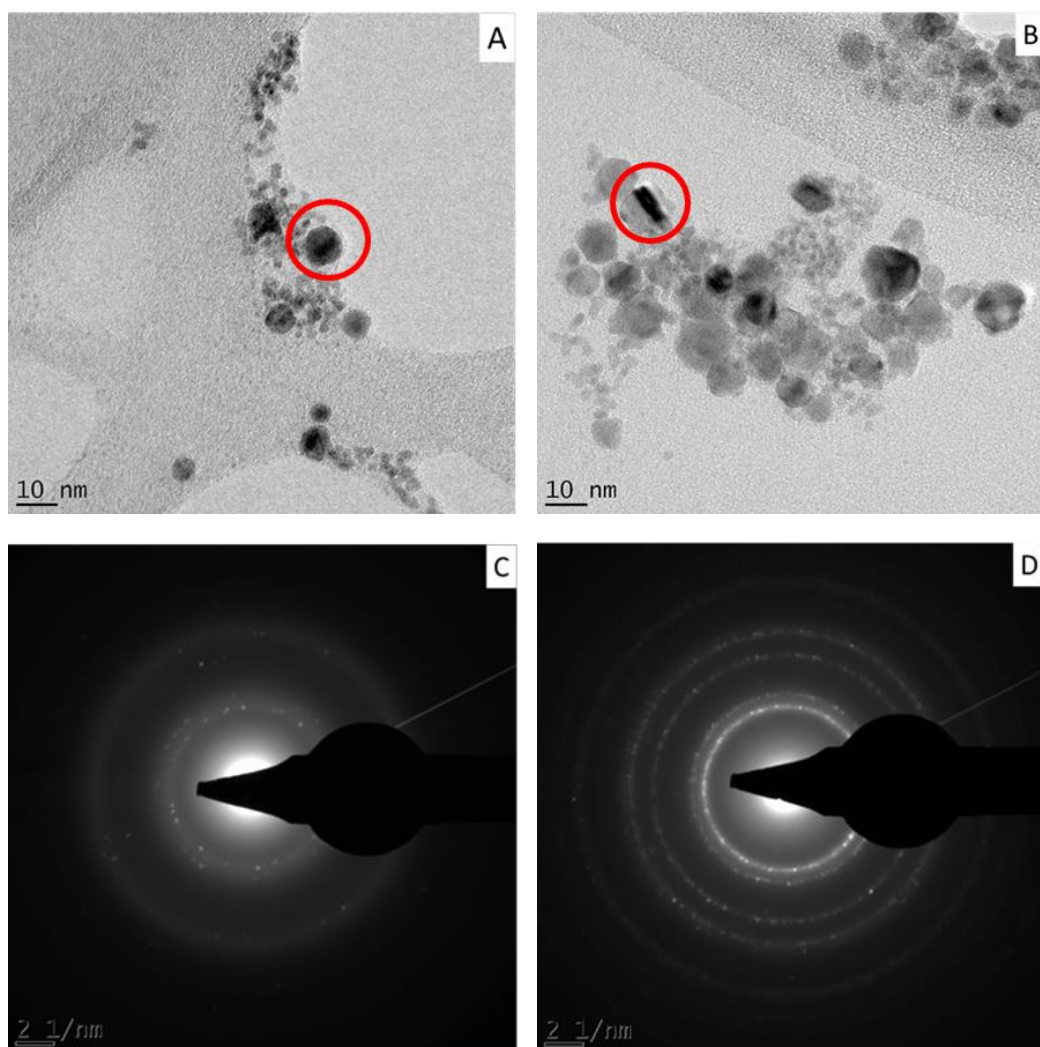
Figure 3.21: HRTEM images obtained for A) OAE-PdNPs and B) AE-PdNPs, and the SAED images obtained for C) the OAE-PdNPs and D) the AE-PdNP samples.

The Selected Area Electron Diffraction (SAED) patterns obtained are shown in Figure 3.21 C) and D) for OAE-PdNPs and AE-PdNPs, respectively. The latter demonstrates the crystallinity of the PdNPs synthesized from aqueous extracts, with the AE-PdNPs revealing a more polycrystalline nature as often seen with NPs, with the SAED pattern revealing that this sample has the most electrons being diffracted. With this information in hand, it was expected that the AE-PdNPs would show at least three or four, well-resolved reflections in the XRD powder patterns (Section 3.3.2.3).

Figure 3.22 shows higher resolution HRTEM images obtained for the PdNPs in order to get more information on the shape/morphology and size of the PdNPs. Figure 3.22 (A and C) are the images for AE-PdNPs, while B and D are the images obtained for the PdNPs. The AE-PdNPs were shown again in order to enable comparison with the 'model' PdNPs (PVP-PdNPs). Figure 3.22 (B and D) shows that the PVP-PdNPs appear to be cubic and triangular in shape, with an average size of

8 nm (using ImageJ) when 10 NPs were measured. The SAED images are shown in Figure 3.22 (F) for the PVP-PdNPs, alongside the AE-PdNPs in E). The SAED images for the PVP-PdNPs reveals that fewer electrons were diffracted and that, perhaps, the XRD powder patterns would be disappointing. The PVP-PdNPs are also, therefore, expected to be smaller in size when compared to the AE-PdNPs, which may limit the AE-PdNPs ability as a catalyst. As it is reported that larger PdNPs have less catalytic activity than smaller PdNPs (Li , et al., 2002).
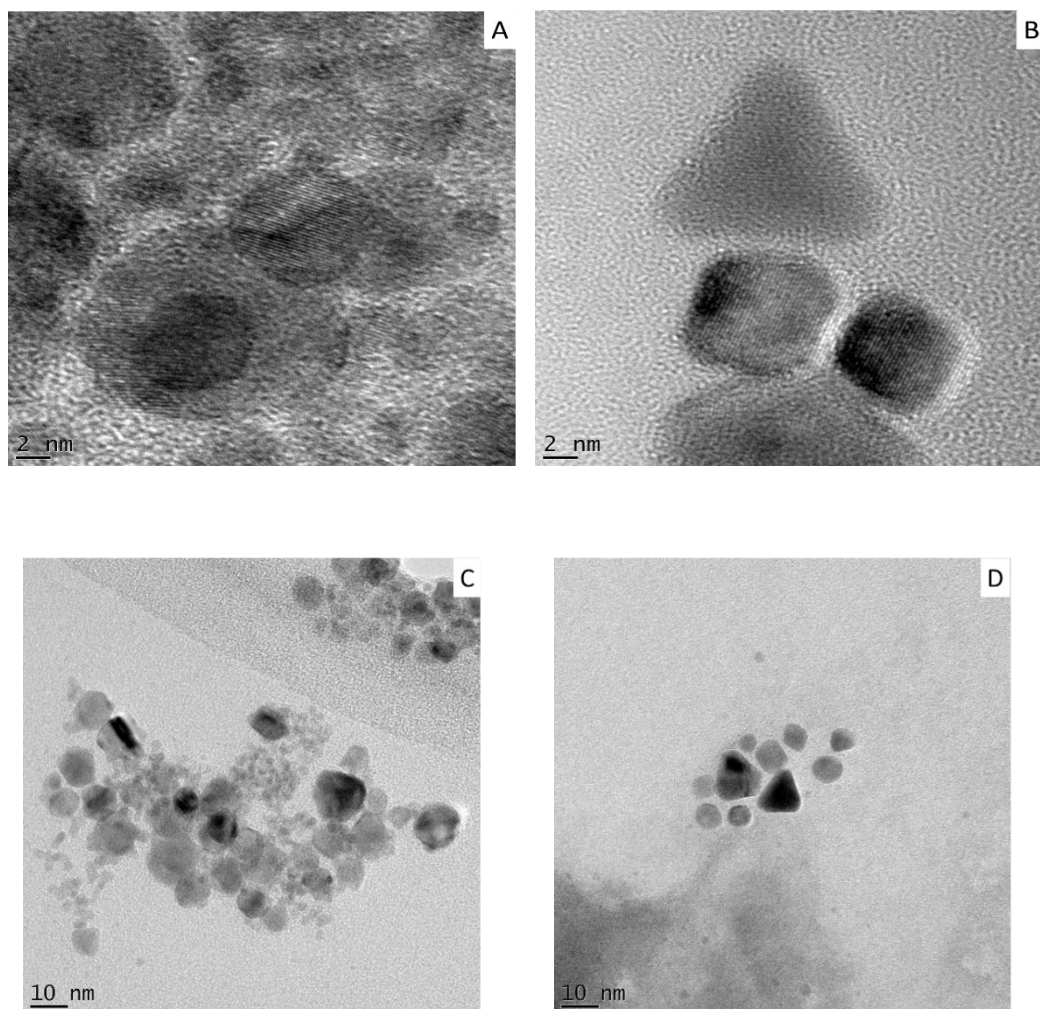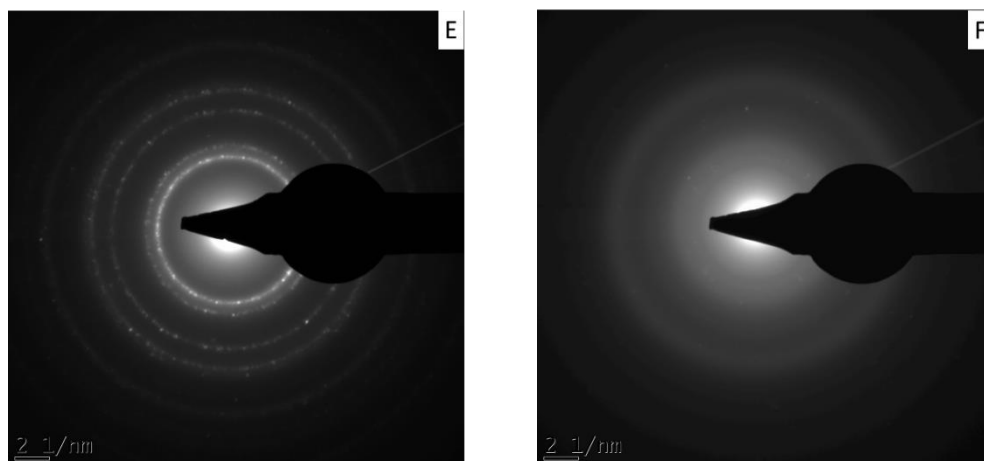
Figure 3.22: HRTEM images obtained for A) and C) AE-PdNPs and B) and D) PVP-PdNPs, and the SAED images obtained for E) the AE-PdNPs and F) the PVP-PdNP samples.

3.3.2.3. X-Ray powder Diffraction

The XRD powder patterns obtained for the AE-PdNPs (A) and PVP-PdNPs (B) are shown in Figure 3.23. The data obtained from the XRD powder patterns gave insight into the crystalline size and structure of the PdNPs. The powder pattern for AE-PdNPs (Figure 3.23 (A)) is more interesting and reveals a few sharp, low-intensity reflections at 2Θ = 40.50°, 46.20° and 66.26°. These diffraction angles correspond to the (1 1 1), (2 0 0) and (2 2 0) crystalline planes of the AE-PdNPs. The XRD reflection patterns are characteristic of elemental Pd^0 and were indexed according to the Joint Committee on Powder Diffraction Standards (JCPDS) file 00-046-1043 (Momeni & Nabipour, 2015). The PdNPs, therefore, have a face-centred cubic (fcc) crystal structure according to the crystalline planes revealed. The sharp signals found at 2Θ = 28.50° and 31.70° are attributed to sodium chloride (NaCl) and potassium chloride (KCl) that is most likely present in the aqueous seaweed extract. Figure 3.23 (B) is the XRD diffraction pattern obtained for the PVP-PdNPs. The PVP-PdNP sample submitted for XRD was, unfortunately, a sticky, gummy paste. In an attempt to obtain XRD spectra, the sticky paste was smeared onto a microscope slide (ClearScan by Lasec, 76 x 26 x 1 mm) and air-dried. The diffraction reflection patterns are not clearly visible in the figure, which could be due to the sample preparation, but a crystalline nature was also not revealed in the SAED image (Figure 3.22 F) obtained for the PVP-PdNPs. A number of articles, that employed the same method for the synthesis of PVP-PdNPs, did not show XRD powder patterns (Narayanan & El-Sayed, 2003) (Li , et al., 2002). It could, therefore, be that the nature of the PVP polymer masks any diffractions patterns that could be observed. However, the HR-TEM images that the PVP-PdNPs do have some crystallinity. The broad humps visible in the diffractograms for both sets of NPs is due to the presence of amorphous organic material.
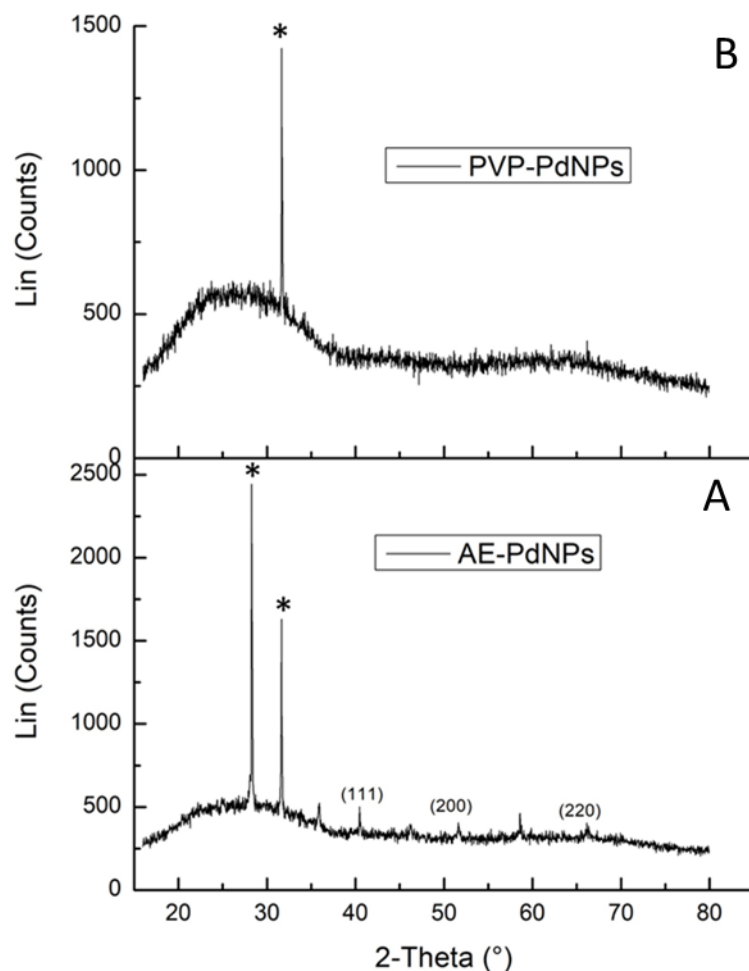
Figure 3.23: The XRD patterns for the PdNPs, AE-PdNPs (A) and PVP-PdNPs (B). The asterisks (*) indicate the presence of NaCl and KCl.

3.3.2.4. EDX (Energy Dispersive X-ray) analysis

The EDX data obtained provide information about the elemental composition of the sample. Figure 3.24 shows the expected palladium signals as well as the presence of carbon, oxygen, silica, and copper. Figure 3.24 also indicates the presence of sulphur and aluminium. The large peak for copper (Cu) is due to the copper grid that was used to hold the specimens under the electron microscope. The carbon and oxygen peaks are likely due to the presence of organic molecules such as polysaccharides and polyphenols (and absorbed O_2), while sulphur may be due to the presence of sulphated polysaccharides associated with brown algae. Silicon is often present in the samples prepared and may come from the glassware used. However, Al remains unaccounted for. The EDX analysis of the PVP-PdNPs was not run, due to the EDX equipment being down during the time that the synthesis and characterization of the PVP-PdNPs was carried out.
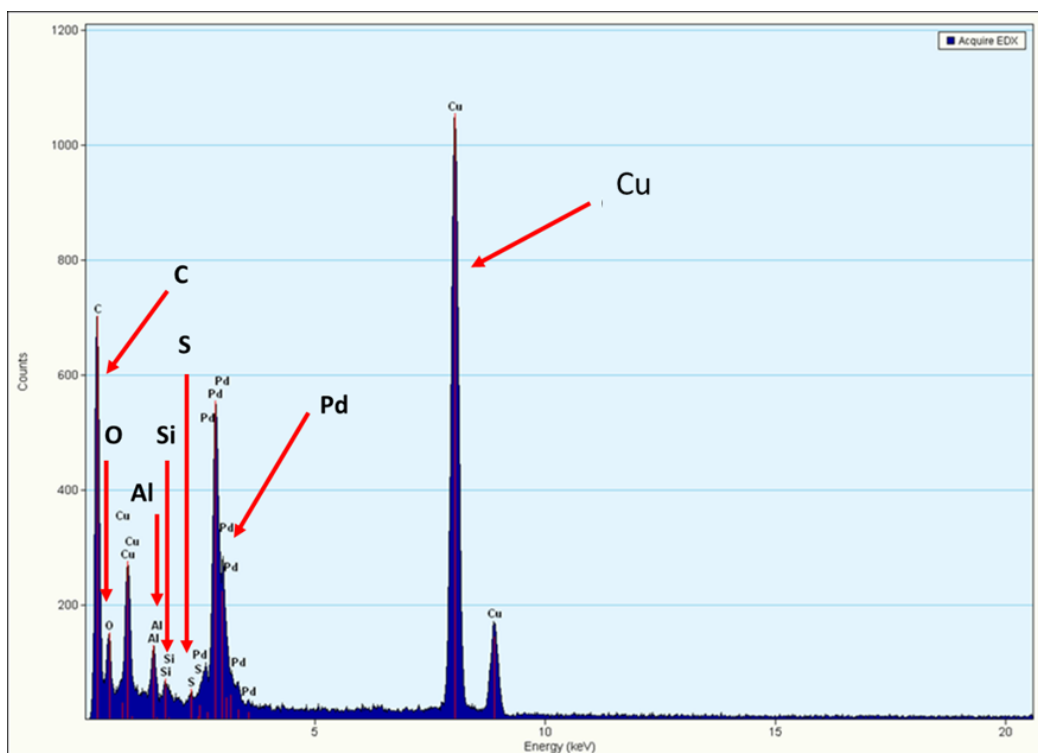
Figure 3.24: The EDX results obtained for the AE-PdNPs.

3.3.2.5. Zeta Potential and Dynamic Light Scattering (DLS)

The zeta potential was measured for both the AE- and PVP-PdNPs by making use of a Zetasizer. A zeta potential value of -17.50 mV was obtained for the AE-PdNPs, while a value of -9.69 mV was obtained for the PVP-PdNPs (Table 3.2). Helmenstine (2019) reported that nanoparticles which have a value greater than -15.00 mV will start to agglomerate, therefore the AE-PdNPs are regarded to be more stable than the PVP-PdNPs, as the PVP-PdNPs has a value that is closer to zero mV. Negative values were expected since polysaccharides are capping the NPs (Bozic, *et al*., 2018). Comparison between the two sets of NPs is difficult however, as different solvents were employed.

Table 3.1: Zeta Potential measurements for the different PdNPs, H_2O was used as a solvent for AE-PdNPs while ethanol was used for PVP-PdNPs.

Zeta Potential Measurements

	AE-PdNPs	PVP-PdNPs
Zeta potential	-17.50 mV	-9.69 mV
Standard Deviation	5.06 mV	18 mV
Conductivity	0.488 mS/cm	1.35 mS/cm
Effective Voltage	148.7 V	148.7 V

*H_2O was used as the solvent for AE-PdNPs, while ethanol was used for the PVP-PdNPs

55

The DLS measurements were also carried out and it reports on the hydrodynamic radius (d_H) of the NP. The hydrodynamic radius is the size of the NP together with the capping agent which is attached to the surface of the NPs (Mmola, *et al.*, 2016). The results obtained for the PdNPs indicates that the size of the PVP-PdNPs is larger (at 99.0 nm) than the AE-PdNPs (at 65.3 nm), the opposite of what was revealed by HR-TEM. The significant difference in size is due to the ease with which heavy metals are detected using HRTEM, while carbon (being a much lighter element) is not easily revealed. The size difference between the hydrodynamic radii for the PVP polymer capped PdNPs compared to the aqueous extracts (which are mostly composed of polysaccharides), is likely due to the larger molecular weight of the PVP polymer compared to the polysaccharide constituents. Taking the HR-TEM results into consideration, the PVP-PdNPs would have the least surface area available, as the NPs are smaller and the polymer closely surrounds the surface of the nanoparticles, which will make it less active in catalytic reactions.

Table 2.3: DLS Results obtained for the PdNPs. H_2O was used as a solvent for AE-PdNPs while ethanol was used for PVP-PdNPs.

Dynamic Light Scattering (DLS) Measurements

Sample	Hydrodynamic radius (d_H) nm	Polydispersity Index (PDI)
AE-PdNPs	65.28	0.320
PVP-PdNPs	99.01	0.207

The polydispersity index (PDI) presents information about the dispersity of the NPs. Mmola *et al*. (2016) and Bhatterjee (2016) reported that PDI values which are in the ranges of 0.2-0.5 are an indication of the broad size distribution for the nanoparticles. The results in Table 3.3 shows PDI values of 0.320 and 0.207 for the AE-PdNPs and PVP-PdNPs respectively. This correlates well with the broad size distribution shown in the HR-TEM images obtained for the NPs.

3.3.2.6. Inductively Coupled Plasma—Atomic Emission Spectroscopy (ICP-AES)

Table 3.4 shows the ICP-AES analysis results obtained for the PdNPs, given in mg/L (or ppm). The AE-PdNPs were found to contain 44.8 ppm, while the PVP-PdNPs sample contains 28.9 ppm of Pd. Therefore, the AE-PdNPs have a higher content of palladium loading. Since the same molar equivalents of Pd were used to produce the NPs and given that the assumption that all the Pd^{2+} ions are converted to Pd^0 to form PdNPs, it therefore means that the AE-PdNPs sample likely contains the most amount of Pd per sample. This assumption could be correct, as the HR-

TEM images do shows that the AE-PdNPs have the most PdNPs when compared with PVP-PdNPs.

Table 3.3: ICP-AES results obtained for the different PdNPs, where H_2O was used as a solvent.

ICP-AES Analysis	
Sample	**Pd (mg/L or ppm)**
AE-PdNPs	44.80
PVP-PdNPs	28.90

3.4. The catalytic activity of the PdNPs synthesized in Suzuki-Miyaura carbon-carbon coupling reactions

The catalytic activity for the AE-PdNPs was evaluated using a model carbon-carbon coupling reaction. The Suzuki-Miyaura coupling reaction employing phenylboronic acid and 4-iodoanisole was used. The scheme (Scheme 3.1) for the Suzuki-Miyaura reaction is shown below, where an organoboron species (**3.1**) is coupled with a halide (**3.2**) using a palladium NP catalyst and a base (K_2CO_3) to form a carbon-carbon single bond:
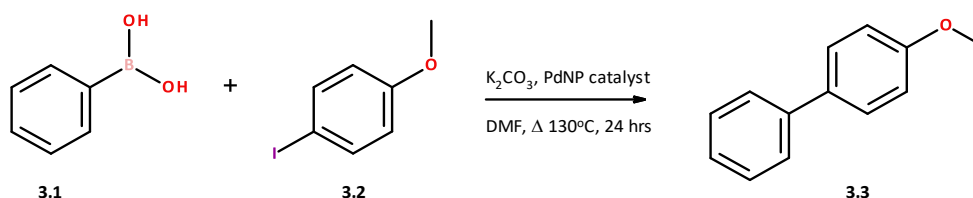
Scheme 3.1: Model Suzuki-Miyaura coupling reaction to produce the product 1-methoxy-4-phenyl benzene (3.3).

The Pd catalyst used in this study is the AE-PdNPs previously prepared. The set of NPs was tested for its catalytic ability in a model reaction, to see if it can be used as a catalyst in various organic reactions.

3.4.2.1. AE-PdNPs as the catalyst

Briefly, 25 mg of the freeze-dried aqueous extract (AE) was dissolved in 25 mL of deionized water to prepare a solution of 1 mg/mL. 14.25 mL of this solution was mixed with 750 µL of a K_2PdCl_4 (0.1M) solution containing 135 mL of deionized water. The synthesis was carried out for 24 h at 80°C under reflux.

Briefly, 18.4 mg of phenylboronic acid (**3.1**, 0.15 mmol eq.), 23.6 mg of 4-iodoanisole (**3.2**, 0.10 mmol eq.), 27.5 mg of potassium carbonate (0.20 mmol eq.), 1.8 mg of the AE-PdNPs catalyst (40.18 mL)and 400 µL of dimethylformamide were all added together in a round bottom flask and heated for 24 h at 130 °C under

inert conditions. The product formed was first extracted with diethyl ether and then with ethyl acetate. The organic layer was then dried under reduced pressure. The crude product was used as is.

The product obtained after extraction from the reaction mixture was not further purified and was analysed as is for NMR spectroscopy. During the first set of NMR analysis, there was no clear ^{13}C spectra, thus the compound was subjected to preparatory Thin Layer Chromatography (TLC) using 9:1, ethyl acetate: hexane as the eluent. 1D NMR data (^{1}H and ^{13}C spectra) were then successfully acquired for the product. The data obtained is tabulated in Table 3.5 in the experimental section.

The ^{1}H NMR spectrum (Figure 3.25) reveals aromatic proton signals in the region of 6.90 ppm – 7.60 ppm, which are expected for the compound. The aromatic signals integrate to 9 protons, consistent with the number of protons that are present on both the aromatic rings. The proton spectrum also hints at the highly symmetrical nature of the product, where the aromatic protons δ_H 6.95, 7.42, 7.54 (two doublets overlapping) integrate to 2. Figure 3.25 also reveals the characteristic signal expected for the methoxy group deshielded at 3.86 ppm, and integrating to 3 protons.
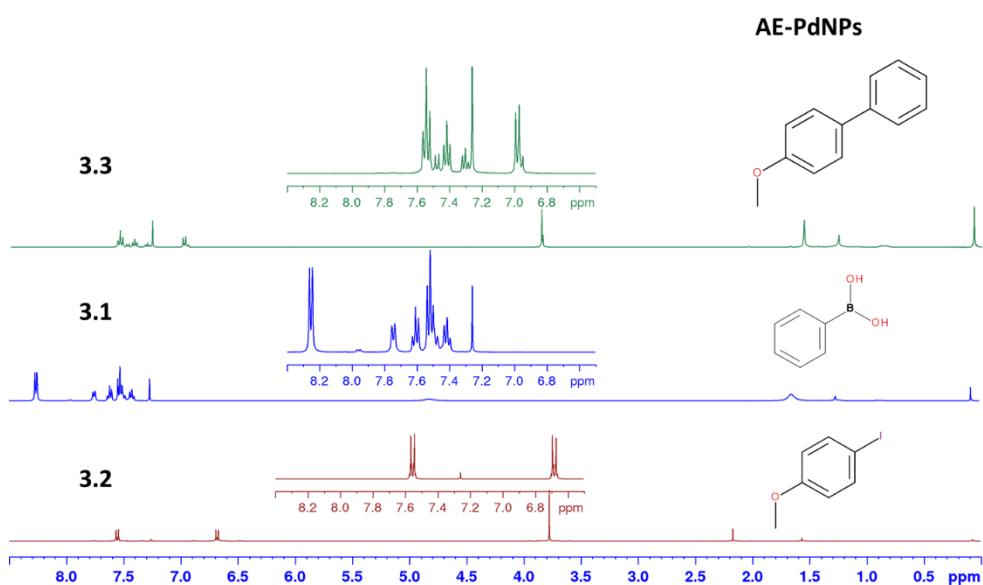
Figure 3.25: The ^{1}H spectrum (CDCl$_3$; 400 MHz) of 1-methoxy-4-phenyl benzene and the starting materials 3.1 and 3.2 (also in CDCl$_3$).

Figure 3.26 reveals the ^{13}C NMR spectrum for the compound, revealing 8 aromatic carbon signals as well as a signal characteristic of a methoxy carbon at δ_C 55.3 (C-9). There is no signal present at approximately 88.0 ppm, an indication that the

signal for the iodo-substituent has disappeared and that the 4-iodoanisole were converted to 1-methoxy-4-phenyl benzene. Once again, the symmetrical nature of the product is hinted by the intensity of the carbon signals. As is expected, the quaternary C signals at δ_C 159, 140 and 133 (C1, C2 and C3 respectively) are low in intensity. The intensity of the protonated aromatic signal at δ_C 126.6 is much less than its counterparts, revealing the position of this signal on the structure as C-7. The remaining signals were assigned by analysing the 1D and 2D data acquired for product 3.3. The data is tabulated in Table 3.5 in the experimental section 3.7 and the assignment compared to literature (since this is a well-known compound).
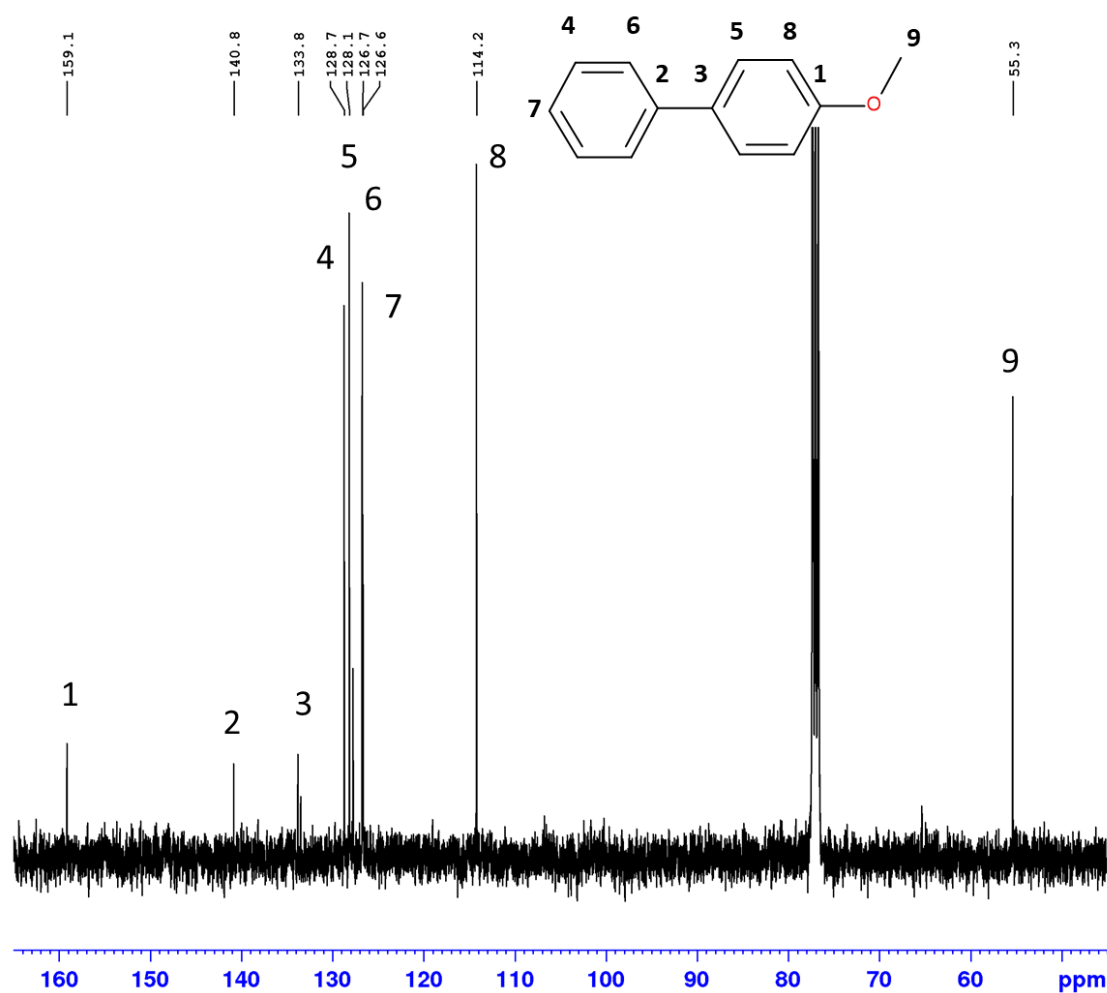
Figure 3.26: ^{13}C spectrum (CDCl$_3$; 100 MHz) of 1-methoxy-4-phenyl benzene. Inset: The proposed assignment of carbons on the structure.

3.5. Conclusion

It is clear that the aqueous extracts of *E. radiata* have the ability to form palladium nanoparticles. The antioxidant assays performed on the two aqueous extracts

59

(OAE and AE) showed that both samples have the potential to reduce the palladium metal ion Pd^{2+} to Pd^0 to form the PdNPs, with the AE sample outperforming the OAE extract in the total polyphenolic content (408.5 vs. 252.6 μg GAE/mg), total reducing power (926.8 vs. 201.8 μg AAE/mg) and radical scavenging (65% vs. 45%) assays. The organic extraction step, therefore, does not appear to be necessary with *E. radiata* in contrast to that reported by Mmola *et al.* (2016) for *Sargassum incisifolium*. The NMR spectra obtained for the kelp extract OAE and AE indicated that the main component present in both extracts are polysaccharides, while polyphenols were present as a minor constituent. Both polysaccharides and polyphenols are important in the generation of NPs, since the polysaccharides and polyphenols act as the capping and reducing agents, respectively.

The UV-visible spectra for both extracts indicated the disappearance of the absorbance peak at 430 nm of the metal salt which is attributed to Pd^{2+} being reduced to Pd^0, showing that the PdNPs form, as reported in the literature (Turunc, et al., 2017). The HR-TEM images obtained for the extract NPs show that that the NPs have a wide size distribution (averaging 11 nm) and are cubic in shape, while the images for PVP NPs show a variety of shapes, including triangles and cubes, and they are smaller in size (7 nm). The SAED images obtained for the NPs show that the AE-PdNPs appear to be more crystalline than the PVP-PdNPs. In addition, the AE-PdNPs are regarded to be more stable than the PVP-PdNPs, since the zeta potentials obtained are more negative for the AE-PdNPs (-17.5 mV) compared to the PVP-PdNPs (-9.7 mV), which indicates that the PVP-PdNPs will prefer to agglomerate and form bulky palladium materials. The DLS results showed that the overall (surface of NPs + capping agent) size of the AE-PdNPs is smaller than that of the PVP-PdNPs. This could mean that a smaller surface area would be available for the PVP-PdNPs, however testing them in catalytic reactions would be the only way to correctly assess their activity. The ICP-AES analyses revealed the AE-PdNPs to have a higher palladium content than the PVP-PdNPs. It would, therefore, be difficult to directly and adequately compare the results obtained for the two PdNP catalysts in the organic reactions.

AE-PdNPs were employed as a catalyst in a "proof of concept" or model Suzuki-Miyaura coupling reaction (Scheme 3.1). The reaction was successful in forming the 1-methoxy-4-phenyl benzene (**3.3**) model product.

The results that were obtained from the aqueous extracts of the brown marine algae *E. radiata* (kelp) appear to be promising when used in the biosynthesis of palladium nanoparticles (PdNPs). The biosynthetic protocol has been reported to be successful in the literature and could be used as a "Green" synthetic method for the synthesis of metallic nanoparticles (MNPs).

The use of the extracts (AE and OAE) to produce palladium nanoparticles (PdNPs) have been successful, based on the results obtained. The extracts (AE and OAE) both did reduce the palladium metal ion from as Pd^{2+} to Pd^0. This is further confirmed using UV-visible spectroscopy (as shown in section 3.3.2.1).

Therefore with the results showing that both extracts are able to form PdNPs, the AE sample appears to be best suited, as it complies with the Green Chemistry principles to make no/limit the use of organic solvents to improve the performance of the extract. Thus, only the AE-PdNPs were taken forward in the organic coupling reactions to be carried out.

3.6. Experimental data

Compound 3.3: 1-methoxy-4-phenyl benzene
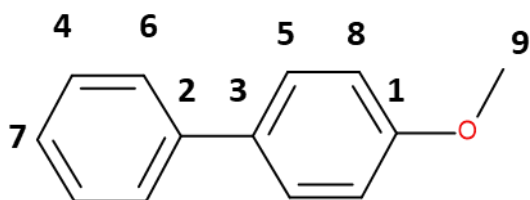
^{1}H NMR (CDCl$_3$, 400 MHz): 3.86 (s, H-9), 6.98 (d, 8.80 Hz, H-8), 7.30 (t, 8.80 Hz, H-7), 7.54* (m, H-6), 7.54* (m, H-5), 7.42 (t, 8.80 Hz, H-4). ^{13}C NMR (CDCl$_3$, 100 MHz): 159.1 (C-1), 140.8 (C-2), 133.8 (C-3), 128.7 (C-4), 128.1 (C-5), 126.7 (C-6), 126.6 (C-7), 114.2 (C-8), 55.3 (C-9).

* H-5 and H-6 have doublet signals that overlap and appear as a triplet in the ^{1}H NMR spectrum.

Table 3.4: Tabulated NMR data obtained from 1D and 2D NMR spectra for 1-methoxy-4-phenyl benzene (3.3).

Atom #	δC (mult.)	δH (integ., mult., *J*(Hz))	COSY	HMBC
1	159.1 (C)	-	-	-
2	140.8 (C)	-	-	-
3	133.8 (C)	-	-	-
4	128.7 (CH)	7.42 (2H, t, *J* = 8.8 Hz)	H-6, H-5, H-7	C-2
5 *	128.1 (CH)	7.54 (4H, m)	H-4, H-8	C-1, C-2, C-3
6 *	126.7 (CH)	7.54 (4H,m)	H-4	C-1, C-2, C-3, C-7
7	126.6 (CH)	7.30 (1H, t, *J* = 8.8 Hz)	H-4	C-6
8	114.2 (CH)	6.95 (2H, d, *J* = 8.8 Hz)	H-5, H-6	C-1, C-3
9	55.3 (CH_3)	3.86 (3H,s)	-	C-1

* H-5 and H-6 are overlapped.

3.7. Bibliography

Anderson, R., Stegenga, H. & Bolton, J., (2016). *Seaweeds of the South African South Coast.* [Online]
Available at: https://southafrseaweeds.uct.ac.za
[Accessed 17 October 2019].

Aseyev, S. A., Weber, P. M. & Ischenko, A. A. (2013) 'Ultrafast Electron Microscopy for Chemistry, Biology and Material Science', *Journal of Analytical Sciences, Methods and Instrumentation,* 3, pp. 30-53.

Bhatterjee, S. (2016) 'DLS and Zeta potential-What they are, what they are not?', *J.Control.Release,* 235, pp. 337-351.

Bozic, M., Elschner, T., Tkancic, D., Hribernik, S., Kleinschek, K. S. and Kargl, R. (2018) 'Effect of different surface active polysaccharide derivatives on the formation of ethyl cellulose particles by the emulsion-solvent evaporation method', *Cellulose,* 25, pp. 6901-6922.

Eustis, S. & El-Sayed, M. A. (2006) 'Why gold nanoparticles are more precious than pretty gold: Noble metal surface plasmon resonance and its enhancement of the radiative and nonradiative properties of nanocrystals of different shapes', *Chem. Soc.Rev.,* 35, pp. 209-217.

Giannini, C., Ladisa, M., Altamura, D., Siliqi, D., Sibillano, T. and De Caro, L. (2016) 'X-ray Diffraction: A Powerful Technique for the Multiple-Length-Scale Structural Analysis of Nanomaterials', *Crystals,* 6(8), pp. 1-22.

Gomez-Guzman, M., Rodriguez-Nogales, A., Algieri, F. & Galves, J. (2018) 'Potential role of seaweed Polyphenols in Cardiovascular-Associated Disorder', *Marine Drugs,* 66(250), pp. 1-21.

Gomez-Ordonez, E. & Ruperez, P. (2011) 'FTIR-ATR spectroscopy as a tool for polysaccharide identification in edible brown and red seaweeds', *Food Hydrocolloids,* 25, pp. 1514-1520.

Guiry, M. & Guiry, G., (2019). *AlgaeBase.* [Online]
Available at: https://www.algaebase.org
[Accessed 3 October 2019].

Hamers, L., (2014). *Nano-Sensors: Small size, big impact.* [Online]
Available at: http://sustainable-nano.com/2014/09/23/nano-sensors-small-size-big-impact/
[Accessed 29 October 2019].

Helmenstine, . A. M., (2019). *Definition of Zeta Potential.* [Online]
Available at: https://www.thoughtco.com/definition-of-zeta-potential-605810
[Accessed 25 September 2019].

Jiang, Y. & Gao, Q. (2006) 'Heterogeneous Hydrogenation Catalyses over Recyclable Pd(0) Nanoparticle Catalysts Stabilized by PAMAM-SBA-15 Organic-Inorganic Hybrid Composites', *J. Am. Chem. Soc.,* 128(3), pp. 716-717.

Kettemann, F., Wuithschick, M., Caputo, G., Kraehnert, R., Pinna, N., Rademann, K. and Polte, J. (2015) 'Reliable palladium nanoparticle syntheses in aqueous solution: the importance of understanding precursor chemistry and growth mechanism', *CrystEngComm,* 17, pp. 1865-1870.

Kripal, R., Gupta, A. K., Srivastava, R. K. & Mishra, S. K. (2011) 'Photoconductivity and photoluminescence of ZnO nanoparticles synthesized via co-precipitation method', *Spectrochim. Acta Part A: Mol. Biomol. Spec.,* 79, p. 1605– 1612.

Li, Y., Boone, E. & El-Sayed, M. A. (2002) 'Size Effects of PVP-Pd Nanoparticles on the Catalytic Suzuki Reactions in Aqueous Solution', *Langmuir,* 18, pp. 4921-4925.

Manzoor, U., Islam, M., Tabassam, L. & Rahman, S. U. (2009) 'Quantum confinement effect in ZnO nanoparticles synthesized by co-precipitate method', *Physica E,* 41, p. 1669–1672.

Mmola, M., Le Roes-Hill, M., Durrell, K., Bolton, J. J., Sibuyi, N., Meyer, M. E., Beukes, D. R. and Antunes, E. (2016) 'Enhanced Antimicrobial and Anticancer Activity of Silver and Gold Nanoparticles Synthesised Using *Sargassum incisifolium* Aqueous Extracts', *Molecules,* 21(1633), pp. 1-22.

Momeni, S. & Nabipour, I. (2015) 'A Simple Green Synthesis of Palladium Nanoparticles with *Sargassum* Alga and Their Electrocatalytic Activities Towards Hydrogen Peroxide', *Appl. Biochem. Biotechnol.,* 176, pp. 1937-1949.

Monsur, H. A., Jaswir, I., Simsek, S., Amid, A. and Alam, Z. (2017) 'Chemical structure of sulfated polysaccharides from brown seaweed (*Turbinaria turbinata*)', *International Journal of Food Properties,* 20(7), pp. 1457-1469.

Narayanan, R. & El-Sayed, M. A. (2003) 'Effect of Catalysis on the Stability of Metallic Nanoparticles:Suzuki Reaction Catalyzed by PVP-Palladium Nanoparticles', *J. Am. Chem. Soc.,* 125, pp. 8340-8347.

Oliveira, D. G., Rosa, C. H., Vargas, B.P., Rosa, D. S., Silveira, M. V., de Moura, N.F. and Rosa, G. R. (2015) 'Introducing Undergraduates to Research Using a Suzuki–Miyaura cross-coupling organic chemistry miniproject', *J. Chem. Edu.,* 92, p. 1217–1220.

Quintanilla, A., Butselaar-Orthlieb, V. C. L., Kwakernaak, C., Sloof, W. G., Kreutzer, M. T. and Kapteijn, F. (2010) 'Weakly bound capping agents on gold nanoparticles in catalysis: Surface poison?', *J. Catal.,* 271, pp. 104-114.

Rajan, K., Roppolo, I., Chiappone, A., Bocchini, S., Perrone, D. and Chiolerio, A. (2016) 'Silver nanoparticle ink technology: state of the art', *Nanotechnology, Science and Applications,* 9, p. 1–13.

Shekhar, S. H. S., Lyons, G., McRoberts, C., McCall, D., Carmichael, E., Andrews, F. and McCormack, R. (2012) 'Brown seaweed species from Strangford Lough: compositional analyses of seaweed species and biostimulant formulations by rapid instrumental methods', *J. Appl. Phycol.,* 24(5), pp. 1141-1157.

Tobwala, S., Fan, W., Hines, C. J., Folk, W. R. and Ercal, N. (2014) 'Antioxidant potential of *Sutherlandia frutescens* and its protective effects against oxidative stress in various cell cultures', *BMC Complementary and Alternative Medicine,* 14(271), pp. 1-11.

Turunc, E., Binzet, R., Gumus, I., Binzet, G. and Arslan, H. (2017) 'Green synthesis of silver and palladium nanoparticles using *Lithodora hispidula* (Sm.) *Griseb*. (*Boraginaceae*) and application to the electrocatalytic reduction of hydrogen peroxide', *Materials Chemistry and Physics*, 202, pp. 310–319.

Viswadevarayalu, A., Ramana, P. V., Sumalatha, J. & Reddy, S. A. (2016) 'Biocompatible Synthesis of Palladium Nanoparticles and Their Impact on Fungal Species', *Journal of Nanoscience and Technology,* 2(3), p. 169–172.

Chapter 4: Application of palladium nanoparticles in coupling reactions

4.1. Introduction

This chapter deals with the application of the various palladium nanoparticles synthesized for catalysis in the assorted carbon-carbon coupling reactions. In this chapter, the catalytic activity and selectivity of the AE-PdNPs are compared to the model PVP-PdNPs. Chapter 4 is divided into three sections according to the reactions employed:

1st section (Section 4.3.1) deals with:

- the materials and the synthetic routes employed for the Suzuki-Miyaura carbon-carbon coupling reactions.
- the results obtained from the various Suzuki-Miyaura coupling reactions for both sets of PdNPs.

Section one concludes with a comparison of the results for the NPs.

2nd section (Section 4.3.2) deals with:

- the materials and the synthesis method used for the Heck carbon-carbon coupling reactions.
- the results obtained from the various Heck coupling reactions for both the PdNPs.

Section two concludes with the results being compared with each other.

3rd section (Section 4.3.3) briefly deals with:

- the materials and synthetic protocol of the Sonogashira carbon-carbon coupling reactions.
- the results obtained from the various Sonogashira coupling reactions for both the PdNPs.

The chapter concludes with the final view from the results obtained for the catalytic reactions.

4.2. Materials and Methods

4.2.1. Materials

Phenylboronic acid, 4-iodoanisole, 4-bromoacetophenone, 4-iodoacetophenone, potassium carbonate, dimethylformamide, 1-iodo-2-nitro-benzene, 1-iodo-4-nitro-benzene, anhydrous sodium sulphate, phenylacetylene, butyl acrylate, tributylamine (TBA), tetrabutylammonium acetate (Bu$_4$NOAc) and ethyl acetate were all purchased from Sigma Aldrich and used without further purification.

4.2.2. General procedures

4.2.2.1 Suzuki-Miyaura carbon-carbon coupling reaction
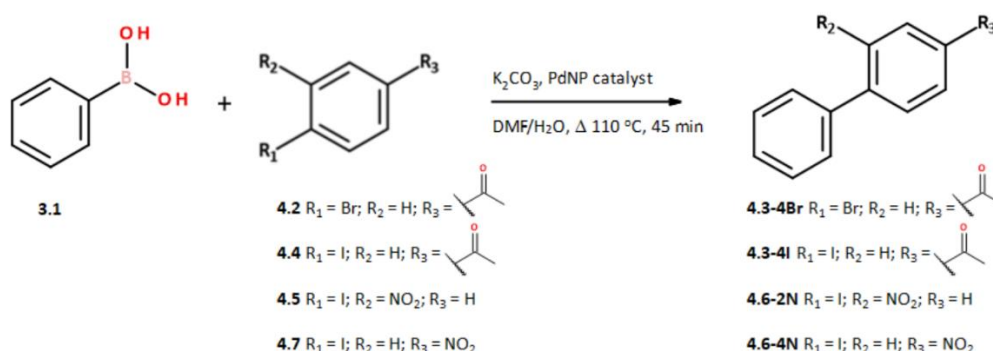
Scheme 4.1: General synthetic procedure used in the Suzuki-Miyaura reaction

Representative procedure:

The synthetic protocol used was modified and adopted from literature (Trilla, *et al.,* 2008), where 0.131 g of phenylboronic acid (**3.1**, 1.05 mmol), 0.143 g of 4-bromoacetophenone (**4.2**, 0.7 mmol) or 0.172 g of 4-iodoacetophenone (**4.4**, 0.7 mmol), 0.194 g of K$_2$CO$_3$ (1.4 mmol), 7.22 mL (0.32 mg Pd) of the AE-PdNPs (or 7.22 mL of PVP-PdNP) catalyst and 1.4 mL of a DMF/H$_2$O (95:5) water mixture was all added in sequence together and allowed to reacted in a 100 mL round bottom flask (RBF) under inert conditions for 45 min at 110 °C. After the reactions were completed, water was added to the RBF and the mixture filtered under vacuum. The product formed was extracted with ethyl acetate and the organic layer separated from the aqueous layer. The organic layer was dried over anhydrous sodium sulphate and passed through a syringe fitted with cotton wool to trap any of the sodium sulphate and other large particles. The solvent was removed under reduced pressure to give the crude products. The samples were not purified further. Instead of 4-iodoacetphenone, 1-iodo-2-nitrobenzene (**4.5**) and 1-iodo-4-nitrobenzene (**4.7**) were employed as substrates using the same reaction conditions.

4.2.2.2 Heck carbon-carbon coupling reaction

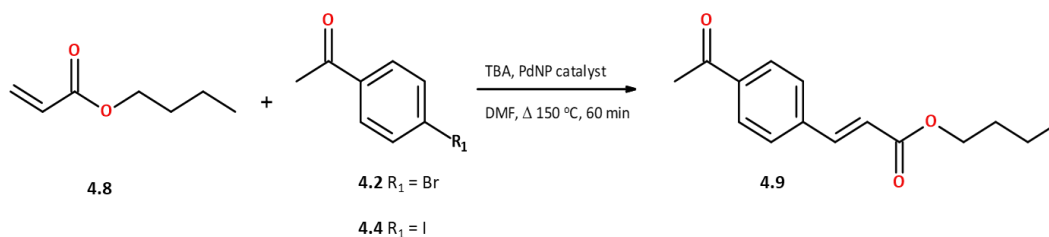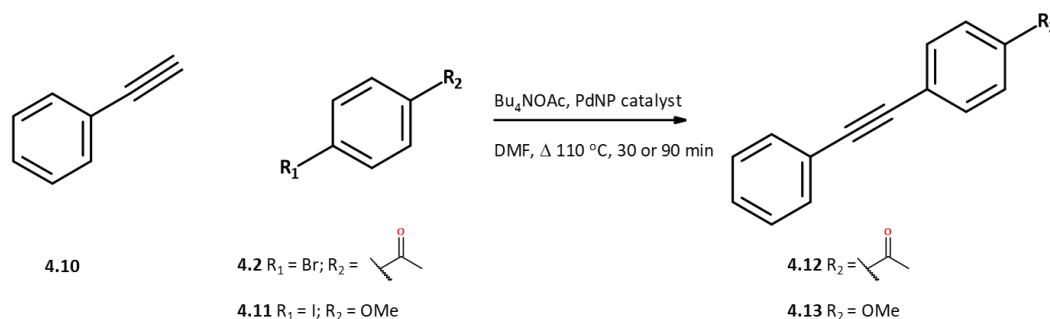Scheme 4.2: General synthetic procedure used in the Heck reaction.

Representative procedure:

The synthetic protocol used was modified and adopted from literature (Trilla, *et al.*, 2008), where *n*-butyl acrylate (**4.8**, 655 µL, 4.5 mmol), 0.61 g of 4-bromoacetophenone (**4.2**, 3 mmol) or 0.738 g of 4-iodoacetophenone (**4.4**, 3 mmol), tributylamine (TBA, 1075 µL, 4.5 mmol), 3.61 mL (0.16 mg Pd) of the AE-PdNPs (or 3.61 mL of PVP-PdNP) catalyst and 2.00 mL of a DMF was all added together and allowed to reacted in a 100 mL RBF under inert conditions for 60 min at 150 °C. After the reactions were finished, water was added to the RBF and the mixture filtered under vacuum. The product formed was extracted with ethyl acetate and the organic layer was separated from the aqueous layer. The organic layer was dried over anhydrous sodium sulphate and passed through a syringe fitted with cotton wool to trap any of the sodium sulphate and other large particles. The solvent was removed under reduced pressure to give crude product (**4.9**).

4.2.2.3 Sonogashira carbon-carbon coupling reaction

Scheme 4.3: General synthetic procedure used in the Sonogashira reaction.

Representative procedure:

The synthetic protocol used was modified and adopted from literature (Trilla, *et al.*, 2008), where phenylacetylene (**4.10**, 505 µL, 4.5 mmol), 0.61 g of 4-bromoacetophenone (**4.2**, 3 mmol) or 0.709 g of 4-iodoanisole (**4.11**, 3 mmol), Bu$_4$NOAc (1.398 g, 4.5 mmol), 12.0 mL (0.54 mg Pd) of AE-PdNPs (or 12.0 mL of

PVP-PdNP) catalyst and 2.0 mL of a DMF was all added together and allowed to react in a 100 mL RBF under inert conditions for 30 or 90 min at 110 °C. After the reactions were done, water was added to the RBF and mixture were filtered under vacuum. The product formed was extracted with ethyl acetate and the organic layer was separated from the aqueous layer. The organic layer was dried over anhydrous sodium sulphate and passed through a syringe fitted with cotton wool to trap any of the sodium sulphate and other large particles. The solvent was removed under reduced pressure, which allows for a resulting crude product (**4.12** or **4.13**) to be collected.

4.2.2.4: Yield calculations

The yields of the products were calculated using quantitative NMR (qNMR), as qNMR is considered to be a very sensitive and accurate technique often used in synthetic chemistry (Rizzo & Pincriroli, 2005). The method involved the use of an internal standard and the sample was prepared so that the sample solution contains 10.022 mM DCM in 500 µL of $CDCl_3$, to which 20 mg of each sample was added. The data was then analysed using the Bruker Topspin 4.0.7 qNMR software.

4.2.2.5: UV-visible spectroscopy

UV-visible analyses were also used as a quick analytical tool to determine whether the products had indeed formed and to obtain additional information. UV-vis spectra were acquired on the starting materials and the products that formed. Distilled DCM was used as the solvent and as a blank. Briefly, stock solutions were prepared with a concentration of 1mg/mL. For the analysis, 40 µL of the stock solution was mixed with 2.96 mL of DCM to obtain a final volume of 3.00 mL.

4.3. Results and discussion

Each of the Suzuki-Miyaura, Heck and Sonogashira carbon-carbon coupling reactions were carried out in duplicate using the two PdNPs synthesized i.e. the AE-PdNPs and PVP-PdNPs. The products that were obtained were labelled AE and PVP for the reactions carried out with AE-PdNPs and PVP-NPs, respectively.

4.3.1. Suzuki-Miyaura coupling reaction

4.3.1.1 Reaction of halogenated acetophenones with phenylboronic acid (SM1 and SM2)

The Suzuki-Miyaura carbon-carbon coupling reactions with halogenated acetophenones was done with phenylboronic acid as a starting material. The halogenated acetophenones that were chosen were 4-bromoacetophenone and 4-iodoacetophenone and these were chosen to determine whether the PdNP catalysts showed any selectivity and also to understand which halogenated acetophenone (I or Br) is preferred by the respective catalyst. Of the two halogenated acetophenones, a preference for the 4-iodoacetophenone is expected, as the iodo group will be a better leaving group than the bromo substituent, since the former is less electronegative than the bromo group.

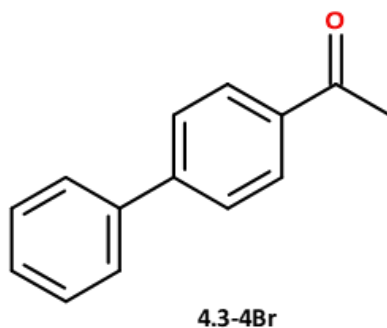*4-Bromoacetophenone as the substrate (SM1):*

4.3-4Br

Figure 4.1: The product 1-(4-phenylphenyl)ethanone (4.3-4Br).

Following the reaction of the organohalide with the boronic acid using both sets of PdNPs, the product 1-(4-phenylphenyl)ethanone (**4.3-4Br**) (denoted SM1 for the bromo-substituted starting material) was extracted successfully, and the sample was not was not subjected to a purification step in order to assess the success of the reaction. Purification of the compound may introduce a loss of product, resulting in errors when calculating the percentage yield. The crude product obtained was a white, flakey powder in a 91.45 and 89.70 % yield for the AE- and PVP-PdNPs, respectively. 1D data (^{1}H and ^{13}C spectra), as well as 2D NMR data (COSY, HSQC, HMBC), were acquired for the product. The product was therefore fully assigned as seen in Figure 4.4, and the data tabulated in Table 4.1.

The ^{1}H NMR spectra obtained for the starting materials (**3.1** and **4.2**; labelled reaction SM1) used and the product 1-(4-phenylphenyl)ethanone (**4.3-4Br**) using both the AE-and PVP-PdNPs as catalysts is shown in Figure 4.2. The

disappearance/residual presence of the proton signal at δ_H 8.25 (B-O$\underline{H_2}$) can serve as an indication of the success of the coupling reaction. Both sets of spectra (Figure 4.2 C and D) reveal the expected aromatic signals in the δ_H 7.35-8.05 ppm region that integrates to 9 protons, as well as a methyl signal (integrating to 3) at δ_H 2.64 ppm. The spectrum obtained for the PVP-PdNPs (Figure 4.2 D) also shows the presence of residual DMF (at $\sim\delta_H$ 3.0).
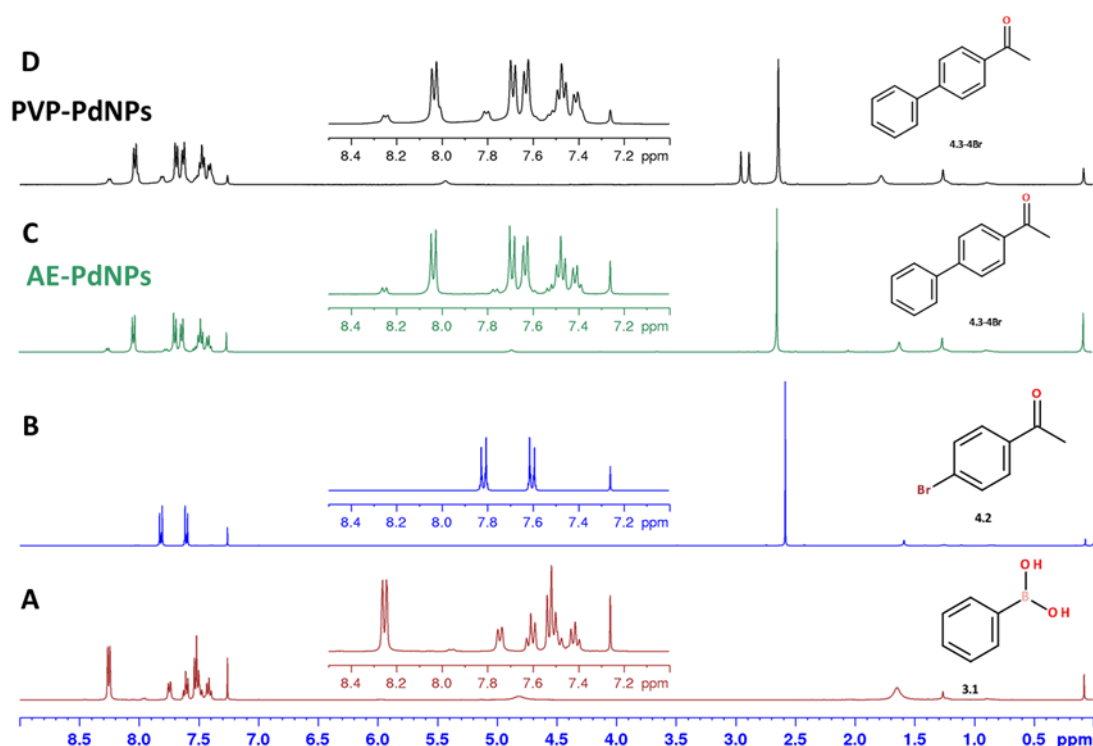
Figure 4.2: ^1H NMR data (CDCl$_3$, 400 MHz) for the SM1 reaction product 1-(4-phenylphenyl)ethanone (4.3-4Br, C, D) using the AE-PdNPs (C) and PVP-PdNPs (D) as catalysts. The starting materials phenylboronic acid (A) and 4-iodoacetophenone (B) are also shown

Figure 4.3 shows the ^{13}C spectra for the product 1-(4-phenylphenyl)ethanone (**4.3-4Br**), revealing 9 aromatic carbon signals (where 2 sets of carbon signals have double the intensity of other protonated carbons due to chemical equivalence), one deshielded carbon signal at δ_C 196.8 for the ketone and one methyl carbon that resonating at δ_C 25.7 ppm.
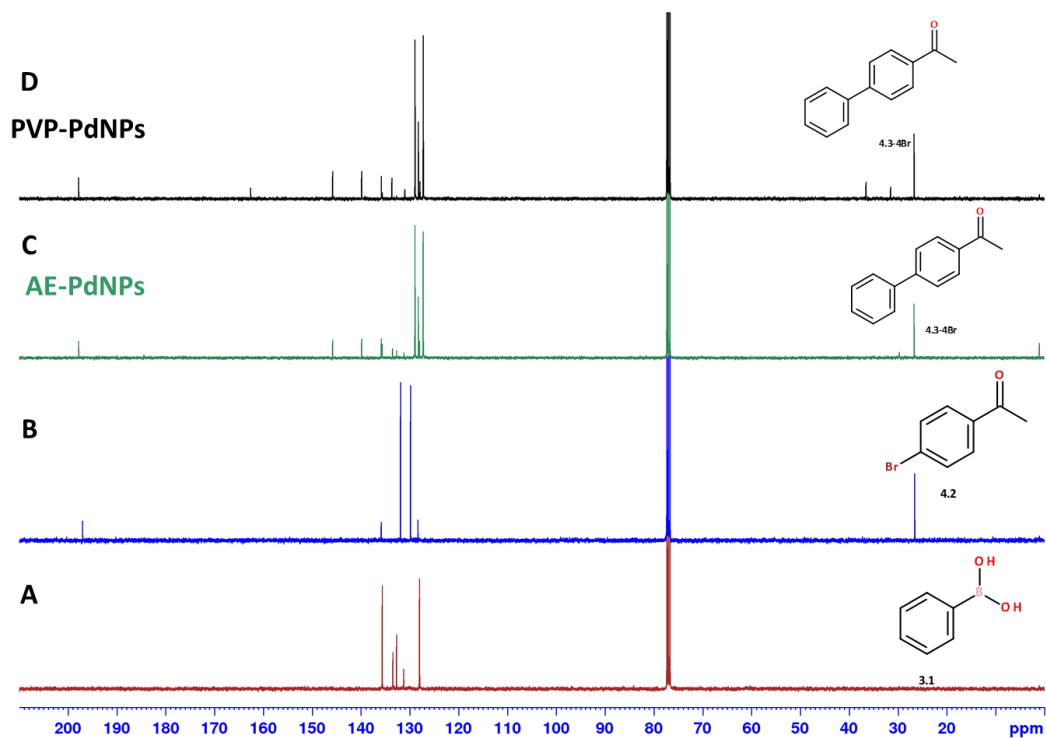
Figure4.3: The ^{13}C NMR data (CDCl$_3$) for the product 1-(4-phenylphenyl)ethanone (4.3-4Br, C, D) from AE-PdNPs (C) and PVP-PdNPs (D) as catalysts. The starting materials phenylboronic acid (A) and 4-iodoacetophenone (B) is also shown.

The HMBC experiment (Figure 4.4) is the most useful of all the 2D experiments as it provides data regarding the connectivity between the two aromatic rings and as well as the ketone moiety. It also helps with the assignment of carbon atoms and serves as confirmation a successful reaction. Important correlations were observed between H10 and C1, between H9 and C3, and between H8 and C2 (Figure 4.5). The data obtained is tabulated in Table 4.1. Figure 4.5 illustrates the central correlations observed for 1-(4-phenylphenyl)ethanone (**4.3-4Br**). Additional correlations were observed, and all assisted with the assignment of the different atoms.

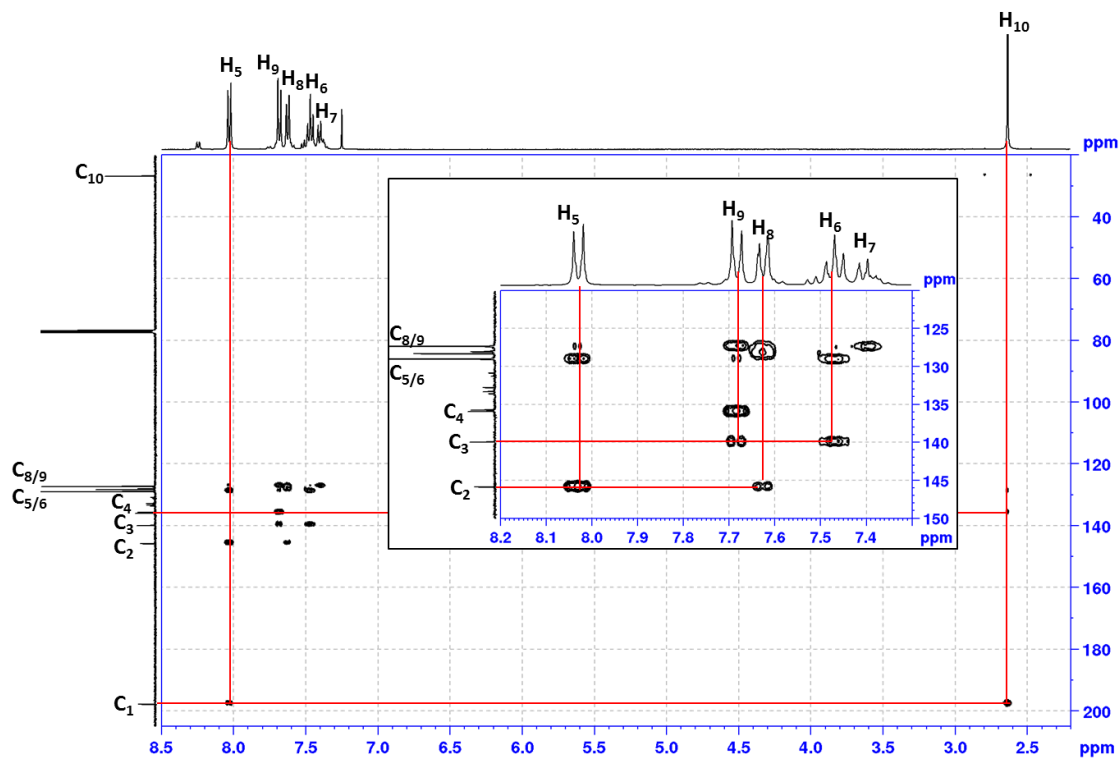*Figure 4.4: The HMBC spectrum (CDCl₃) for 1-(4-phenylphenyl)ethanone (4.3-4Br).*

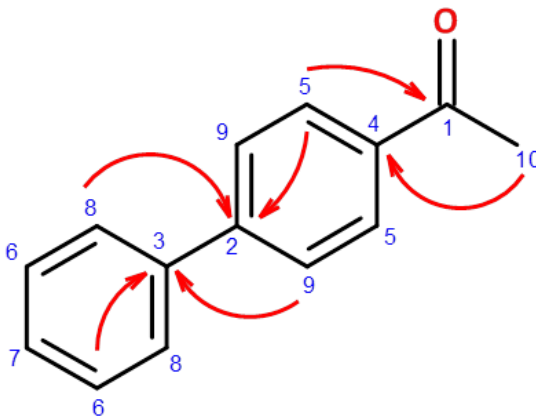*Figure 4.5: The important correlations which illustrate the formation of 1-(4-phenylphenyl)ethanone (4.3-4Br), the numbering is based on ^{13}C chemical shift.*

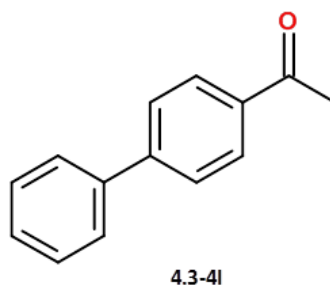*4-Iodoacetophenone as the substrate (SM2):*

4.3-4I

Figure 4.6: The product 1-(4-phenylphenyl)ethanone (4.3-4I).

After the product 1-(4-phenylphenyl)ethanone (**4.3-4I**) obtained was extracted, it was not purified to assess the success of the reaction. The crude product obtained was a white-light yellow, flakey powder in a 91.84 and 89.29 % yield for the AE- and PVP-PdNPs, respectively. 1D data (^{1}H and ^{13}C spectra), as well as 2D data (COSY, HSQC, HMBC), were acquired for the product. The product was therefore fully assigned as **4.3-4I** (Figure 4.9), and the data tabulated in Table 4.1.

The ^{1}H NMR spectra for the product 1-(4-phenylphenyl)ethanone (**4.3-4I**) using both the AE- and PVP-PdNPs as catalysts in reaction SM2 (denoted SM2 for the iodo-substituted starting material) is shown in Figure 4.7. The expected aromatic signals in the 7.35-8.05 ppm region were once again found to integrate to 9 protons, while a deshielded methyl signal (integrating to 3H) was observed at 2.64 ppm. Some residual boronic acid starting material was once again observed at ~8.25 ppm. However, no unreacted iodo-acetophenone was found in the product spectra.

Figure 4.7: The ^{1}H NMR data (CDCl$_3$, 400 MHz) for the product 1-(4-phenylphenyl)ethanone (4.3-4I, C, D) from AE-PdNPs (C) and PVP-PdNPs (D) as catalysts. The starting materials phenylboronic acid (A, in DMSO-d6) and 4-iodoacetophenone (B) is also shown.

Figure 4.8 shows the ^{13}C spectra obtained for the product 1-(4-phenylphenyl)ethanone (**4.3-4I**) and it is revealing 9 aromatic carbon signals where 2 sets of methane carbon signals had double the intensity of other protonated carbons, showing the chemical equivalence of the carbon signals, a signal at δ_C 196.8 attributed to the ketone and one methyl carbon resonating at 25.7 ppm.
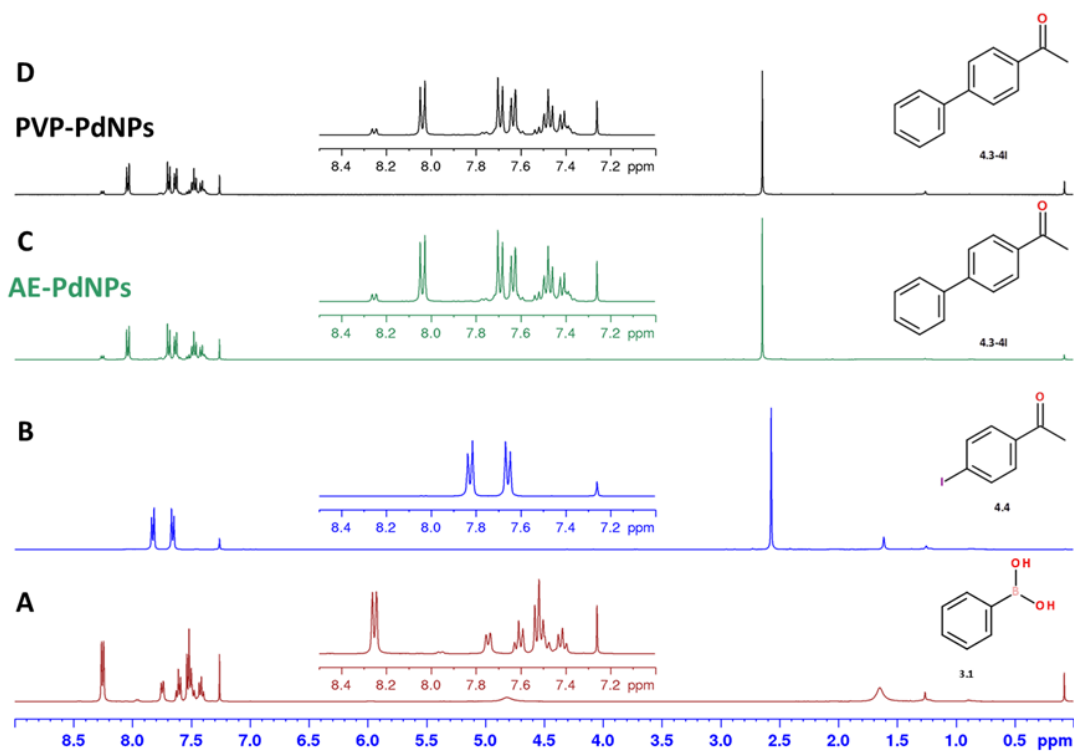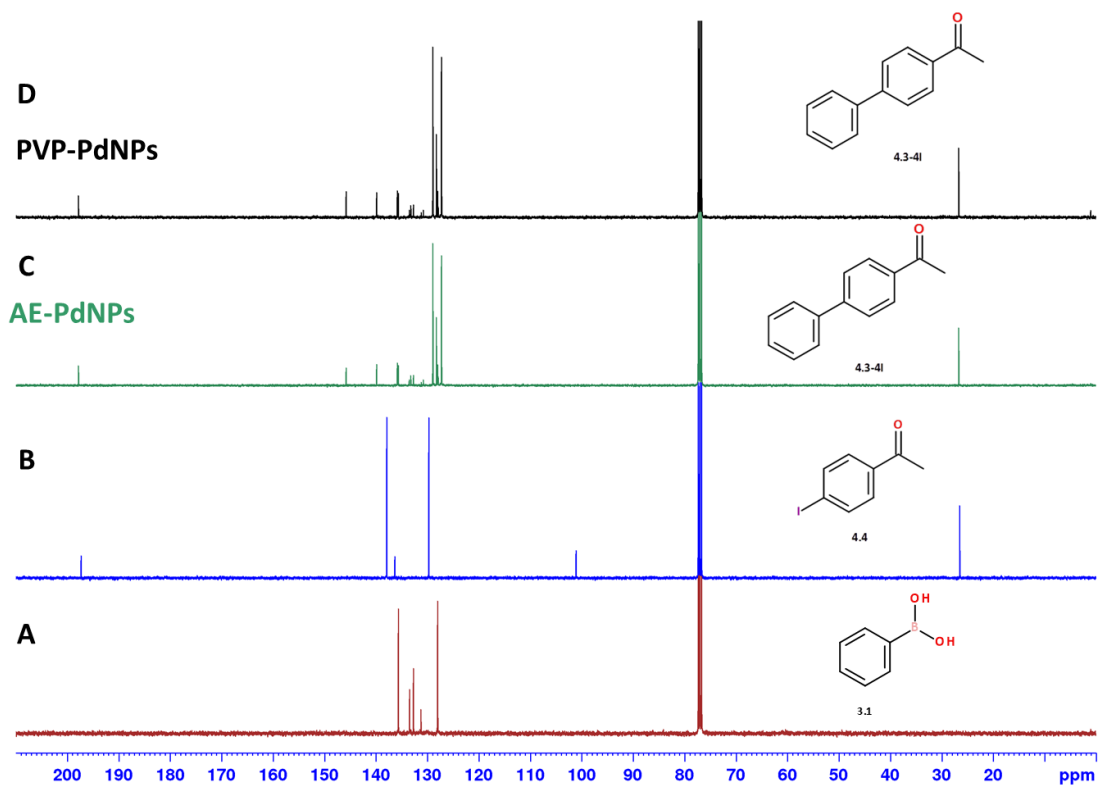
Figure 4.8: The ¹³C NMR data (CDCl₃; 100 MHz) for the product 1-(4-phenylphenyl)ethanone (4.3-4I, C, D) from AE-PdNPs (C) and PVP-PdNPs (D) as catalysts. The starting materials phenylboronic acid (A) and 4-iodoacetophenone (B) is also shown.

Figures 4.9 illustrates the same key 2D correlations observed for the 1-(4-phenylphenyl)ethanone (**4.3-4I**) product. These correlations were identical to those of compound **4.3-4Br** and will not be discussed further.

Figure 4.9: The important correlations which illustrate the formation of 1-(4-phenylphenyl)ethanone (4.3-4I), the numbering is based on ¹³C chemical shift.

Table 4.1: Representative NMR data obtained for the products 1-(4-phenylphenyl) ethenone (4.3-4Br and 4.3-3I).

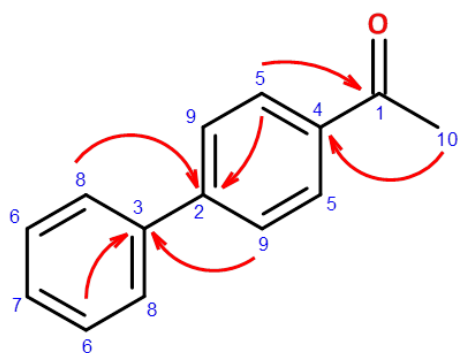| Atom #	Δ_C (mult.)	δ_H (integ., mult., J(Hz))	COSY	HMBC
1	196.8(C)	-	-	-
2	144.8 (C)	-	-	-
3	138.9 (C)	-	-	-
4	134.8(C)	-	-	-
5	127.9 (CH)	8.04 (2H, d, 8.2 Hz)	H6	C1, C2, C6
6	127.9 (CH)	7.48 (2H, t, 7.3 Hz)	H5	C3, C5
7	127.2 (CH)	7.42 (1H, d, 7.3 Hz)	H8	C9
8	126.3 (CH)	7.69 (2H, d, 8. 2 Hz)	H7, H9	C3, C4, C9, (C5/C6)
9	126.2 (CH)	7.63 (2H, d, 8.2 Hz)	H8	C7
10	25.7 (CH$_3$)	2.64 (3H, s)	-	C1

The reaction sequence SM2 is expected to produce the same product as SM1, since a change in the halogenated acetophenones should not cause a different product to form. GC-EIMS data collected for the products obtained from SM1 and SM2 coupling reactions both revealed a base peak corresponding to the molecular ion at 196.2 amu, which is the expected mass of the product 1-(4-phenylphenyl)ethanone (Figure 4.10) at a retention time of 24.4 min for both catalysts (Table 4.4). The same molecular ion peak was reported by (Islam, et al., 2010). Alpha cleavage of the methyl group leads to formation of the mass fragment *m/z* 181.2, which is then followed by the loss of carbon monoxide to give fragment *m/z* 152.2 (Figure 4.10).

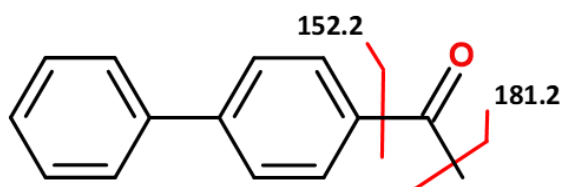*Figure 4.10: The major mass fragments obtained for both 1-(4-phenylphenyl)ethanone (m/z 192.2) products, 4.3-4I and 4.3-4Br.*

The mass spectroscopic data thus illustrates the successful formation of compound 1-(4-phenylphenyl)ethenone. The GC-MS data is tabulated in Table 4.4.

FTIR data (Figure 4.11) of the products formed from the SM1 and SM2 reactions revealed notable peaks at 2998 cm^{-1} and assigned as a C-H stretch of alkanes. Peaks at 1677 cm^{-1} and 1601 cm^{-1} were assigned to the ketone and alkenes of the aromatic ring system, respectively (Trilla, *et al.*, 2008).
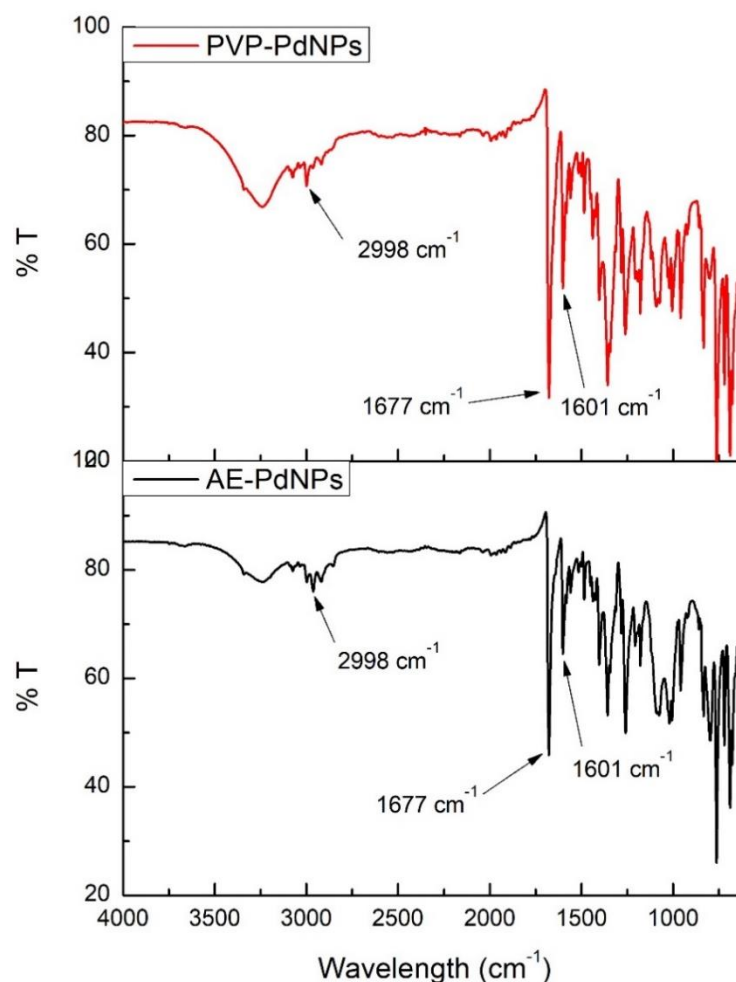
Figure 4.11: The FTIR spectra of 1-(4-phenylphenyl)ethanone produced using the two PdNP catalysts.

Using DCM as a solvent, UV-Visible spectra (Figure 4.12) were also collected on the starting materials and the products formed via the SM1 and SM2 reactions, since a substantial red shift is expected because of the increase in conjugation upon formation of the product. Phenyl boronic acid reveals a λ_{max} at ~230 nm and a small, broad absorption band at 270 nm. 4 bromoacetophenone shows a λ_{max} at 255 nm, with the 4-iodoacetophenone revealing a 15 nm red shift to give a λ_{max} at 270 nm. All four products produced revealed the expected red shift in wavelength to give a λ_{max} at 284 nm. Although the extinction coefficient was not calculated for

the samples, the product produced using the PVP-PdNPs catalyst and the iodo substrate, produced the most intense absorption. This may be due to a calculation error in preparing the sample solution. The spectra for the products also hint at traces of the phenylboronic acid starting material (at 230 nm), as also seen in the ^{1}H NMR spectra.

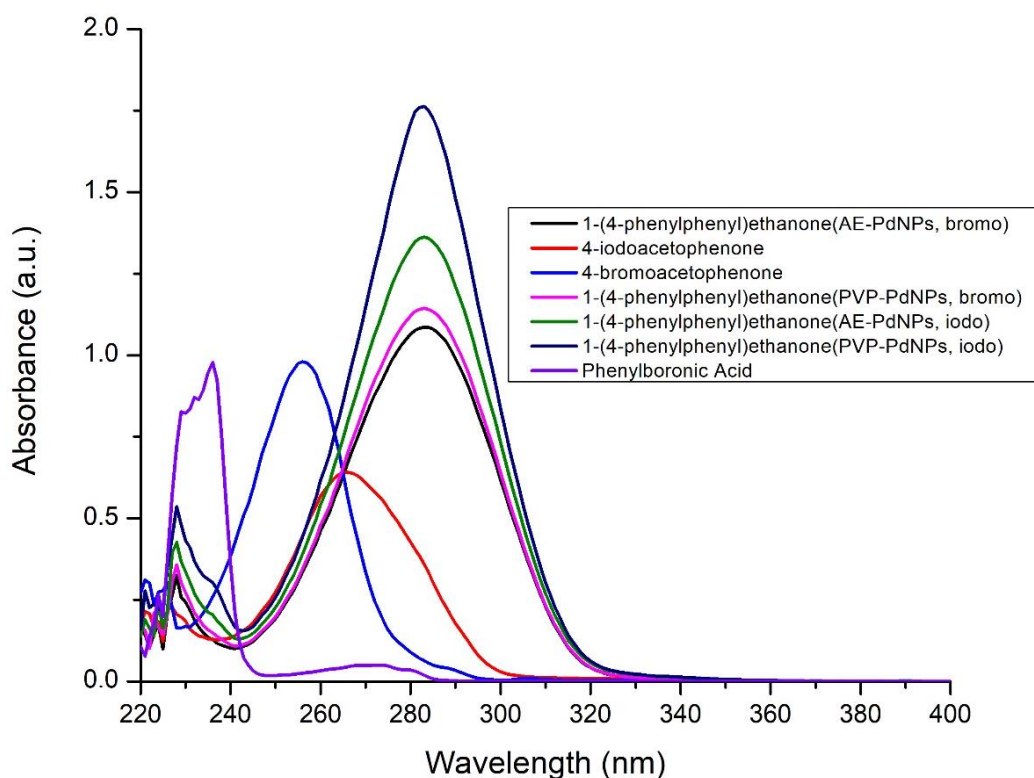*Figure 4.12: The UV-visible spectra obtained for the starting materials and products 1-(4-phenylphenyl)ethanone, all λ$_{max}$ at 284 nm. (Solvent DCM).*

4.3.1.2 Reaction of halogenated nitrobenzenes with phenylboronic acid (SM3 and SM4)

The Suzuki-Miyaura carbon-carbon coupling reaction using halogenated nitrobenzenes (1-iodo-2-nitrobenzene (**4.5**) (reaction denoted as SM3) and 1-iodo-4-nitrobenzene (**4.7**) (reaction denoted as SM4) was also carried out with phenylboronic acid. The halogenated nitrobenzenes were chosen to understand the selectivity of the palladium nanoparticle catalysts, to understand which halogenated nitrobenzene is preferred by the catalysts. It is also important to understand the selectivity of the catalysts when the nitro-group is changed from the ortho- to the para-position on the benzene ring system and how this change will influence the yield of product formed. Between the two halogenated nitrobenzenes, it is predicted that the 1-iodo-4-nitrobenzene would be the preferred reagent, as this substrate is less sterically hindered than the 1-iodo-2-nitrobenzene.
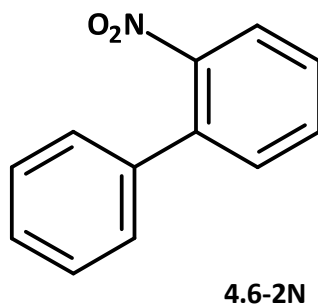
1-Iodo-2-nitrobenzene as the substrate (SM3):

4.6-2N

Figure 4.13: The product 1-nitro-2-phenyl-benzene (4.6-2N) .

Following reaction of 4-iodo-2-nitrobenzene with phenyl boronic acid, the product 1-nitro-2-phenyl-benzene (**4.6-2N**) was successfully extracted with DCM to remove the large DMF signals that would be present in the ^{1}H spectrum. The crude product formed was yellow crystals at 18 °C, but this changed to a sticky yellow oil at RT, indicating that the compound has a low melting point. The yields obtained for the AE- and PVP-PdNPs were quite low at 56 and 40%, respectively, 1D (^{1}H and ^{13}C spectra), as well as 2D NMR data (COSY, HSQC, HMBC), were acquired for the product the data tabulated in Table 4.3 (section 4.5).

The ^{1}H NMR spectra for the product 1-nitro-2-phenyl-benzene (**4.6-2N**) using both AE-and PVP-PdNPs as catalysts in reaction SM3 is shown in Figure 4.14. For both catalysts, the spectra reveal some overlap for the expected aromatic signals (7.27-8.05 ppm), however they integrate to 9 protons. The overlap may be resolved by the HSQC spectrum since the second dimension for ^{13}C will enable the spread of the signals. The proton spectrum for the reaction using PVP-PdNPs (Figure 4.14 D), reveal the presence of some residual phenyl boronic acid and 4-iodo-2-nitrobenzene.

Figure 4.14: The ¹H NMR data (CDCl₃, 400 MHz) for the product 1-nitro-2-phenyl-benzene (4.6-2N, C, D) from AE-PdNPs (C) and PVP-PdNPs (D) as catalysts. The starting materials phenylboronic acid (A) and 1-iodo-2-nitrobenzene (B) is also shown.

Figure 4.15 is the ^{13}C spectrum for the product 1-nitro-2-phenyl-benzene (**4.6-2N**) and it is revealing 10 aromatic carbon signals, though some of these signals may be due to starting materials. Some quarternary signals (C9 and C10) were also found to be absent, making full assignment of the structure difficult.
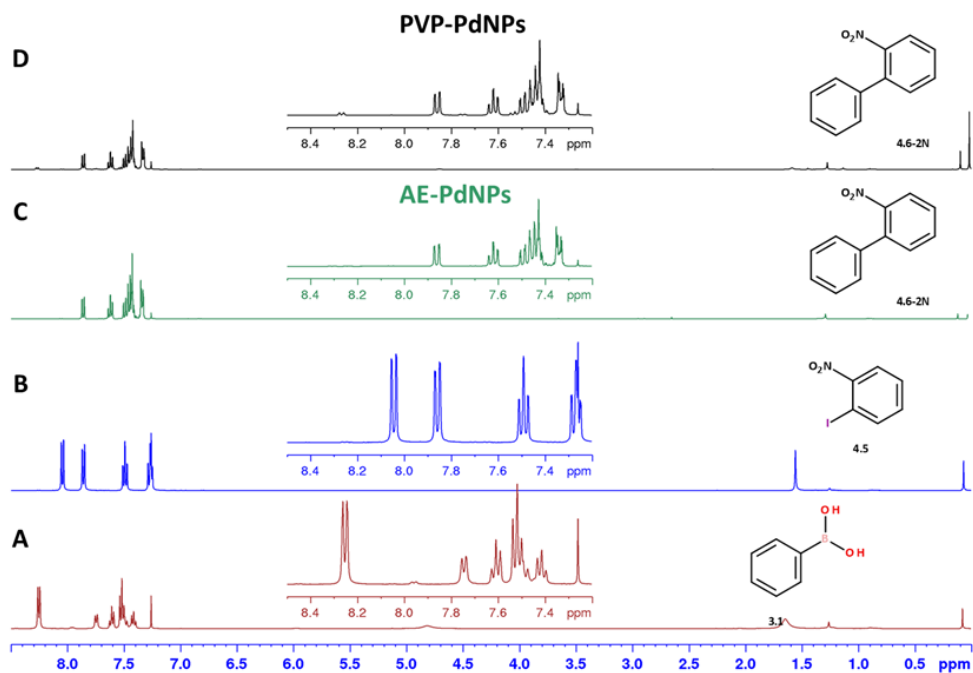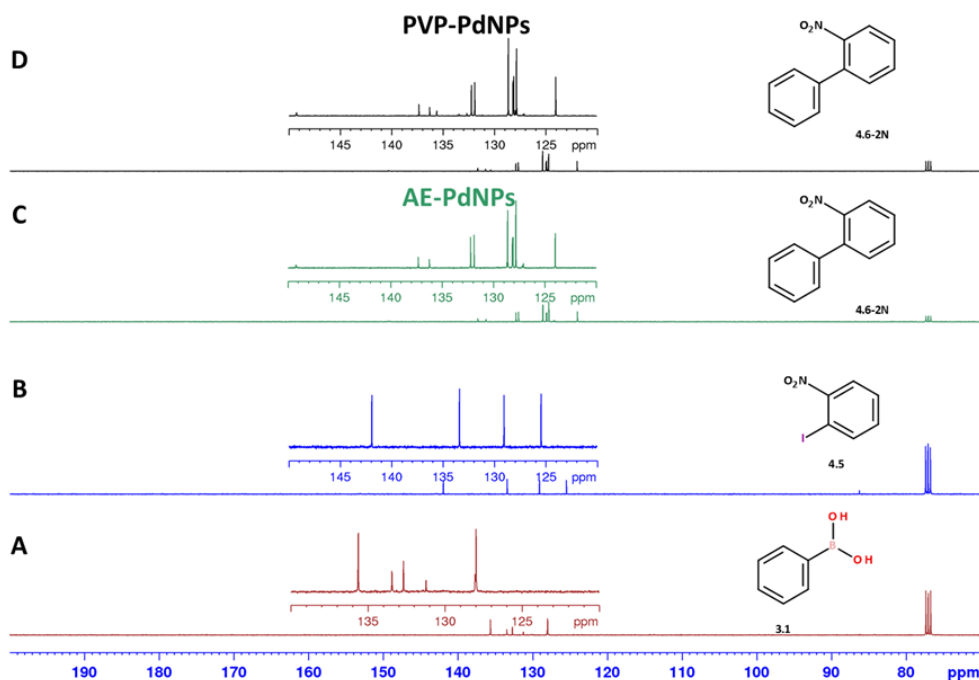
Figure 4.15: The ^{13}C NMR data (CDCl$_3$, 100 MHz) for the product 1-nitro-2-phenyl-benzene (4.6-2N, C, D) from AE-PdNPs (C) and PVP-PdNPs (D) as catalysts. The starting materials phenylboronic acid (A) and 1-iodo-2-nitrobenzene (B) is also shown.

The HMBC spectrum for **4.6-2N** is shown in Figure 4.16. The data obtained were tabulated in Table 4.2. Figure 4.17 illustrate some of the correlations observed from the HMBC data for 1-nitro-2-phenyl-benzene (**4.6-2N**). H2 reveals correlations to C1 and C3, while H3 reveals correlations to C4 and C7. Correlations from H-6 to C5 were the only correlations observed for the second ring. Unfortunately, correlations to the new C-C bond between the aromatic rings were not observed. The NMR data is listed in Table 4.2.

*Figure 4.16: The HMBC spectrum (CDCl₃) obtained for the product 4.6-2N. *? Denotes possible starting material signals.*

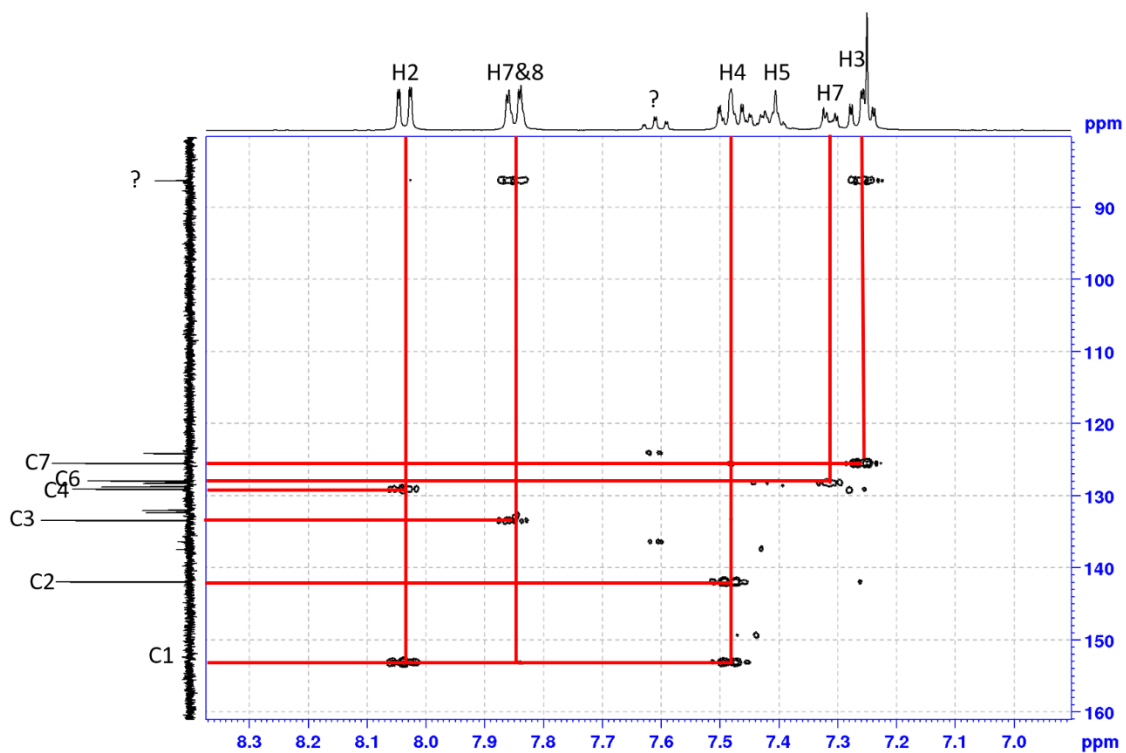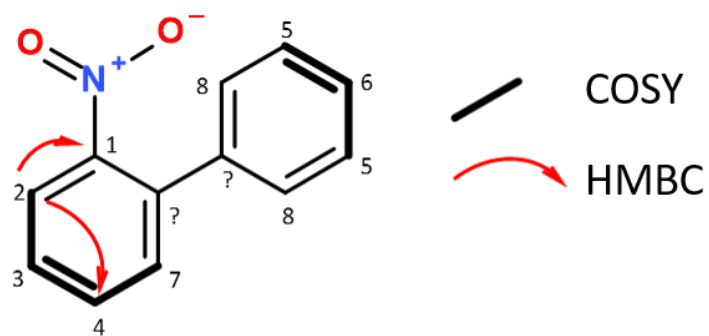*Figure 4.17: Key correlations obtained from 2D NMR data for the product 1-nitro-2-phenyl-benzene (4.6-2N), the numbering is based on ¹³C chemical shifts. *? Denotes absent carbon signals.*

Atom #	δ_C (mult.)	δ_H (integ., mult., J(Hz))	COSY	HMBC
1	153.0 (C)	-	-	-
2	141.9 (CH)	8.05 (1H, dd, 6.8 Hz)	H3	C4, C1
3	133.4 (CH)	7.27 (1H, td, 6.4 Hz)	H4, H2	C7, C4
4	129.0 (CH)	7.48 (1H, td, 6.6 Hz)	H3, H7	C1, C2
5	128.7 (CH)	7.41 (2H, td, 7.0 Hz)	H6	-
6	127.9 (CH)	7.32 (2H, dd, 5.6 Hz)	H5	C5
7	125.4 (CH)	7.86 (1H, dd, 6.6 Hz)*	H4	C3, C1
8	124.1 (CH)	7.86 (1H, dd, 6.6 Hz)*	H4	C3, C1

*overlapped signal

In addition to the NMR data collected for the compound **4.6-2N**, GC-EIMS data was collected to confirm successful formation of the product. The GC-MS data demonstrated the presence of a molecular ion peak at *m/z* 199.2, the expected mass of the product 1-nitro-2-phenyl-benzene (**4.6-2N**) (Figure 4.18) at a retention time of 23.2 min for each of the catalysts. The same molecular ion peak was reported by Gonzalez *et al.* (2005). The loss of one of the oxygen moieties on the nitro functional group and loss of an additional proton corresponded to the fragment *m/z* 182.2. Subsequent loss of N=O gave rise to the fragment *m/z* 152.2 (Figure 4.18). The mass spectroscopic data obtained was consistent with that reported by Gonzalez *et al.* (2005). Both catalysts were thus successful in the formation of 1-nitro-2-phenyl-benzene (**4.6-2N**) product. The data is given in Table 4.4.
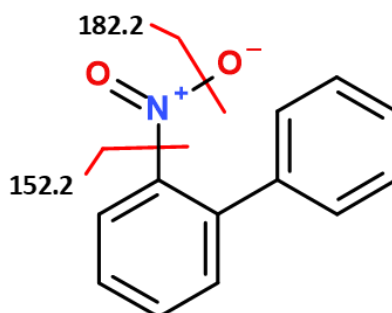

Figure 4.18: The major mass fragments obtained for 1-nitro-2-phenyl-benzene (4.6-2N) (m/z 199.2).

The FTIR data (Figure 4.19) obtained from the products revealed similar spectra with peaks at 1520 cm^{-1} which is assigned the nitro functional group. Signals attributed to the aromatic rings were found at 1350 cm^{-1}. A broad peak at approximately 3500 cm^{-1} was only observed for the AE-PdNP catalyst sample.
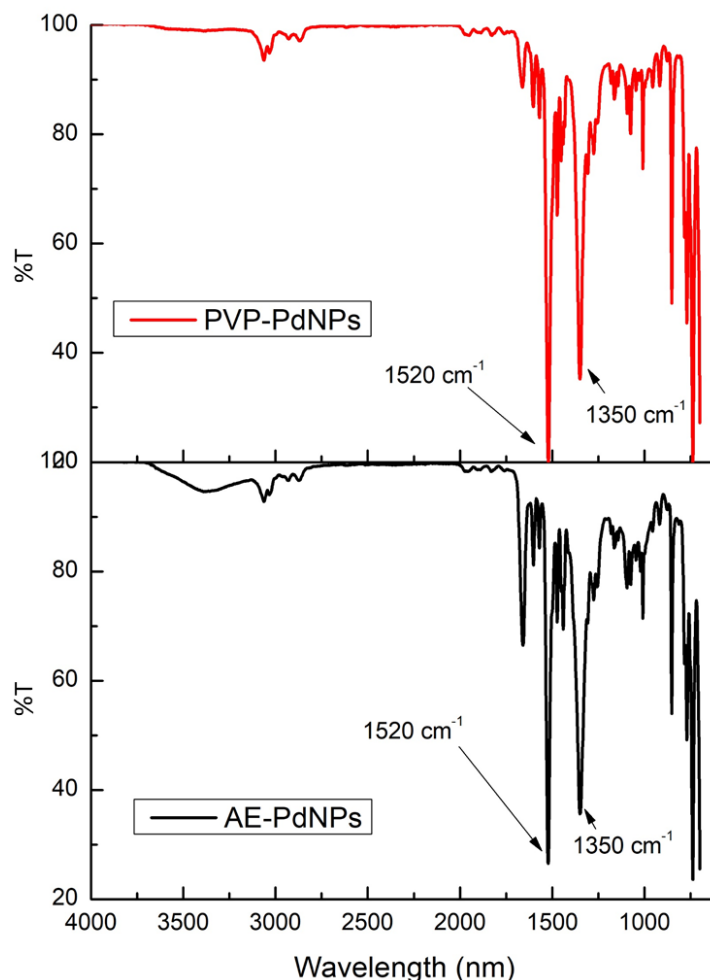
Figure 4.19: The FTIR spectra obtained for 1-nitro-2-phenyl-benzene (4.6-2N) employing the AE-PdNPs and the PVP-PdNPs.

UV-Visible spectra collected for the starting materials and the products obtained from the AE-PdNPs and PVP-PdNPs, is shown in Figure 4.20. The starting material revealed absorbance bands at 230 nm (λ_{max}), 265 and 320 nm. Unexpectedly, the products did not show intense absorption bands at longer wavelengths (due to increased conjugation) showing only λ_{max} at 235 nm and a small absorption band at ~310 nm. This may be due to the presence and electro-withdrawing nature of the NO$_2$ moiety at the *ortho* position, disrupting the planarity of the biphenyl system.
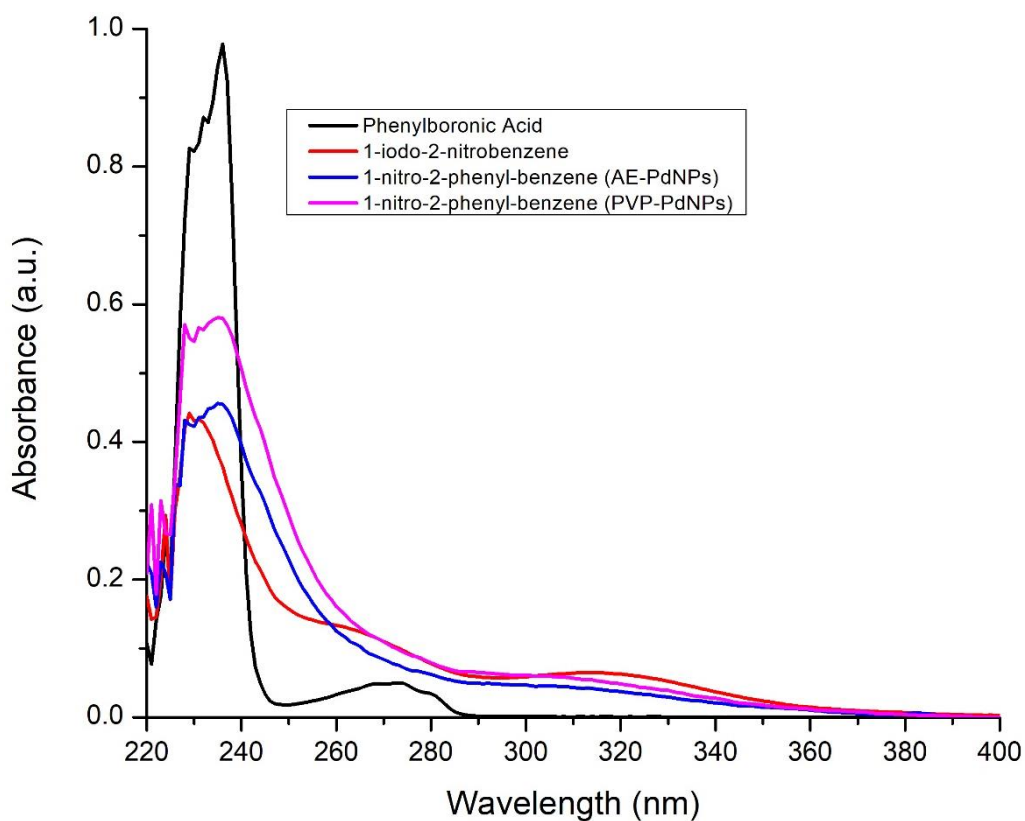
Figure 4.20: The UV-visible spectra obtained for the starting materials (3.1 and 4.5) for 1-nitro-2-phenyl-benzene (4.6-2N). (Solvent DCM).

1-Iodo-4-nitrobenzene as the substrate (SM4):
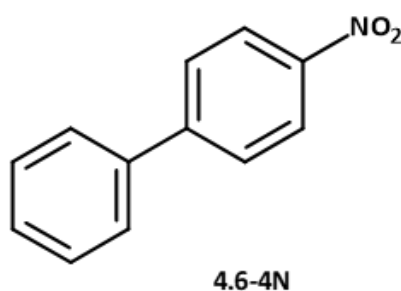
4.6-4N

Figure 4.21: The product 1-nitro-4-phenyl-benzene (4.6-4N).

Following extraction and drying of the crude product 1-nitro-4-phenyl-benzene (**4.6-4N**), a brownish powder was obtained at RT. This indicates that the compound 1-nitro-4-phenyl-benzene has a higher melting point compared to 1-nitro-2-phenyl-benzene. The yields obtained were 93 and 91% for the AE- and PVP-PdNPs. 1D data (^{1}H and ^{13}C spectra), as well as 2D data (COSY, HSQC, HMBC), were acquired for the product. The product was therefore fully assigned as seen in Figure 4.21, and the data tabulated in Table 4.3.

The ¹H NMR spectrum for the product 1-nitro-2-phenyl-benzene (**4.6-4N**) using both AE-and PVP-PdNPs as catalysts in reaction SM4 is shown in Figure 4.22. The spectrum reveals 3 well resolved aromatic signals integrating to 6 protons, together with 2 overlapped signals integrating to 3, in the 7.40-8.40 ppm region, as expected.

Figure 4.22: The ¹H NMR data (CDCl₃, 400 MHz) for the product 1-nitro-4-phenyl-benzene (4.6-4N, C, D) from AE-PdNPs (C) and PVP-PdNPs (D) as catalysts. The starting materials phenylboronic acid (A) and 1-iodo-2-nitrobenzene (B) is also shown.

Figure 4.23 is the ¹³C spectrum (together with the dept-135 data) for the product 1-nitro-4-phenyl-benzene (**4.6-4N**) revealed 8 aromatic carbon signals as expected for the highly symmetrical molecule. Four sets of carbon signals (δ_C 129.1, 127.8, 127.4 and 124.1) had double the intensity of one of the protonated carbons (at δ_C 128.9). This therefore suggests the position of the protonated carbons within the structure of **4.6-4N**. Quarternary carbons were observed at δ_C 147.7, 147.1 and 138.8. The characteristic I-*C*= signal at 102.7 ppm for the starting material, is not observed in the products.
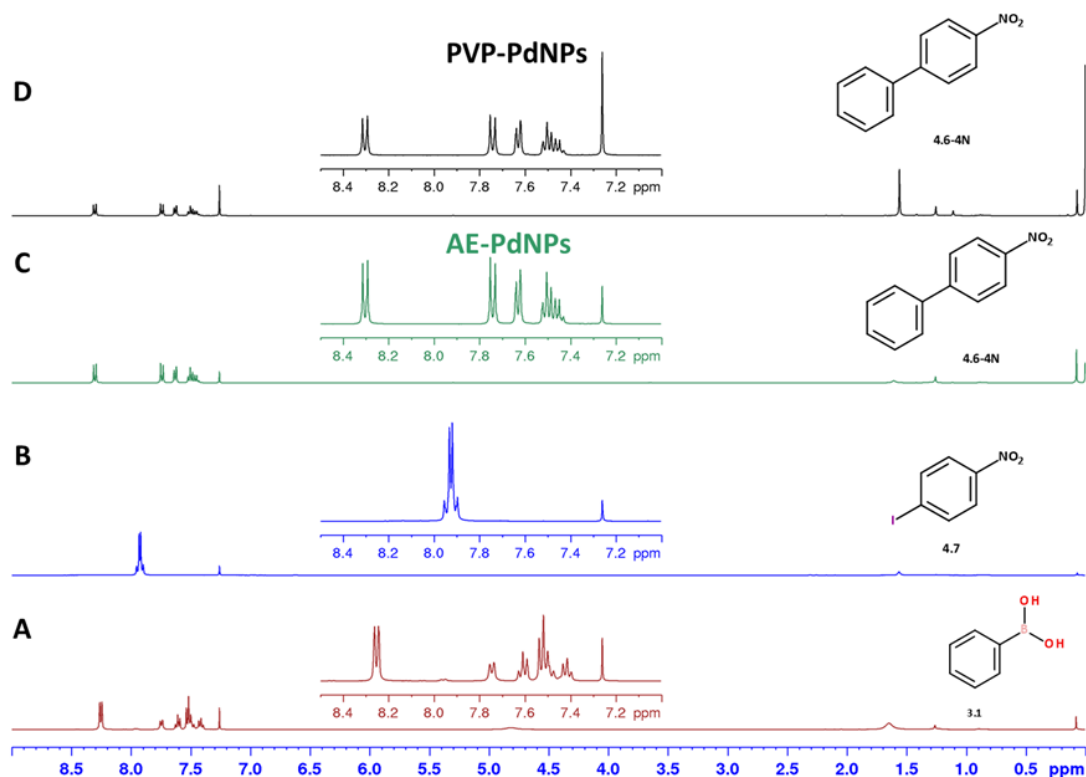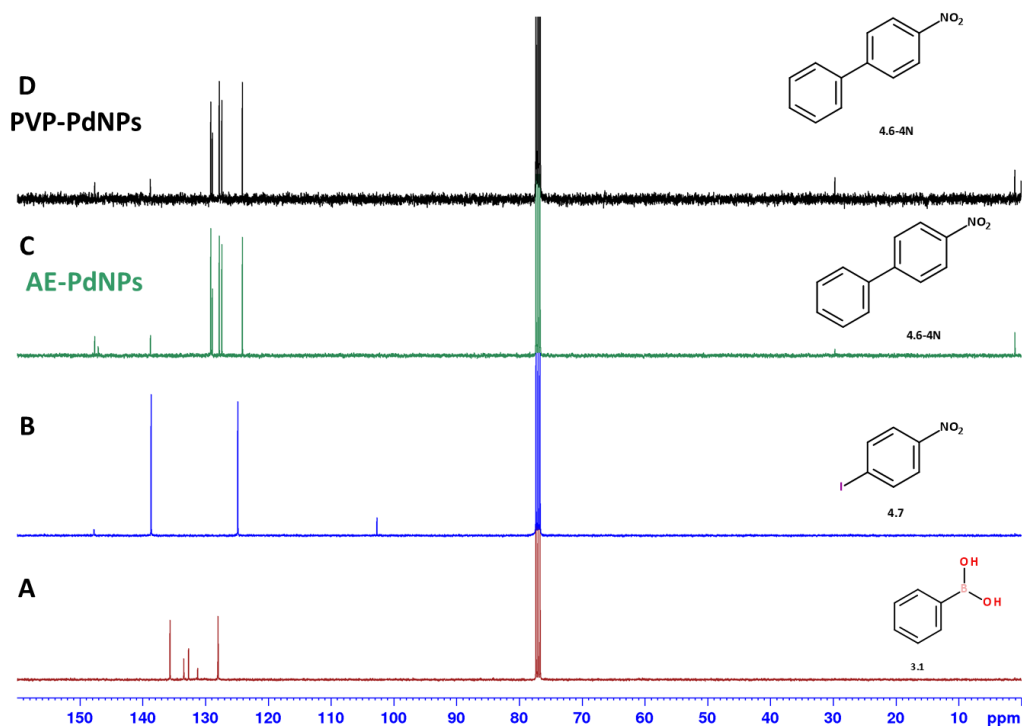
Figure 4.23: The ^{13}C NMR data (CDCl$_3$, 100 MHz) for the product 1-nitro-4-phenyl-benzene (4.6-4N, C, D) from AE-PdNPs (C) and PVP-PdNPs (D) as catalysts. The starting materials phenylboronic acid (A) and 1-iodo-2-nitrobenzene (B) is also shown.

Figures 4.25 illustrates some of the key correlations that were observed in the HMBC NMR data for 1-nitro-4-phenyl-benzene (**4.6-4N**). The most important correlations are those of H6 showing correlations to C2, C3 and C8. The proof that the new carbon-carbon bond was formed between the two aromatic rings, are the correlations between H6 and C3, and H7 to C2. The placement of C4 and C5 was based on the intensity of the C5 signal in the ^{13}C spectrum (Figure 4.23). The HMBC spectrum (Figure 4.24) thus confirmed the connectivity between the two aromatic rings, and that the SM4 reaction was indeed successful. Additional 2D data (including COSY spectra) helped assign the structure of **4.6-4N** and these are listed in Table 4.3.

Figure 4.24: HMBC spectrum (CDCl$_3$) of 1-nitro-4-phenyl-benzene (4.6-4N), which shows the correlations for H6 and H8.

Figure 4.25: Key 2D NMR correlations observed for 1-nitro-4-phenyl-benzene (4.6-4N), the numbering is based on ^{13}C chemical shifts.
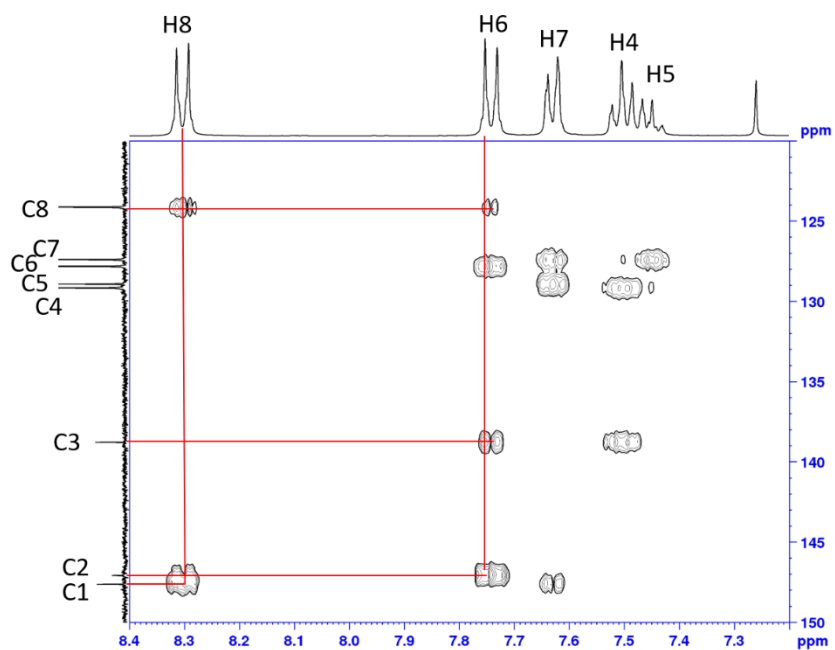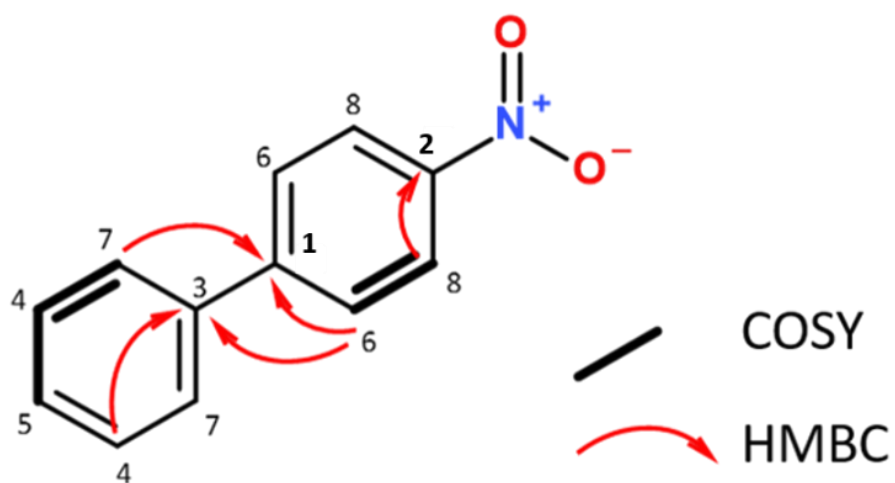
Atom #	δ_C (mult.)	δ_H (integ., mult., J(Hz))	COSY	HMBC
1	147.6 (C)	-	-	-
2	147.1 (C)	-	-	-
3	138.8 (C)	-	-	-
4	129.1 (CH)	7.51 (1H, m)	H7	C3, C7(lr)
5	128.9 (CH)	7.45 (2H, m)	-	C7
6	127.8 (CH)	7.74 (2H, d, 8.8 Hz)	H8	C2, C3, C8
7	127.4 (CH)	7.63 (2H, d, 7.1 Hz)	H4	C1, C5
8	124.1 (CH)	8.31 (2H, d, 8.8 Hz)	H6	C1, C2

GC-MS data did not show a molecular ion at m/z 199.2, which is the expected mass of the product 1-nitro-4-phenyl-benzene (**4.6-4N**), however, it did reveal a fragment at m/z 183.2 which is due to the loss of one of the oxygen atoms of the nitro group (Figure 4.26). The retention time for this product was found to be 20.9 min for the AE-PdNP catalyst (Table 4.4). Unfortunately, the GC-MS chromatogram revealed no product for the PVP-PdNP catalyst, which may be due to operator error, as the NMR data was clear.
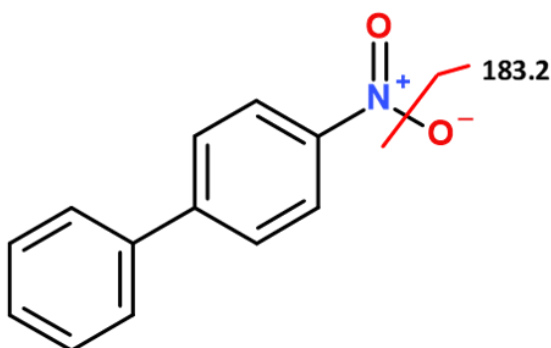
Figure 4.26: The only mass fragment obtained for 1-nitro-4-phenyl-benzene (4.6-4N).

The FTIR (Figure 4.27) data which was obtained from the compound showed a signal at 1510 cm^{-1} which is assigned for a nitro-functional group present on an

aromatic compound. Besides this peak, the aromatic carbon peaks were also found for the compound at 1340 cm⁻¹.
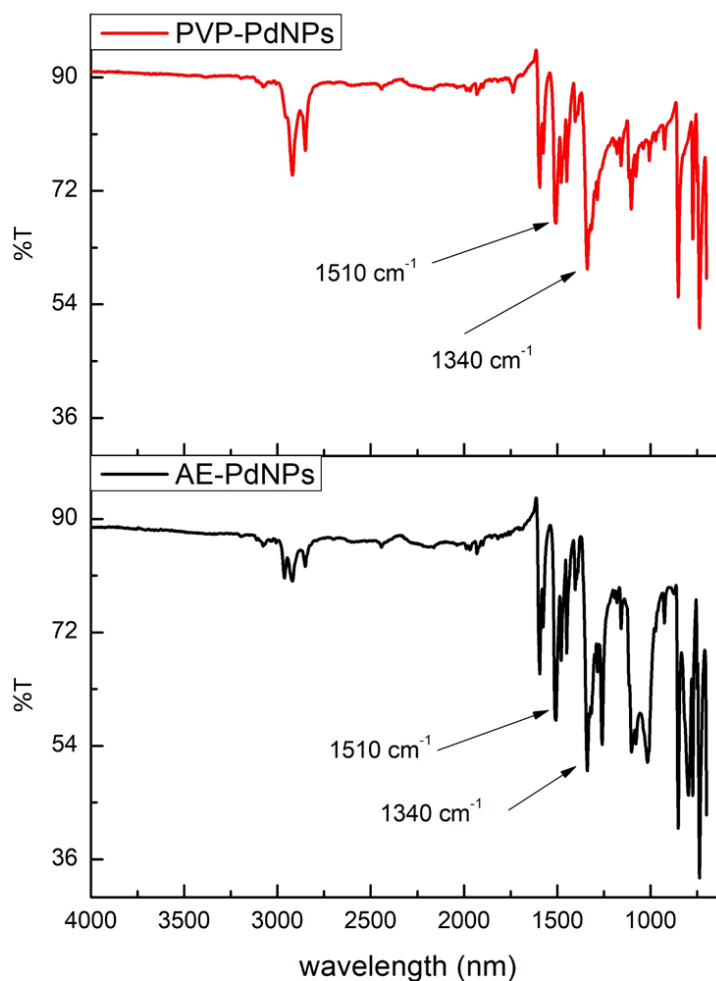
Figure 4.27: The FTIR spectrum of 1-nitro-4-phenyl-benzene (4.6-4N).

UV-Visible spectra (Figure 4.28) of the starting materials and products for both catalysts are shown in Figure 4.29. 1-iodo-4-nitrobenzene showed an absorbance at 300 nm (in comparison to compound **4.6-2N** which showed only weak absorption bands), while the products for each of the catalysts revealed a 10 nm red shift to longer wavelengths (λ_{max} 310 nm), confirming an increase in conjugation.
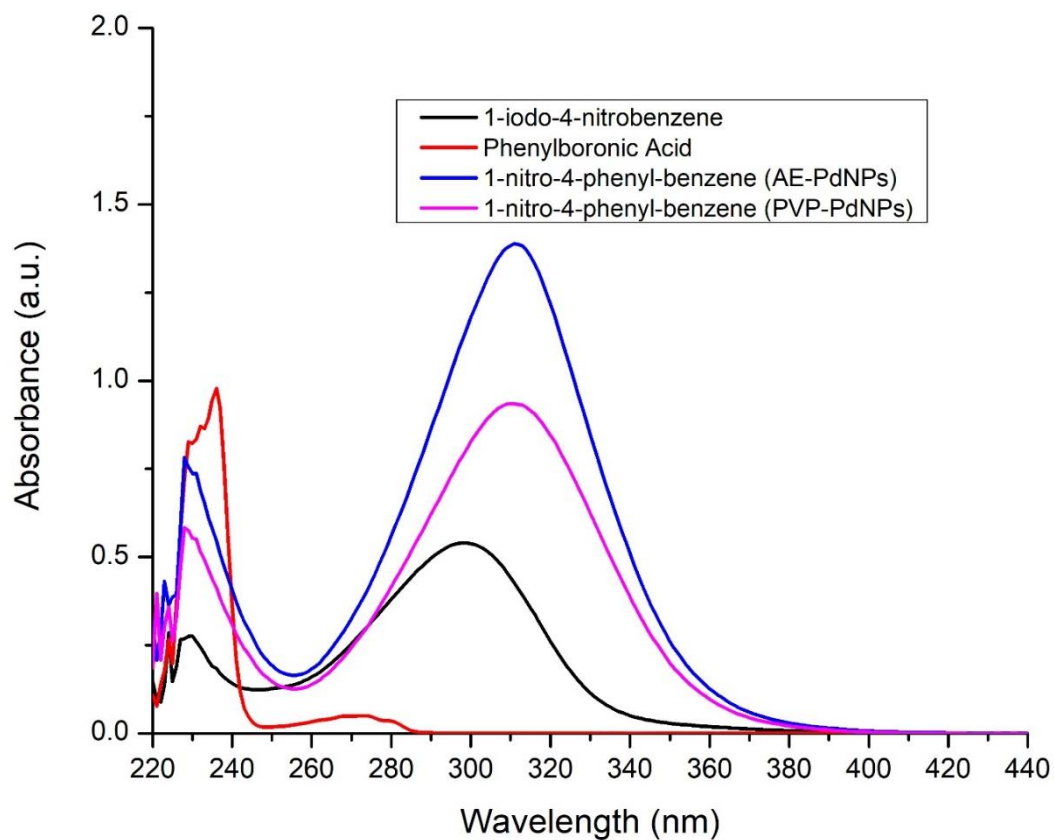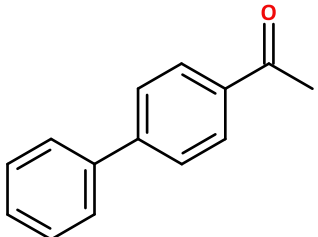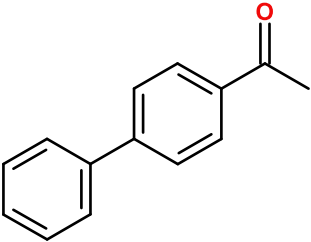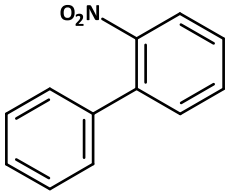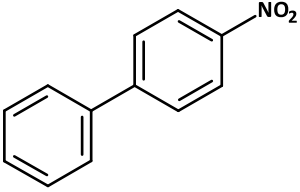
Figure 4.28: UV-visible spectra for the starting materials (3.1 and 4.7) and the product 1-nitro-4-phenyl-benzene (4.6-4N), both the products did undergo a red shift to λ_{max} 310 nm. (Solvent DCM).

Table 4.4: Retention times (GC), calculated and observed molecular masses and percentage yields obtained for the Suzuki-Miyaura carbon-carbon coupling reactions using the AE- and PVP-PdNPs synthesized.

Reaction	Product	Rt (min)	*m/z*	% Yield
			$C_{14}H_{12}O$ (196.24 amu)	
SM1	**4.3-4Br**	AE: 24.41	AE: Found: 196.2	AE: 91.5
		PVP: 24.38	PVP: Found: 196.2	PVP: 89.7
	1-(4-phenylphenyl)ethanone			

C₁₄H₁₂O (196.24 amu)

SM2

4.3-4I

1-(4-phenylphenyl)ethanone

	$C_{14}H_{12}O$ (196.24 amu)		

AE: 24.38   **AE:** Found: 196.2   **AE:** 90.8

PVP: 24.37   **PVP:** Found: 196.2   **PVP:** 89.3

C₁₂H₉NO₂ (199.20 amu)

SM3

4.6-2N

1-nitro-2-phenyl-benzene

AE: 23.20   **AE:** Found: 199.2   **AE:** 55.7

PVP: 23.22   **PVP:** Found: 199.2   **PVP:** 39.7

C₁₂H₉NO₂ (199.20 amu)

SM4

4.6-4N

1-nitro-4-phenyl-benzene

AE: 20.91   **AE:** **183.2   **AE:** 92.6

PVP: *n/a   **PVP:** *Found: n/a   **PVP:** 90.7

---

* Not available on GC-MS spectrum.

** Molecular ion not observed, only fragment ion corresponding to the loss of one oxygen atom found.

4.3.1.3. Discussion on the success of Suzuki-Miyaura coupling reactions

The NMR, GC-MS and UV/Vis data obtained for the products **4.3-Br**, **4.3-4I**, **4.6-4N**, except for **4.6-2N**, confirmed the success of the reactions. Use of the 1-iodo-2-nitrobenzene as substrate was not as successful (with yields obtained as low as 39%), although there were some indications (NMR, GC-MS) that the product had formed. qNMR was used to determine the successful conversion of the starting reagents to the product, it was clear that AE-PdNPs allowed for greater success in forming the products since it consistently gave the highest yields. The use of a 4-bromo- substrate (**4.2**) compared to a 4-iodo substituted starting material (**4.4**) did not significantly impact the % yield of the products since the yields obtained were 91.2 % for the AE-PdNPs and 89.5% for the PVP-PdNPs. Nitro substitution at the ortho vs. para position on the aromatic ring, did show a marked difference with the AE- and PVP-PdNPs producing yields of 56 and 40%, respectively for the ortho substituted substrate (**4.5**). This contrasts with the results obtained for the para substituted substrate (**4.7**) where compound **4.6-4N** was produced in yields of 93 and 91% for the AE- and PVP-PdNPs, respectively. The ~40% difference in yield implies that steric hindrance is the problem. However, for all reactions carried out the AE-PdNPs appears to have a slight advantage in Suzuki-Miyaura carbon-carbon coupling reactions.

4.3.2. Heck coupling reaction

4.3.2.1. The reaction of halogenated acetophenones with butyl acrylate (Heck1 and Heck2)

The PdNP catalysed Heck C-C coupling between the unsaturated aryl halide (**4.2** or **4.4**) and an activated alkene (**4.8**) in the presence of tributylamine as a base was attempted. The Heck coupling reaction with halogenated acetophenones was carried out using butyl acrylate (**4.8**) as the substrate. The halogenated acetophenones chosen were 4-bromoacetophenone (**4.2**) and 4-iodoacetophenone (**4.4**) to understand selectivity of the PdNP catalysts and the halogenated acetophenones. Of the two halogenated acetophenones, it is expected that 4-iodoacetophenone would be the preferred reagent, as the iodo group is a better leaving group then the bromo moiety, as the latter is more electronegative. The base that is used also needs to be considered, as it is responsible for the removal of a proton from the double bond.

4-Bromoacetopenone as the substrate (Heck 1):
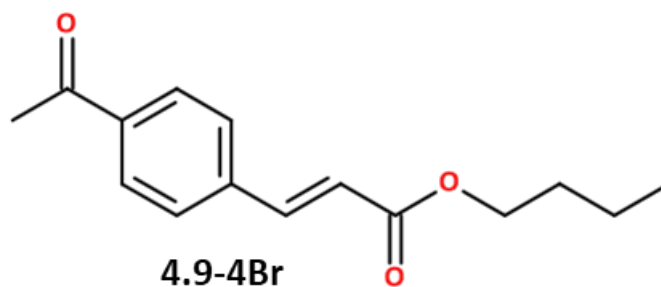
Figure 4.29: Butyl (E)-3-(4-acetylphenyl)prop-2-enoate (4.9-4Br).

The product obtained following the reaction of the halide and the alkene was extracted and further purified using silica gel chromatography, to remove excess DMF still present in the samples, to give a yellow oil. The product was purified in this case, as DMF masked signals pertaining to the product which did not allow for unequivocal assignment. The product obtained was a yellow oil. 1D data (^{1}H and ^{13}C spectra) was acquired for the product.

The ^{1}H NMR spectra for the yellow oil (**4.9-4Br**) using the AE-and PVP-PdNPs catalysts in the reaction is shown in Figure 4.30. Aromatic signals pertaining to the aryl moiety was observed in the 7.0-8.0 ppm region, integrating to 4 protons, together with the methyl signal at 2.64 ppm. The methylene and the methyl protons belonging to the acrylate were also observed at 0.7 to 0.8 ppm. However, the protons attributed to the terminal methylene (=CH_2-CH-C=O), which would be a clear indication of conjugation, were still observed, disclosing that the reaction was not successful for either of the catalysts. This was confirmed by the ^{13}C NMR spectra obtained.
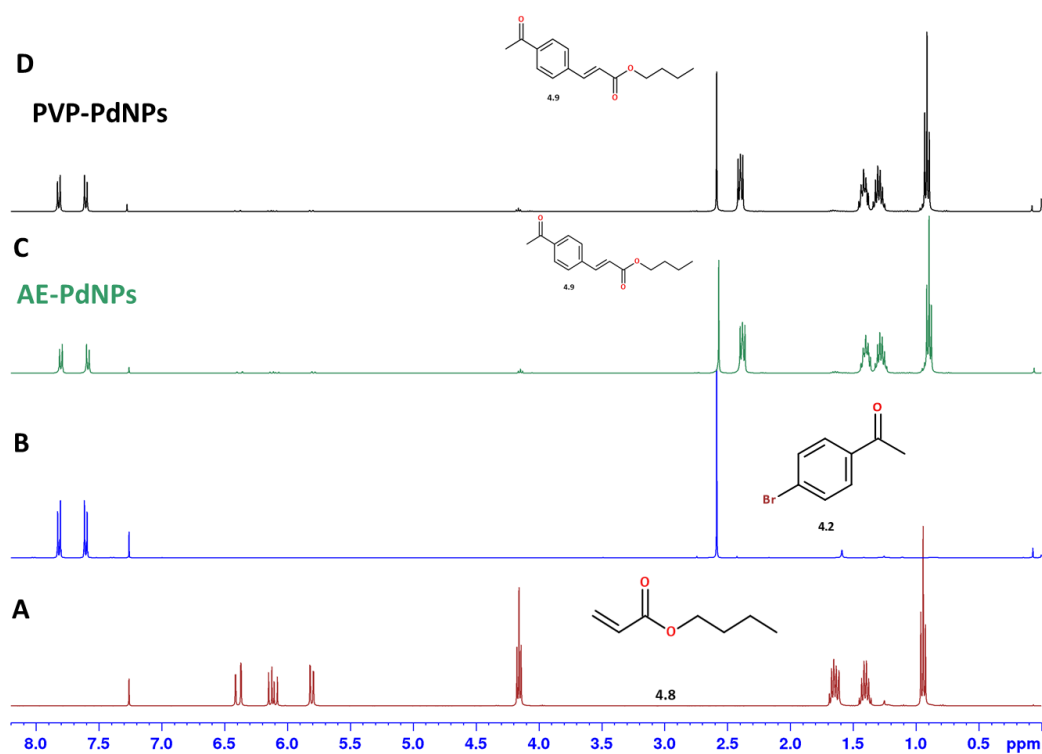
Figure 4.30: The ^{1}H NMR data (CDCl$_3$, 400 MHz) for the product obtained from AE-PdNPs (C) and PVP-PdNPs (D) catalytic reactions. The starting materials butyl acrylate (A) and 4-bromoacetophenone (B) is also shown.

Figure 4.31 shows the ^{13}C spectra obtained for reaction product (**4.9-4Br**), revealing the requisite aromatic ring signals and methylene signals pertaining to the butyl moiety. However, the terminal methylene signals of the acrylate remained. Once again indicating that the reaction was not successful. This was confirmed by analysis of GC-MS data where the characteristic 1:1 isotopic cluster pattern for a brominated compound at *m/z* 198.0 was observed (Table 4.6).
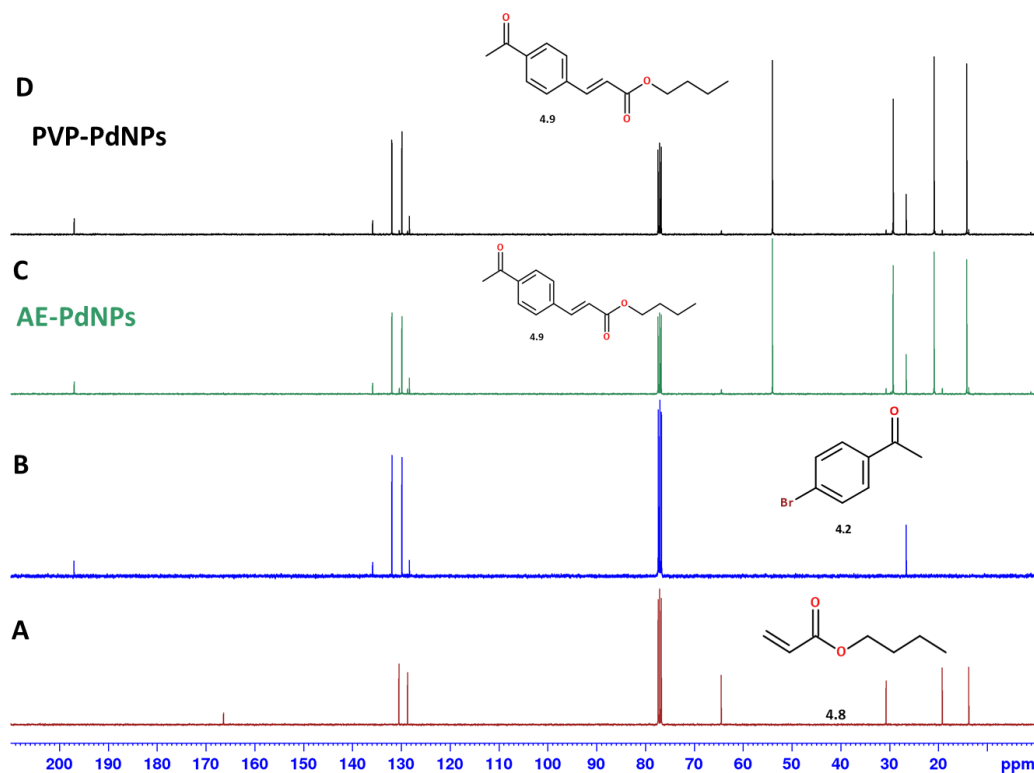
Figure 4.31: The ¹³C NMR data (CDCl₃, 100 MHz) for the product obtained using the AE-PdNP (C) and PVP-PdNP (D) catalysts. The starting materials butyl acrylate (A) and 4-bromoacetophenone (B) are also shown.

UV-visible spectroscopy revealed that the butyl acrylate remained unchanged showing a λ_{max} at 257 nm (Figure 4.32) for both the products.
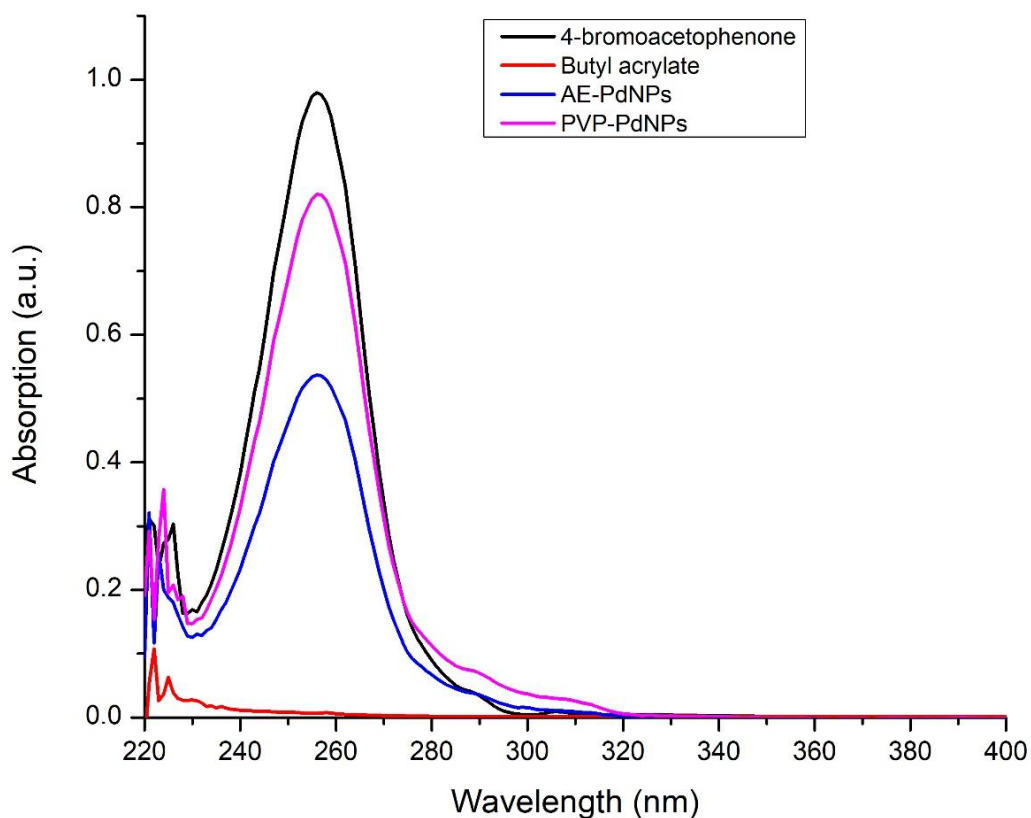
Figure 4.32: The UV-visible spectra of the starting materials and the product obtained (4.9-4Br). (Solvent DCM).

4-Iodoacetopenone as the substrate (Heck2):
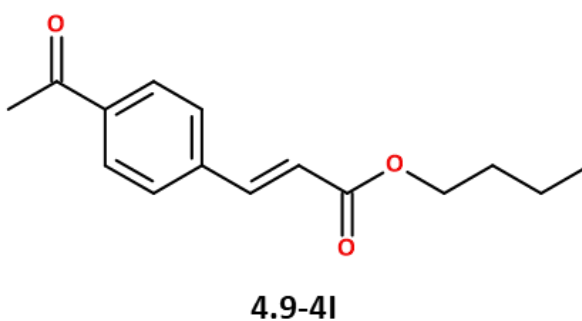
4.9-4I

Figure 4.33: Butyl (E)-3-(4-acetylphenyl)prop-2-enoate (4.9-4I).

In this reaction 4-iodoacetophenone was used as the aryl halide (**4.4**). Figure 4.33 illustrates the expected product, butyl (*E*)-3-(4-acetylphenyl)prop-2-enoate (**4.9-4I**), which was further purified using silica gel chromatography to remove the excess DMF still present in the samples. The product obtained was a yellow oil in a 71 and 69% yield for the AE- and PVP-PdNPs, respectively. 1D data (^{1}H and [13]C

spectra), as well as 2D data (COSY, HSQC, HMBC), were acquired for the product. The data is tabulated in Table 4.6.

The ^{1}H NMR spectra for the products **4.9-4I** obtained using both the AE-and PVP-PdNPs as catalysts in reaction Heck2 is shown in Figure 4.34. The expected aromatic signals for a symmetrical molecule are observed at δ_H 7.95 (d, 2H) and 7.59 (d, 2H), while the methylene signals for the butyl chain are observed at 1.69, 1.40 and at 4.21 ppm for the CH_2-O moiety. The methyl ketone is observed at δ_H 2.60 (s, 3H) while the remaining methyl signal is observed at δ_H 0.96 (3H). The signals for the terminal methylene at δ_H 6.50 and 5.74 have disappeared, replaced by signals at 7.68 (d, 1H) and 6.51 (d, 1H) ppm. Measuring the coupling constants for the latter signals reveals a large coupling constant at 16.0 Hz, indicating that the geometry about the double bond is trans. All protons remain accounted for the product **4.9-4I**.
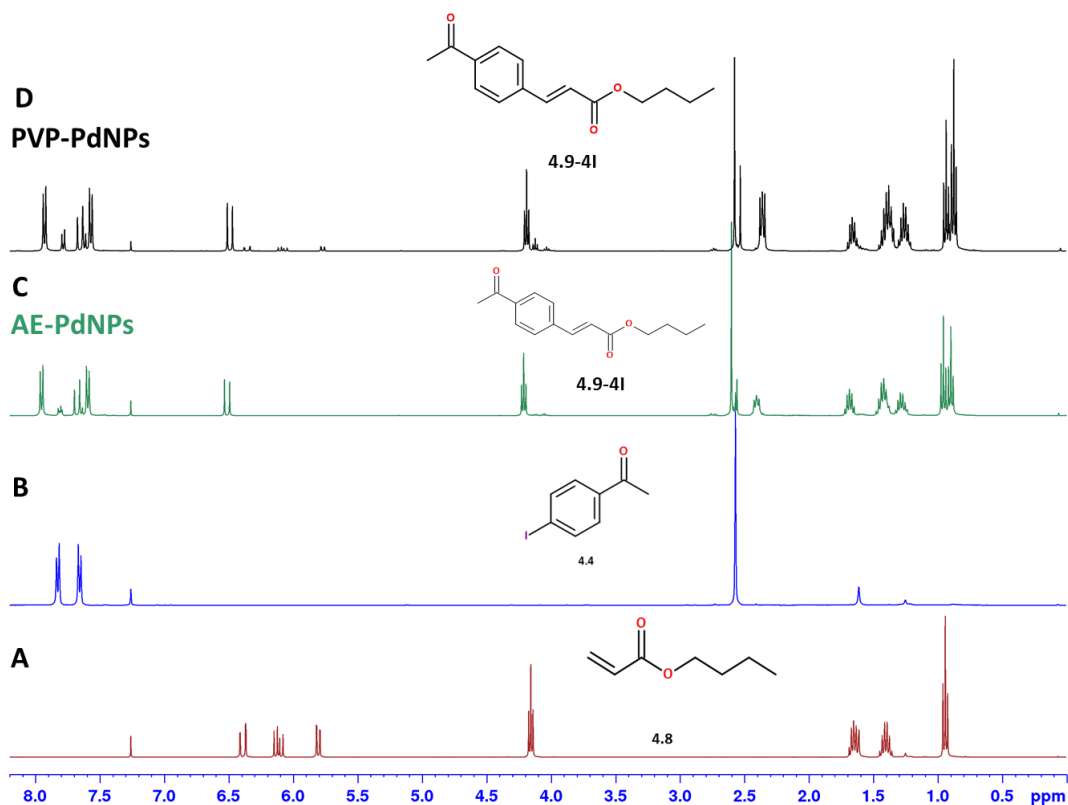
Figure 4.34: 1H NMR spectra (CDCl3, 400 MHz) for the product butyl (E)-3-(4-acetylphenyl)prop-2-enoate (4.9-4I) using AE-PdNPs (C) and PVP-PdNPs (D) as catalysts. The starting materials butyl acrylate (A) and 4-iodoacetophenone (B) is also shown.

Figure 4.35 shows the ^{13}C spectra acquired for the product **4.9-4I** (C, D) and the starting materials (A, B). The spectra for the products both reveal 13 carbon signals including 4 quarternary carbons at 197.3 (C=O), 166.5 (O=C-O), 138.8 and 137.9

ppm. Four methine signals, 2 with double the intensity of the other methines, due to the symmetrical ring system, at 128.8 and 128.1 ppm, as well as two methine signals attributed to the double bond were observed at δ_C 142.9 and 120.8. Of the remaining 5 carbon signals, 2 methyls were observed at δ_C 26.7 (O=C-CH_3) and 14.0. The latter is assigned to the methyl group on the butyl chain. Finally, three methylene signals were observed at δ_C 19.1, 30.7, and 64.6 (CH_2-O).
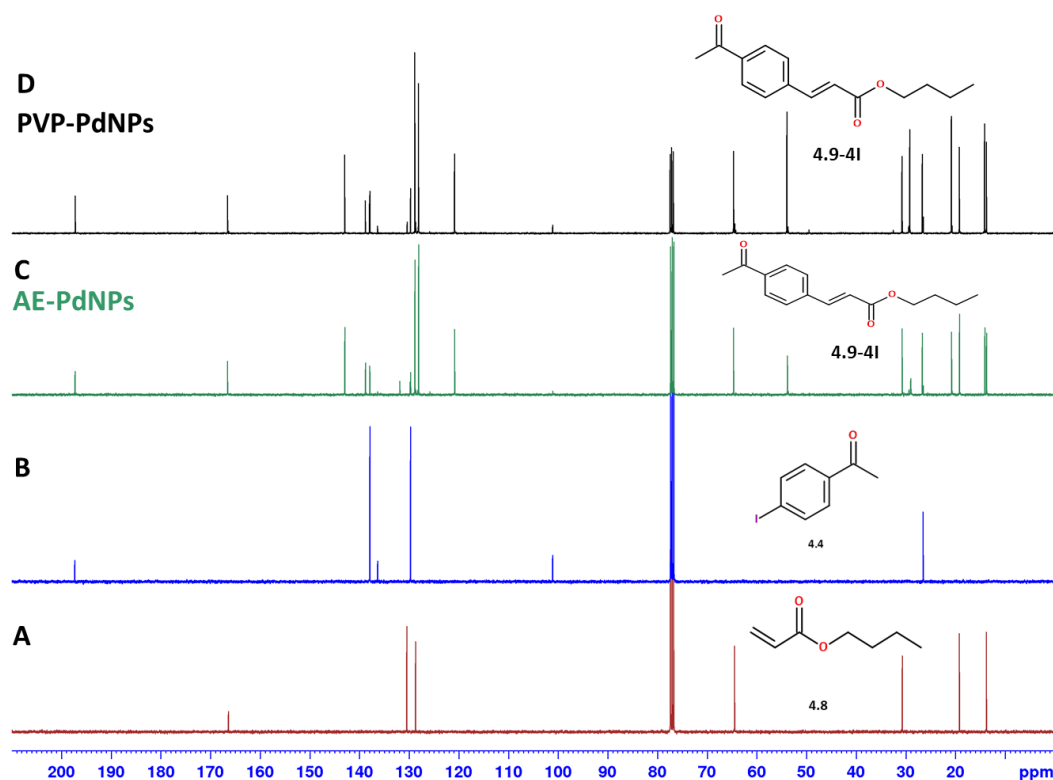
Figure 4.35: The ^{13}C NMR data (CDCl$_3$, 100 MHz) for the product butyl (E)-3-(4-acetylphenyl)acrylate (4.9-4I) from AE-PdNPs (C) and PVP-PdNPs (D) as catalysts. The spectra for the starting materials butyl acrylate (A) and 4-iodoacetophenone (B) is also shown.

2D NMR data (Table 4.5) confirmed the positions and assignment of the product **4.9-4I**. The HMBC spectra (Figure 4.36) revealed correlations showing that product formation was successful. A number of important correlations were observed including H8 (on the double bond) to C2 (O-C=O), the methine at C3 (HC=CH-C=O), the quarternary carbon C4 together with the methine at C7 on the aromatic ring. Similarly, correlations for H3 were observed to C8, C2, C4 and C7. The aromatic ring proton H7 revealed concomitant correlations to C3 and C5. This together with COSY and the 1D data allowed the full assignment of the product **4.9-4I**. The data obtained is tabulated in Table 4.5.
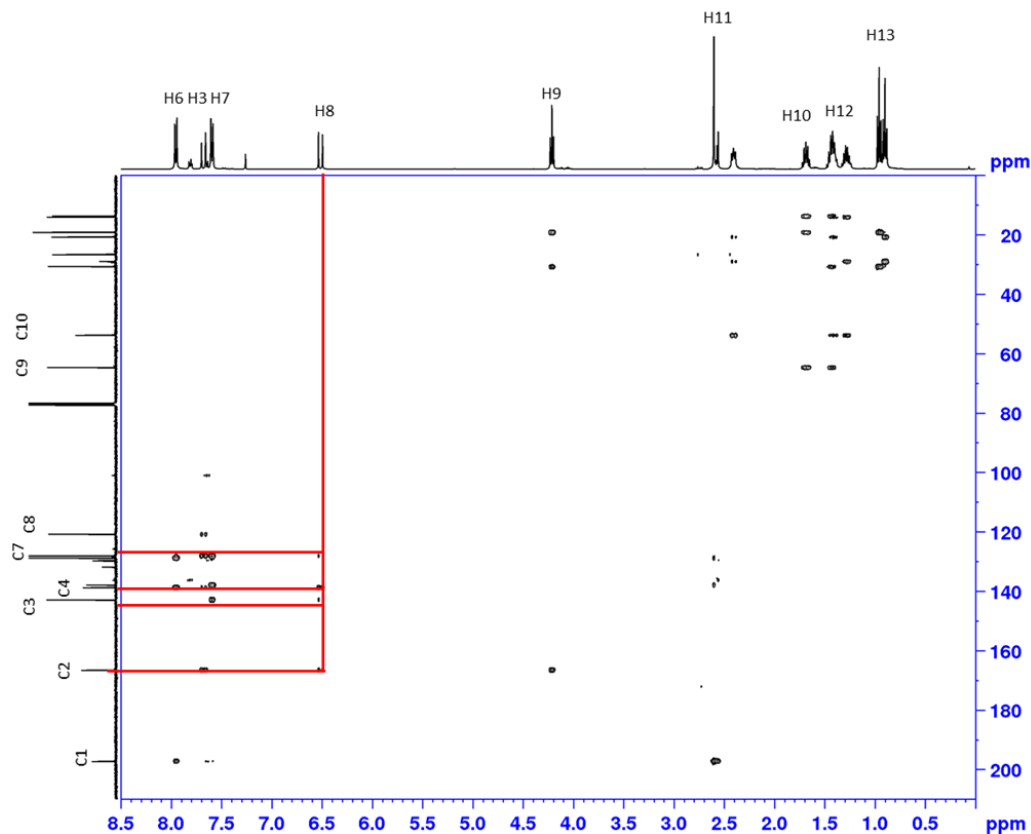
Figure 4.36: The HMBC spectrum (CDCl₃) obtained for butyl (E)-3-(4-acetylphenyl)prop-2-enoate (4.9-4I).

Figures 4.37 illustrate the most important correlations that are observed from the HMBC NMR data for butyl (*E*)-3-(4-acetylphenyl)prop-2-enoate (**4.9-4I**). The most important correlations are those of C8, which have correlations with C2, C3, C4 and C7. The proof that a new carbon-carbon bond did occur between the aromatic ring and the alkene, is the correlation between C3 and C2, as C2 are on the benzene ring, while C7 which have a correlation with C3 that is on the alkene group. These NMR results are in accordance with that reported by Trilla *et al.* (2008). Additional correlations were observed, and these are listed in Table 4.5.
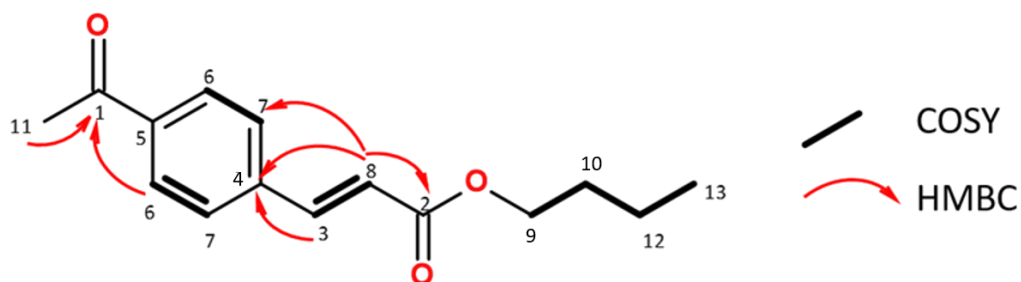
Figure 4.37: Key 2D NMR correlations observed for butyl (E)-3-(4-acetylphenyl)prop-2-enoate (4.9-4I), the numbering is based on the ¹³C chemical shifts.

Table 4.5: The data obtained from the 1D and 2D NMR on the product butyl (E)-3-(4-acetylphenyl)prop-2-enoate(4.9-4I).

Atom #	δ_C (mult.)	δ_H (integ., mult., *J*(Hz))	COSY	HMBC
1	197.3 (C)	-	-	-
2	166.5 (C)	-	-	-
3	142.9 (CH)	7.68 (1H, d, 16.0 Hz)	H8	C2, C4, C7, C8
4	138.8 (C)	-	-	-
5	137.9 (C)	-	-	-
6	128.8 (CH)	7.95 (2H, d, 8.3 Hz)	H7	C1, C5
7	128.1 (CH)	7.59 (2H, d, 8.3 Hz)	H6	C3, C5
8	120.8 (CH)	6.51 (1H, d, 16.0 Hz)	H3	C2, C3, C4, C7
9	64.6 (CH$_2$)	4.21 (2H, t, 6.7 Hz)	H10	C10, C12
10	30.7 (CH$_2$)	1.69 (2H, m)	H9	C9, C12, C13
11	26.7 (CH$_3$)	2.60 (3H, s)	-	C1, C5, C6
12	19.1 (CH$_2$)	1.42 (2H, m)	H10, H13	C9, C10, C13
13	14.0 (CH$_3$)	0.96 (3H, t, 7.3 Hz)	H12	C10, C12

GC-MS data revealed the presence of the molecular ion peak at 246.2 m/z (Figure 4.38), which is the expected mass of the product butyl (E)-3-(4-acetylphenyl)prop-2-enoate (**4.9-4I**). The main fragmentation ion peaks observed were found at *m/z* 231.2, 217.2 and 175.2. The retention times for the products obtained from both catalysts was 27.3 min (Table 4.6).
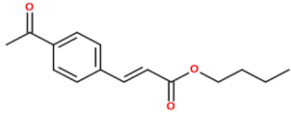
Figure 4.38: The major mass fragments obtained for butyl (E)-3-(4-acetylphenyl)prop-2-enoate (4.9-4I).

Reaction	Product	Rt (min)	m/z	% Yield
			$C_{15}H_{18}O_3$ (246.2 amu)	
Heck2		AE: 27.32	AE: Found: 246.2	AE: 70.6
	4.9-4I	PVP: 27.30	PVP: Found: 246.2	PVP: 68.7
	butyl (*E*)-3-(4-acetylphenyl)prop-2-enoate			

FTIR spectra revealed a stretch at 1683 cm^{-1} which is assigned to the alkene, as well as peaks at 2958 cm^{-1}, 1256 cm^{-1} and 1168 cm^{-1}.
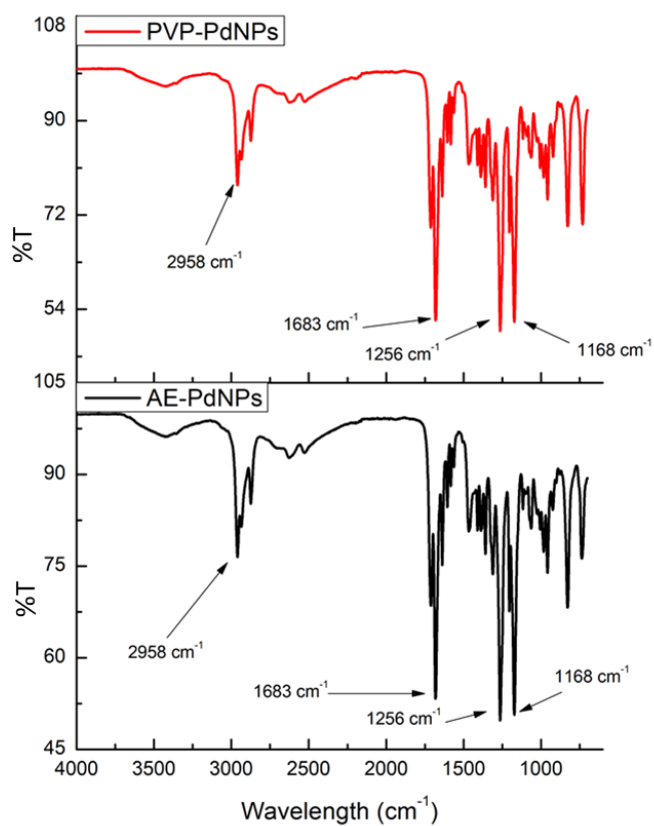
Figure 4.39: FTIR spectra obtained for butyl (E)-3-(4-acetylphenyl)prop-2-enoate (4.9-4I).

The UV-Visible spectra obtained for the starting materials and the final products are shown in Figure 4.40. A λ_{max} was observed at 270 nm. As expected, coupling between the acrylate and 4- iodoacetophenone induced a significant red shift of 23 nm to give a λ_{max} at 293 nm. The product obtained using the AE-PDNP catalyst appears to have an increased absorption intensity, together with a sharper band.
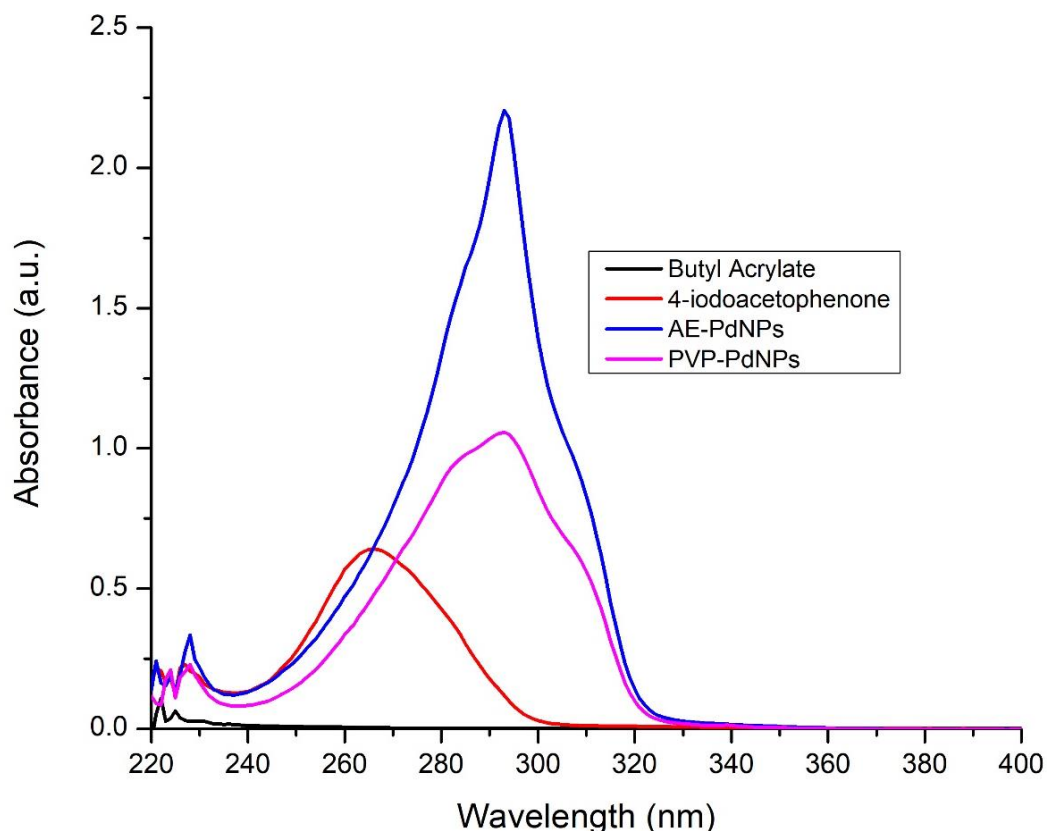
Figure 4.40: The UV-visible spectra obtained for (E)-3-(4-acetylphenyl)prop-2-enoate (4.9-4I) and the starting materials. The products did undergo a red shift to a λ_{max} at 293 nm Solvent (DCM).

4.3.2.2. Discussion on the Heck coupling reactions

The Heck coupling reaction was completed successfully only when 4-iodoacetophenone was used as the substrate. The use of 4-bromoacetophenone was not successful at all, indicating the selectivity of the reaction. qNMR was used to determine the successful conversion of the starting reagents to the product **4.9-4I**. It was clear that AE-PdNPs had a slightly better catalytic effect considering the yields obtained (71 and 69% for the AE- and PVP-PdNPs, respectively). GC-MS, NMR and UV-visible spectroscopy all confirmed the success of the NP catalysts in producing the product using 4-iodoacetphenone, while the opposite was true for the bromo substrate. Therefore, both sets of PdNPs were successful in this reaction to produce product **4.9-4I**, favouring the iodo-substrate only.

4.3.3. Sonogashira coupling reaction

4.3.3.1. The reaction of halogenated substrates with phenylacetylene (Sono1 and Sono2)

The Sonogashira carbon-carbon coupling reaction with halogenated substrates (4-bromoacetophenone (**4.2**) and 4-iodoanisole (**4.11**)) was carried out with phenylacetylene (**4.10**) as the second substrate. These halogenated substrates were chosen to understand the selectivity between the PdNPs catalysts for the substrate and also to understand which halogenated substrate the catalysts would favour in the formation of the expected products.

4-bromoacetophenone as the substrate (Sono1):
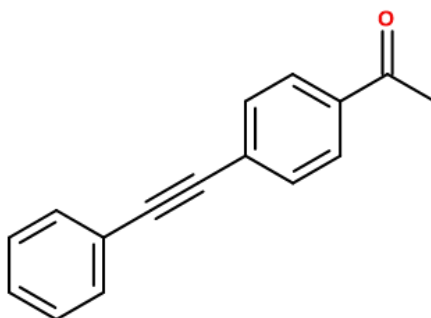
4.12

Figure 4.41: The expected product 1-(4-acetylphenyl)-2-phenylacetylene (4.12).

A dark brown powdered product was obtained following work-up of the reaction. 1D data (^{1}H and ^{13}C spectra) were acquired for the product. The ^{1}H NMR spectrum for the product 1-(4-acetylphenyl)-2-phenylacetylene (**4.12**) using both AE-and PVP-PdNPs as catalysts in reaction Sono1 is shown in Figure 4.42. It is revealing the aromatic signals in the 7.40-8.05 ppm region that integrates to 9 protons, as well as methyl signal found at 2.60 ppm.
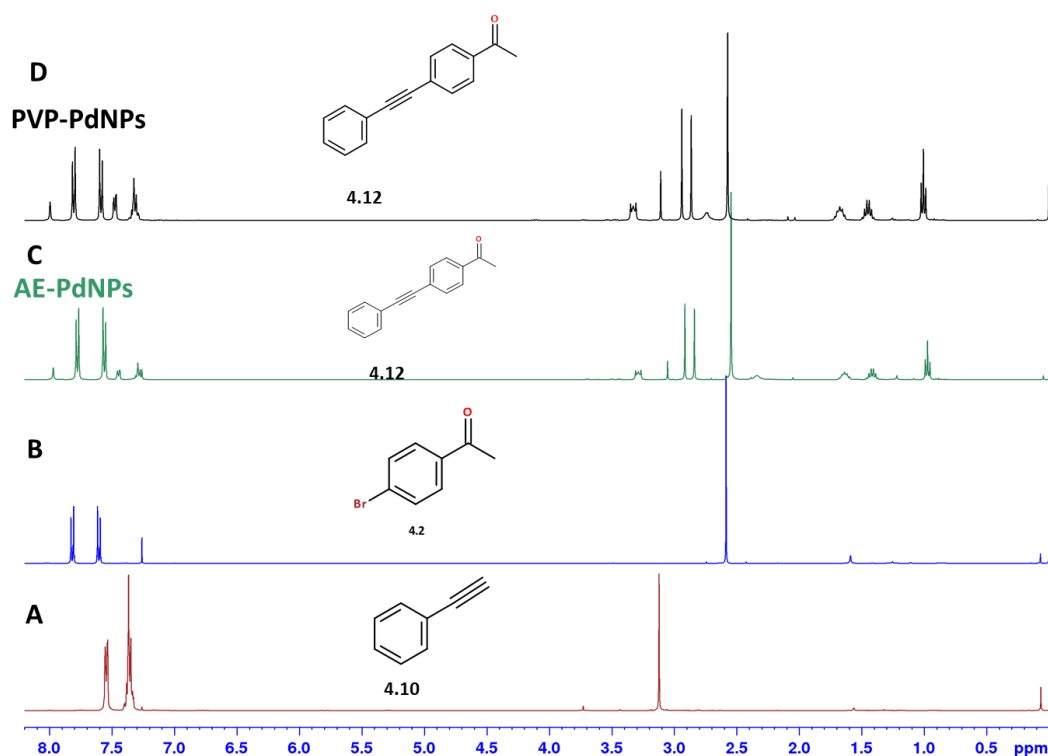
Figure 4.42: The ^{1}H NMR data (CDCl$_3$, 400 MHz) obtained for the product obtained using the AE-PdNPs (C) and PVP-PdNPs (D) catalysts. The proton spectra for the starting materials phenylacetylene (A) and 4-bromoacetophenone (B) is also shown.

The ^{1}H NMR spectra for the product **4.13** using both AE-and PVP-PdNPs as catalysts in reaction Sono1. The spectra for both products appear to be unreacted starting materials. This was confirmed by the ^{13}C NMR spectra, which revealed only the presence of starting materials.

The second reaction carried out, Sono2, also showed the presence of starting materials (**4.10** and **4.11**) in the 1H NMR and ^{13}C NMR spectra (Figure 4.43). No further analyses were attempted and due to time constraints, the reaction was not pursued further.
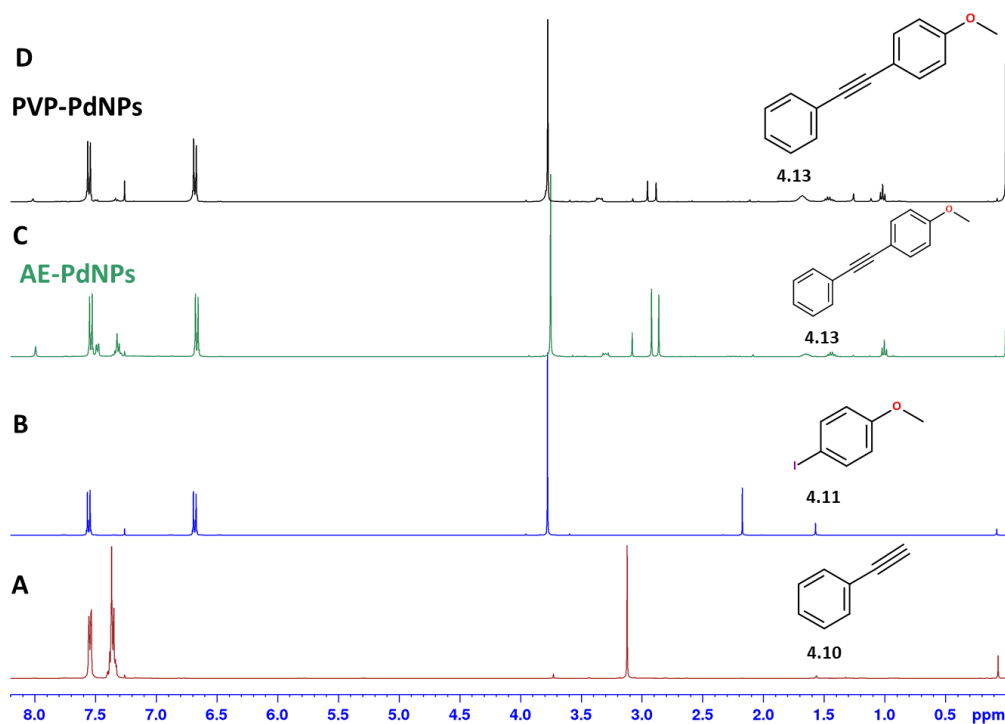
Figure 4.43: The ^1H NMR data (CDCl₃, 400 MHz) for the product 1-(4-methoxyphenyl)-2-phenylacetylene (4.13, C, D) from AE-PdNPs (C) and PVP-PdNPs (D) as catalysts. The starting materials phenylacetylene (A) and 4-iodoanisole (B) is also shown.

4.3.3.2. Discussion on Sonogashira coupling reaction

Both the Sonogashira products did not show the expected signals in the ^1H and ^{13}C NMR spectra. The failure of the experiments could be due to the selectivity and nature of the PdNPs.

4.4. Conclusion

Based on the NMR, GC-MS, and in some cases, the UV-Visible spectroscopic data, it appears that the AE-PdNPs, as a catalyst outperformed the "model catalyst" PVP-PdNPs in the Suzuki-Miyaura and Heck coupling reactions. The AE-PdNPs produced higher product % yields in all the reactions, which is an indication that the biosynthetic catalyst can be employed for manufacturing purposes. For both catalysts, the Suzuki-Miyaura coupling reactions SM1 and SM2, some form of selectivity is observed where the 4-bromoacetophenone substrate is preferred to the 4-iodoacetophenone, unexpectedly, since the iodo group is considered to be an easier leaving group compared to the bromo moiety. However, in the Heck coupling reactions 1 and 2, both PdNP catalysts clearly favoured 4-

iodoacetophenone as a substrate the expected product did not form, with 4-bromoacetophenone.

When the PdNPs were used in the Suzuki-Miyaura coupling reactions involve nitro substituted substrates, both the PdNPs preferred the nitro substituent in the para-position on the aromatic ring, compared to the ortho substituted substrate. This shows that, although the PdNPs could form the sterically hindered compound to some extent, it does not perform that well. Further studies would be necessary to improve the yield.

4.5. Bibliography

Gonzalez, R. R., Liguori, L., Carrillo, A. M. & Bjørsvik, H.-R. (2005) 'Synthesis of 2-Nitro- and 2,2'-Dinitrobiphenyls by Means of the Suzuki Cross-Coupling Reaction', *J. Org. Chem,* 70, pp. 9591-9594.

Islam, S. M., Mondal, P., Roy, A. S., Mondal, S. and Hossain, D. (2010) 'Heterogeneous Suzuki and copper-free Sonogashira cross-coupling reactions catalyzed by a reusable palladium(II) complex in water medium', *Tetrahedron Letters,* 51, p. 2067–2070.

Rizzo, V. & Pincriroli, V. (2005) 'Quantitative NMR in synthetic and combinational chemistry', *Journal of Pharmaceutical and Biological Analysis,* 38, pp. 851-857.

Trilla, M., Pleixats, R., Man, M. W. C., Bied, C. and Moreau, J. J. E. (2008) 'Hybrid Organic-Inorganic Materials fromDi-(2-p yridyl)methyl-amine-Palladium Dichloride Complex as Recoverable Catalysts for Suzuki, Heck and Sonogashira Reactions', *Adv. Synth. Catal.,* 350, pp. 577-590.

Chapter 5: Conclusion and future work

This chapter deals with the conclusions drawn from the work carried out and recommended future work for the project.

5.1. Synthesis and characterisation of palladium nanoparticles

Aqueous extracts of the brown marine algae, *Ecklonia radiata*, were successfully prepared and characterised. The aqueous extract (AE) and organic aqueous extract (OAE) from the brown algae were subjected to various characterisation methods such as NMR, FTIR, UV-visible and antioxidant assays, in order to determine the major components present in these extracts and to assess their capability in reducing the palladium metal salt. The presence of polysaccharides and polyphenols as the major and minor components, respectively were confirmed using NMR and the assays. The two aqueous extracts (AE and OAE) were compared, showing that AE possessed the greatest polyphenol content. Extraction of the seaweed with organic solvents prior to the water extraction, are probably to blame for the OAE losing some of its polyphenolic content. Overall, AE does have an additional advantage over OAE sample, as it better complies with green chemistry objectives that were set out for the project in producing PdNPs. Even though both extracts were able to generate PdNPs, the OAE sample did so in much less efficient manner, given the UV-vis spectra obtained and assay data.

The aqueous extract was shown to be able to reduce the Pd metal salt from Pd^{2+} to the zero valent metal, where the polyphenols are surmised to play an important role. The capping of the nanoparticles, in order to stop the nanoparticles from undergoing agglomeration, is thought to be the role of the polysaccharides present in the extract. The synthesis of the AE-PdNPs was easily achieved in a one-step method at room temperature using only water as the solvent, eliminating the need for the use of toxic reducing reagents typically needed such as $NaBH_4$. In contrast, the PVP-PdNPs requires a time consuming, multi-step reaction sequence. Also, the method to synthesise PVP-PdNPs makes use of expensive chemicals and reagents, giving the synthesis of PdNPs using an aqueous extract of a highly renewable resource an advantage over PVP capped PdNPs.

The PdNPs were characterised using different techniques and the results obtained does explain the nature of the PdNPs to some extent. The method used to produce the AE-PdNPs appears to produce the highest Pd loading for the NPs, compared to the PVP-PdNPs. This was corroborated by HRTEM, although HRTEM images are only obtained from a small area of the grid, and ICP-AES, since the Pd loading for the AE-PdNPs was found to be 48.8 ppm compared to PVP-PdNPs which had 28.9 ppm. The SAED images show the polycrystalline nature of the NPs clearly for the AE-PdNPs, indicating clear crystal lattice planes, which the PVP-PdNPs did not. These data were confirmed by XRD powder patterns, where the reflections revealed a face-centred cubic crystal phase for the AE-PdNPs. Zeta potential measurements confirmed the presence of negatively charged capping agents for both NPs, with the AE-PdNPs considered to be more stable based on the data obtained (at -17.5 mV for the AE-PdNPs vs -9.69 mV for the PVP capped NPs). DLS revealed the hydrodynamic radii of the NP to be 65 nm and 99 nm for the AE- and PVP-PdNPs. This appears to be in contrast to the average sizes obtained from the HRTEM images (12 nm (AE-PdNPs) vs.7 nm (PVP-PdNPs)). This is explained by the technique itself, where heavier elements like Pd, are more easily observed compared to organic material. Thus, the difference in TEM and DLS size determinations is due to the presence of a capping agent on the NP surface.

Synthesis of the PdNPs was therefore deemed to be successful, meeting a few of the aims and objectives set out for the study. The use of green synthetic methods can therefore be used for the formation of PdNPs, as it allows for non-toxic waste generation and should not limit the applications that NPs can be used in.

5.2. Carbon-carbon coupling reactions (Suzuki-Miyaura, Heck, Sonogashira)

Based on literature studies, PdNPs have been successfully used to catalyse various organic reactions such as Suzuki-Miyaura, Heck and Sonogashira carbon-carbon coupling reactions. Thus, one of the objectives was to use PdNPs as catalysts in the carbon-carbon coupling reactions. The success of these coupling reactions in industry, albeit using Pd complexes instead of PdNPs, does make the use of PdNPs as catalysts very promising, given the high surface to volume ratio inherent in NPs.

The carbon-carbon coupling Suzuki-Miyaura, Heck and Sonogashira reactions were attempted using the AE-PdNPs and PVP-PdNPs, the latter used as a 'model' NP catalyst. Following reaction of the variously substituted organohalides with boronic acids (Suzuki-Miyaura), butyl acrylate (Heck) or phenyl acetylene (Sonogashira), the product was interrogated by NMR (1D and 2D), qNMR, GC-MS,

FTIR and UV-Vis spectroscopy to determine if the reactions were indeed successful.

qNMR revealed that for the Suzuki-Miyaura coupling reactions, that a bromo substrate consistently slightly favoured over an iodo substituted starting material. However, product yields obtained for either reaction were >85%. To interrogate the effect of steric hindrance on the success or yield of the reaction using 1-iodo-2-nitrobenzene and 1-iodo-4-nitrobenzene, both PdNPs favoured the less steric hindered *para* substrate as expected. However, the reactions were not a complete failure, with the AE-PdNPs being responsible for a yield of 56%, with the PVP-PdNPs giving a significant lower yield at 40%. The AE-PdNPs consistently catalysed a higher yield for the products in Suzuki-Miyaura coupling reactions than its PVP counterpart.

The use of the PdNPs in the Heck coupling reactions was fairly successful, demonstrating some selectivity in these reactions. The reaction of 4-bromoactophenone butyl acrylate with both sets of PdNPs was a complete failure. However, when 4-iodoacetophenone was used, product yields of up to 70% were obtained (using the AE-PdNPs). PdNP catalysts therefore favour the iodo substrate in a reaction with butyl acrylate. The AE-PdNPs once again outperformed the model PVP-PdNPs in the Heck coupling reaction as the AE-PdNPs consistently produced higher yields 71% compared to the PVP-PdNPs with yields of 69%.

The Sonogashira coupling reactions failed to produce the expected products. The failure of the catalysts in these reactions could be due to various reasons, one of which could be that both the PdNPs were solutions and not powders, solutions such as water (AE-PdNPs) and ethanol (PVP-PdNPs) may cause the substrate phenylacetylene to interact with it and not with the other substrates. Sanz *et al.* (2007) have reported that phenylacetylene may undergo hydration when there is water or an alcohol present in the reaction media.

The PdNP catalysts were clearly efficient in the Suzuki-Miyaura carbon-carbon coupling reactions, giving >90% for the desired products and ~50% yields with sterically crowded substrates. Heck coupling reactions clearly favoured the use of iodo moieties as leaving groups. The aims and objectives of the study was mostly achieved, since the AE-PdNPs were successfully synthesised using green chemistry principles, showing many advantages over the model PVP-PdNP catalysts.

5.3. Future work

A few studies need to be carried out in order to substantiate the findings in this thesis. Even though the AE-PdNPs were synthesised from *Ecklonia radiata,* other more common kelp species could be investigated in order to make better use of a renewable resource. Full characterisation of the aqueous extract using NMR, HPLC and LC-MS needs to be done. Also, different concentrations of Pd metal salts in order to assess which concentration produces the most efficient, catalytically active PdNPs. Better control in producing a small size distribution is also critical in the production of NP catalysts. More substrates in order to further test the selectivity of the PdNPs in the Suzuki-Miyaura and Heck coupling reactions, could be used where kinetic studies are also carried out. Recyclability tests and turnover frequency (TOF) tests are also very important in the characterisation of a catalyst, as it allow for the understanding to see which PdNPs catalyst could be recycled the most in a catalytic reaction.

5.4. Bibliography

Sanz, S., Jones, L. A., Mohr, F. and Laguna, M. (2007) 'Homogeneous catalysis with gold: Efficient hydration of phenylacetylene in aqueous media', *Organometallics,* 26, pp. 952-957.